UNIVERSIDADE D
COIMBRA

Cláudio Figueiredo Costa

EXPERIMENTAL ENHANCEMENT OF CELLULAR OXPHOS RELIANCE FOR MITOCHONDRIAL HEALTH ASSESSMENTS

DEVELOPMENT AND CHARACTERIZATION OF A RAPID AND EFFICIENT METHOD TO INDUCE OXPHOS IN SKIN FIBROBLASTS, FOR THE ASSESSMENT OF MITOCHONDRIAL TOXICITY AND PROTECTION

Dissertação no âmbito do Mestrado em Biologia Celular e Molecular, orientada pela Doutora Maria Teresa Martins da Cunha Oliveira e pelo Professor Doutor António Joaquim Matos Moreno e apresentada ao Departamento de Ciências da Vida da Faculdade de Ciências e Tecnologia da Universidade de Coimbra.

Setembro de 2018

Faculdade de Ciências e Tecnologia | Departamento de Ciências da Vida
Mestrado em Biologia Celular e Molecular

EXPERIMENTAL ENHANCEMENT OF CELLULAR OXPHOS RELIANCE FOR MITOCHONDRIAL HEALTH ASSESSMENTS

Development and characterization of a rapid and efficient method to induce OXPHOS in skin fibroblasts, for the assessment of mitochondrial toxicity and protection

Cláudio F. Costa
Teresa Cunha-Oliveira
António J. Moreno

Coimbra
September, 2018

E pluribus unum

in *Moretum,* **Virgílio**

This work was performed at the Mitochondrial Toxicology and Experimental Therapeutics (MitoXT) group, at the Center for Neuroscience and Cell Biology of University of Coimbra, Portugal, under the supervision of Dr. Teresa Cunha-Oliveira (CNC, UC) and Dr. António J. Moreno (DCV, UC) and also of the group leader, Dr. Paulo J. Oliveira (CNC, UC).

The work presented in this dissertation was funded by FEDER/COMPETE/national funds by FCT under research grants PTDC/DTP-FTO/2433/2014, POCI-01-0145-FEDER-029297 and POCI-01-0145-FEDER-007440.

Agradecimentos

Findo um ano de muito trabalho, precedido de quatro muito semelhantes, serve este monte de papéis como culminação, sendo que muitas seriam as palavras que podia escrever nesta secção, sem sequer de correr o risco de exagerar.

As minhas primeiras palavras terão de ir necessariamente para a Dra. Teresa Oliveira, por não raras vezes ser uma cabeça mais pensadora do que eu, por ser uma voz de otimismo até perante os cenários mais negativos, e, principalmente, pela imensa paciência que teve nos últimos anos. Sem o seu contributo, muito provavelmente, seria muito menos capaz de fazer ciência, pelo que, certamente, no futuro, quaisquer que sejam os desafios que abrace, o seu cunho estará sempre presente. Espero, muito sinceramente, ter estado à altura de toda e qualquer expectativa em mim depositada. O segundo agradecimento é direcionado ao Dr. Paulo Oliveira, por proporcionar todas as condições à realização deste trabalho, já nem falando do estímulo constante à atividade física! Um agradecimento também ao Prof. Dr. António Moreno por aceitar a supervisão de um aluno que não conhecia à priori, assim como à Dra. Vilma por ter a minha professora de Seahorse e também de Western Blot, sendo a especialista a quem podia sempre recorrer.

Logicamente, não podia deixar de agradecer a todos os membros do MitoXT, um grupo fantástico, no verdadeiro sentido da palavra. Mais em particular, ao Rui, o escravo número 1 sempre que necessário, sempre pronto a ajudar no que fosse necessário, mesmo sabendo que, regra geral, pouco ganharia com isso, algo que, considero eu, o valoriza imenso. Ao Ricardo Amorim, irmão Benfiquista, meu professor de cultura celular, outro que nunca se coibiu de ajudar, e com quem foi um gosto discutir todas a vieiradas e restantes assuntos que nos faziam sofrer de maneira muito semelhante. À Susana, a voz da razão, sempre pertinente, uma pessoa com quem, devido à sua frontalidade, todos deviam conviver na sua vida. Ao José, não só por frequentemente ser o meu taxista, mas também pelo seu sempre proveitoso aconselhamento em imensas questões práticas que foram surgindo ao longo do trabalho, além de ser também um excelente companheiro de café. À Cláudia, a taxista *ex aequo* que, por ser a pessoa mais picuinhas do grupo e ao mesmo tempo dona de uma personalidade tão peculiar, foi uma pessoa com quem deu gosto coexistir, mesmo tendo em conta a sua mais clara lacuna que é a cor clubística. À Inês, a minha colega bioq do grupo, que também gastou do seu tempo em prejuízo próprio em ensinar o que que sabia, e que, estando nós numa situação académica semelhante, foi uma excelente parceira de discussão sobre o futuro que nos espera. Ao João Martins, o tipo de pessoa que devia existir em todos os grupos de trabalho, que, por vezes sem sequer lhe ser pedido, partilhava o seu conhecimento, sempre com uma calma e com uma boa disposição contagiante. Às Adrianas, à Caroline, ao Rodrigo, à Luciana, também elas e ele excelentes companheiros de café. A todos os restantes

membros do grupo, Guida, Filomena, Liljana e Ricardo Marques, assim como a todas as pessoas estrangeiras que foram passando pelo MitoXT e aos alunos de 1º ano de mestrado, por este fantástico ano de coexistência.

Externos ao grupo, urge deixar também um sincero agradecimento à Dra. Sonia Pinho, sem acento, pela colaboração e pela imensa ajuda numa técnica que me era antes completamente estranha. Um agradecimento também à Dra. Cristina e ao Dr. John Jones, assim como ao Ludgero, pela ajuda nas experiências de RMN já realizadas, que só é pena ainda não terem dado resultados. Finalmente, um agradecimento ao grupo liderado pela Prof. Dra. Fernanda Borges, pela cedência de pequenas alíquotas de antioxidantes para o trabalho.

A título mais pessoal, e correndo o risco de deixar alguém de parte, um agradecimento por tudo aos Paulos e Paulas Brandão, Chicória, Carolina, Zé Pinto, Rocha, Bem-Haja, Pedrosa, Abranches, Andreia, Navarro, …, bem como aos velhotes, dos quais destaco o Tozé, e aos bebés, dos quais destaco o Xavier e a Inês Morais, que certamente irão comigo para onde quer que eu vá no futuro. Também aos membros da Estudantina Universitária de Coimbra e aos membros da Orquestra Académica da UC, duas famílias às quais a música felizmente me juntou e que muito me enriqueceram a nível pessoal. Finalmente, um agradecimento também aos arganilenses (Zé Oliveira, Catarina, Zé Castanheira, Nelson, Bruna, Jorge …) e aos membros da Associação Filarmónica de Arganil, que me acompanham há mais tempo do que dura esta vida universitária.

Não podia deixar de dizer obrigado à Susana, por ser o meu yin. Correndo o risco de, daqui por uns tempos, não nos podermos ver à frente, certamente que estes 5 anos teriam sido imensamente diferentes sem ela. Por último, mas não menos importante, à minha FCT particular, com sede fiscal numa pequena aldeia chamada Pombeiras, não só por serem a minha entidade financiadora, mas por incansavelmente me darem na cabeça há mais de 22 anos. Um agradecimento, portanto, ao senhor Arselino e à dona Manuela, extensivo à mais nova manceba da casa.

Table of Contents

List of Acronyms and Abbreviations

Acetyl-CoA	Acetyl-Coenzyme A
ADP	Adenosine Diphosphate
ALT	Alanine Transaminase
AMP	Adenosine Monophosphate
AMPK	AMP-activated protein kinase
ATP	Adenosine Triphosphate
BCA	Bicinchoninic Acid
BSA	Bovine Serum Albumin
cAMP	Cyclic Adenosine Monophosphate
cDNA	Complementary DNA
CN^-	Cyanide
CO_2	Carbon Dioxide
CRLS1	Cardiolipin Synthase 1
Cybrid	Cytoplasmic Hybrids
DAB	Diamidobenzidine
DJ-1	Protein Deglycase
DLAT	Dihydrolipoamide Acetyltransferase
DLD	Dihydrolipoamide Dehydrogenase
DMEM	Dulbecco's Modified Eagle's Medium
DMM	Dimethyl Malonate
DNA	Deoxyribonucleic Acid
DTT	Dithiothreitol
ECAR	Extracellular Acidification Rate
ECM	Extracellular Matrix
ETC	Electron Transport Chain
F-6-P	Fructose 6-Phosphate
$FADH_2$	Flavin Adenine Dinucleotide
FBS	Fetal Bovine Serum
FCCP	Carbonyl Cyanide 4-(trifluoromethoxy)phenylhydrazone
FoxO3	Fork Head Box O3
G-6-P	Glucose-6-Phosphate
G6PDH	Glucose-6-Phosphate Dehydrogenase
GABPA	GA binding protein transcription factor alpha subunit
GABPB1	GA binding protein transcription factor beta-1 subunit
GALE	UDP-Glucose 4-Epimerase
GALK	Galactokinase
GALT	Galactose-1-Phosphate Uridyltransferase
GAPDH	Glyceraldehyde 3-Phosphate Dehydrogenase
GLS	Glutaminase
GLUT	Glucose Transport Proteins
GSH	Glutathione
GSSG	Glutathione Disulfide
GTP	Guanosine Triphosphate
H^+	Proton
H_2O	Water
H_2O_2	Hydrogen Peroxide
HCl	Hydrogen Chloride
$HClO_4$	Perchloric Acid
HGm	High-Glucose medium
HK	Hexokinase
HPLC	High Performance Liquid Chromatography
HRP	Horseradish Peroxidase
HSP60	Heat Shock Protein 60
IC50	Half Maximal Inhibitory Concentration

IgG	Immunoglobulin G
IMM	Inner Mitochondrial Membrane
IMS	Intermembrane Space
KH_2PO_4	Phosphate Buffer
LDH	Lactate Dehydrogenase
LGm	Low-Glucose medium
LHON	Leber's hereditary optic neuropathy
MMP	Matrix Metalloproteinases
mRNA	Messenger RNA
mtDNA	mitochondrial DNA
NADH	Nicotinamide Adenine Dinucleotide (reduced form)
NADPH	Nicotinamide Adenine Dinucleotide Phosphate (reduced form)
NaOH	Sodium Hydroxide
NDK	Nucleoside-Diphosphate Kinase
NHDF	Normal Human Dermal Fibroblast
NRF	Nuclear Respiratory Factors
NTB	NitroTetrazolium Blue
O_2	Molecular Oxygen
$O_2^{\bullet -}$	Superoxide Radical
OAA	Oxaloacetate
OCR	Oxygen Consumption Rate
$^{\bullet}OH$	Hydroxyl Radical
OXPHOS	Oxidative Phosphorylation
OXPHOSm	OXPHOS medium
PBS	Phosphate-Buffered Saline
PDH	Pyruvate Dehydrogenase
PDK1	Pyruvate Dehydrogenase Kinase 1
PEPCK-C	Phosphoenolpyruvate Carboxykinase-C
PFK-1	Phosphofructokinase 1
PGC1α	Peroxisome Proliferator-Activated Receptor Gamma Coactivator-1α
PGM	Phosphoglucomutase
Pi	Inorganic Phosphate
PINK1	PTEN-induced putative kinase 1
PKA	Protein Kinase A
PKM	Pyruvate Kinase
PMSF	Phenylmethylsulfonyl Fluoride
PPARα	Peroxisome Proliferator-Activated Receptor-α
PPP	Pentose Phosphate Pathway
PVDF	Polyvinylidene Difluoride
Q10	Ubiquinone
QH_2	Ubiquinol
qRT-PCR	Quantitative Real Time Polymerase Chain Reaction
RNA	Ribonucleic Acid
RNAseP	ADP-ribosyltransferase polymerase-like 2
ROS	Reactive Oxygen Species
SDS	Sodium Dodecyl Sulfate
SDS–PAGE	Sodium Dodecyl Sulfate–Polyacrylamide Gel
SEM	Standard Error of the Mean
SIRT1	Sirtuin-1
SIRT3	Sirtuin-3
SOD	Superoxide Dismutase
SRB	Sulforhodamine B
tBHP	*tert*-Butyl Hydroperoxide
TCA	Tricarboxylic Acid
TFAM	Mitochondrial Transcription Factor A
TMRM	Tetramethylrhodamine Methylester
TPP	Triphenylphosphonium

UCP	Uncoupling Protein
UDP-Galactose	Uridine Diphosphate Galactose
UDP-Glucose	Uridine Diphosphate Glucose
UV	Ultraviolet

Abstract

Stimulation of oxidative phosphorylation (OXPHOS) in cultured cells has gained relevance in the last decade as a very important tool for studies in the areas of toxicology and biomedicine, namely by unmasking the selective mitochondrial toxicity of chemicals. This may be achieved by removing glucose from culture media, but there is a great variability in the methodology across the literature that compromises the comparisons between different works. Thus, our objective was to standardize and characterize cell culture conditions to enhance OXPHOS reliance in Normal Human Dermal Fibroblasts (NHDF) cell line, with applicability in mitochondrial health assessments.

We used NHDF cells cultured in medium containing 25 mM Glucose (HGm) and gradually adapted, or acutely exposed, to 5 mM Glucose-containing medium (LGm) or to glucose-free galactose-containing medium (OXPHOSm) for different periods. Oxygen consumption rates (OCR) were measured under these conditions using a Seahorse XF^{e}96 Extracellular Flux Analyzer. To understand the importance of different OXPHOSm components for OXPHOS stimulation, we also measured OCR in cells cultured in the presence or absence of glutamine, pyruvate, galactose and uridine. Furthermore, we compared several cellular parameters, such as the expression, levels and activity of several key genes and proteins, mtDNA copy number, mitochondrial network morphology, the cellular energetic state and the effect of toxicants in metabolic activity and ATP levels of the same cells.

Measurements of OCR-associated parameters indicated that gradual cell adaptation in at least one cell passage to OXPHOSm is necessary for OXPHOS stimulation to be observed. Measurements of CYB mRNA expression in cells cultured in OXPHOSm for a different number of passages indicated that cells needed at least two cell passages in OXPHOSm until a plateau of CYB expression was reached, which suggests that the levels of mitochondrial biogenesis take time to stabilize. Our results also suggest that a more OXPHOS-based cellular phenotype is accompanied by changes in the expression and in the levels of several genes and proteins, in mtDNA copy number and in mitochondrial network morphology, without affecting, however, the cellular global energetic state. Also, toxicity of mitochondrial toxicants was increased and more consistent in OXPHOSm-adapted cells, facilitating mitochondrial protection studies.

Together, our results show that the long-term adaptation of NHDF cell line to OXPHOSm increased its OXPHOS-reliance, which did not occur shortly after acute exposure to this medium, sensitizing them for the toxic effects of mitochondrial drugs. These effects were accompanied by molecular changes in cellular metabolic machineries.

***Keywords**: metabolic remodeling; fibroblasts; mitochondrial health; OXPHOS reliance*

Resumo

A estimulação da fosforilação oxidativa (OXPHOS) em células em cultura ganhou relevância na última década como uma ferramenta muito importante para estudos nas áreas da toxicologia e biomedicina, servindo para desmascarar a toxicidade mitocondrial seletiva de químicos. Isto pode ser alcançado pela remoção de glicose do meio de cultura, sendo que, porém, há uma grande variabilidade na metodologia na literatura que compromete as comparações entre diferentes trabalhos. Assim, o nosso objetivo foi padronizar e caracterizar as condições de cultivo celular para aumentar a dependência de OXPHOS em fibroblastos de pele (NHDF), com aplicabilidade em estudos para avaliação de saúde mitocondrial.

Foram usadas células NHDF cultivadas em meio contendo 25 mM glicose (HGm) e gradualmente adaptadas ou expostas de forma aguda a meio contendo 5 mM glicose (LGm) ou galactose (OXPHOSm). As taxas de consumo de oxigénio (OCR) foram medidas nessas condições usando um Seahorse XFe96 Extracellular Flux Analyzer. Para entender a importância dos diferentes componentes do OXPHOSm para a estimulação da OXPHOS, também foram medidas as OCR em células cultivadas na presença ou ausência de glutamina, piruvato, galactose e uridina. Além disso, foram comparados também vários parâmetros celulares, como a expressão, níveis e atividade de vários genes e proteínas, o número de cópias do mtDNA, a morfologia da rede mitocondrial, o estado energético das células e também o efeito de algumas substâncias na atividade metabólica ou nos níveis de ATP das mesmas células.

Medições de parâmetros associados à OCR indicaram que a adaptação gradual das células em pelo menos uma passagem a OXPHOSm é necessária para a estimulação da OXPHOS. Medições da expressão de CYB em células cultivadas em OXPHOSm em diferente número de passagens sugerem que as células precisam de, pelo menos, duas passagens em OXPHOSm até atingir um plateau de expressão de CYB, o que sugere que os níveis de biogénese mitocondrial levam tempo para estabilizar. Os nossos resultados sugerem também que um fenótipo mais oxidativo é acompanhado por mudanças na expressão e nos níveis de vários genes e proteínas, no número de cópias do mtDNA e na morfologia da rede mitocondrial, sem afetar, porém, o estado energético global das células. Além disso, a toxicidade de venenos mitocondriais foi muito maior e mais consistente em células adaptadas a OXPHOSm, facilitando os estudos de proteção mitocondrial.

Em conjunto, os resultados mostram que a adaptação das células NHDF a OXPHOSm aumentou a sua dependência da OXPHOS, algo que não ocorreu logo após exposição aguda a este meio, sensibilizando-as para os efeitos tóxicos das drogas mitocondriais. Estes efeitos foram acompanhados de alterações moleculares nas maquinarias celulares associadas ao metabolismo.

***Palavras-chave**: remodelação metabólica; fibroblastos; saúde mitocondrial; OXPHOS-dependência*

Chapter I
Introduction

Energy is a factor to have into account in every process that occurs in the universe. While some reactions involve release of energy, being called exergonic reactions, others consume energy, being called endergonic reactions. Exergonic reactions are thermodynamically favorable, occurring spontaneously, in theory, while endergonic reactions are unfavorable (Nelson and Cox, 2013).

Biological processes are no exception. For example, biosynthesis of nucleic acids, proteins and other biomolecules requires the usage of energy, mainly but not only in the form of Adenosine Triphosphate (ATP) (Voet and Voet, 2011, Nelson and Cox, 2013). ATP is a nucleoside triphosphate (Figure 1.1) composed by an adenosine nitrogenous base, a ribose and three connected phosphate groups, being an important source of chemical energy. When exergonic cleavage of one phosphate group occurs, generating Adenosine Diphosphate (ADP) and inorganic phosphate (Pi), there is release of energy that is coupled to biological endergonic reactions, that, without this energy, would not occur (Nelson and Cox, 2013).

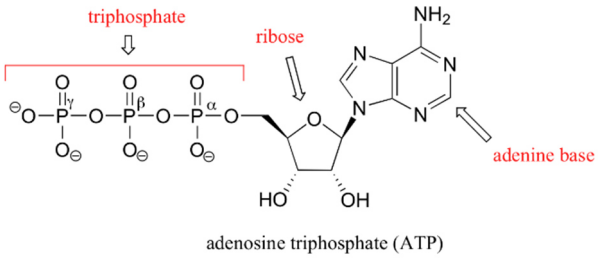

Figure 1.1 ATP molecular structure. *In*

1.1 Carbohydrate cell metabolism and mitochondrial metabolic pathways

There are several metabolic pathways that occur in cells to generate ATP. Glycolysis is one of the most important pathways, occurring in the cytosol and being a catabolic set of ten chemical reactions in which there is degradation of glucose into pyruvate, in a ratio of two pyruvates per glucose (Berg et al., 2002, Nelson and Cox, 2013). In a first phase, designated preparatory or investment phase, which comprises the first five reactions, glucose is converted into two molecules of glyceraldehyde-3-phosphate, consuming two molecules of ATP. After that, in the compensation phase,

comprising the other five reactions, those two molecules of glyceraldehyde-3-phosphate are converted into two molecules of pyruvate, generating four molecules of ATP. Taking everything into account, at the end of glycolysis, the balance is a reward of two ATP molecules. In glycolysis, there is also generation of two molecules of reduced Nicotinamide Adenine Dinucleotide (NADH) (Berg et al., 2002, Nelson and Cox, 2013). Glycolysis is indirectly activated by glucose, since phosphorylation of fructose 6-phosphate (F-6-P) to fructose-1,6-bisphosphate, the most important control point of the pathway, is catalyzed by phosphofructokinase 1 (PFK-1), that is allosterically activated by fructose-2,6-bisphosphate, whose synthesis, by PFK-2, occurs when there is an excess of F-6-P (Berg et al., 2002). Adenosine Monophosphate (AMP) is also an allosteric activator of PFK-1, so, in conditions of energy deficit, cells are stimulated to perform glycolysis (Berg et al., 2002). In addition, glycolysis is activated by fructose 1,6-bisphosphate and inhibited by ATP, glucose-6-phosphate (G-6-P) and alanine (Berg et al., 2002).

Pyruvate may have several fates. In mammalian cells under hypoxia, pyruvate is converted into lactate, in a process called lactic acid fermentation. In this process, which is faster but less efficient than the one described below, there is reduction of pyruvate by NADH, in a reaction catalyzed by lactate dehydrogenase (LDH) (Berg et al., 2002, Yu et al., 2017). Lactate is then exported by the cells through specific carriers, the monocarboxylate transporters, which allow cells to maintain normal intracellular pH (Lin et al., 1998, Dimmer et al., 2000, Grollman et al., 2000, Halestrap and Meredith, 2004, Marie and Shinjo, 2011). In contrast, in cells under normoxia, pyruvate is transported into mitochondria, being a substrate for pyruvate dehydrogenase (PDH) complex. PDH complex is composed by PDH itself, dihydrolipoamide dehydrogenase (DLD) and dihydrolipoamide acetyltransferase (DLAT) and E3-binding protein, and catalyzes pyruvate decarboxylation, in a multi-step reaction that leads to Acetyl-Coenzyme A (Acetyl-CoA) and NADH generation (Berg et al., 2002, Yu et al., 2008, Yu et al., 2017). Acetyl-CoA is then a substrate for tricarboxylic acid (TCA) cycle, also known as Krebs cycle, in honor to Hans Krebs, the German-born British biochemist

that first identified the existence of this metabolic pathway. In the Krebs cycle, Acetyl-CoA is oxidized into carbon dioxide (CO_2), in an eight-step cycle that starts with citrate synthesis from oxaloacetate (OAA) and Acetyl-CoA by citrate synthase and ends with OAA regeneration after L-Malate oxidation by malate dehydrogenase, that may be used to restart the cycle (Nelson and Cox, 2013). This metabolic pathway does not form ATP directly. However, it generates one molecule of guanosine triphosphate (GTP) per cycle, that is easily converted in ATP by nucleoside-diphosphate kinase (NDK) in a reversible reaction (Berg et al., 2002, Nelson and Cox, 2013). Since four of the eight steps of Krebs cycle are reduction–oxidation reactions, there is also generation of several reducing equivalents per cycle, namely, three molecules of NADH, as well as one of reduced Flavin Adenine Dinucleotide ($FADH_2$) inside succinate dehydrogenase (Nelson and Cox, 2013). Acetyl-CoA is also important for other cellular functions, such as protein acetylation (Sadoul et al., 2008).

Another important metabolic pathway in which glucose is oxidized is the Pentose Phosphate Pathway (PPP). PPP has two phases, the oxidative phase and the non-oxidative phase. In the oxidative phase, G-6-P is oxidized into ribulose-5-phosphate and then to ribose-5-phosphate, with reduction of two molecules of Nicotinamide adenine dinucleotide phosphate ($NADP^+$) into its reduced form, NADPH, for each G-6-P oxidized (Nelson and Cox, 2013). NADPH is very important for glutathione (GSH) regeneration from Glutathione disulfide (GSSG) and for biosynthesis of fatty acids and steroids, whereas ribose-5-phosphate is a precursor for synthesis of nucleotides and several coenzymes, such as coenzyme A, NADH or ATP, making PPP a very important pathway for cells undergoing proliferation (Nelson and Cox, 2013). Non-oxidative phase recycles G-6-P with consumption of ribulose-5-phosphate. This phase is particularly important for cells with high NADPH demands (Nelson and Cox, 2013). Regulation of PPP activity is made at the first reaction of the pathway, which is the conversion of G-6-P into 6-phosphoglucono-δ-lactone by G-6-P dehydrogenase (G6PDH), with reduction of $NADP^+$ into NADPH. G6PDH is allosterically activated by $NADP^+$ and inhibited by NADPH, so G-6-P is directed to PPP depending on

NADPH/$NADP^+$ ratio (Voet and Voet, 2011, Nelson and Cox, 2013, Patra and Hay, 2014).

Oxidative phosphorylation (OXPHOS) is another metabolic pathway that occurs in mitochondria, particularly, in inner mitochondrial and cristae membranes, being responsible for most of ATP synthesis (Nelson and Cox, 2013, Saada, 2014). According to Peter Mitchell's chemiosmotic theory (Figure 1.2), this pathway uses energy derived from the oxidation of molecules that were reduced in other pathways to create a proton gradient between mitochondrial intermembrane space (IMS) and inner mitochondrial membrane (IMM), generating, in the intermembrane space, a chemical potential (with matrix alkalinization) and an electrical potential (with the matrix becoming more negative). This electrochemical potential is then used to generate ATP from ADP and Pi (Mitchell, 1961, Nelson and Cox, 2013). This process involves the Electron Transport Chain (ETC), composed by four protein complexes, namely NADH dehydrogenase (complex I), Succinate dehydrogenase (complex II), Coenzyme Q - cytochrome c reductase (complex III) and Cytochrome c oxidase (complex IV) and a fifth OXPHOS complex, called F_1F_O ATP synthase (complex V) (Nelson and Cox, 2013). In complex I, NADH is transformed into its oxidized form (NAD^+) with reduction of ubiquinone (also known as coenzyme Q10) (Q10) to ubiquinol (QH_2), in a reaction that also involves translocation of four protons (H^+) from mitochondrial matrix to IMS, contributing for the proton gradient mentioned before (Nelson and Cox, 2013). One of the most known inhibitors of complex I is rotenone (Prieur et al., 2001, Nelson and Cox, 2013). Complex II is the only membrane-bound enzyme of Krebs cycle, catalyzing the oxidation of succinate to fumarate, coupled with the reduction of FAD to $FADH_2$ inside the enzyme. $FADH_2$ then transfers electrons to Q10, leading to its reduction to

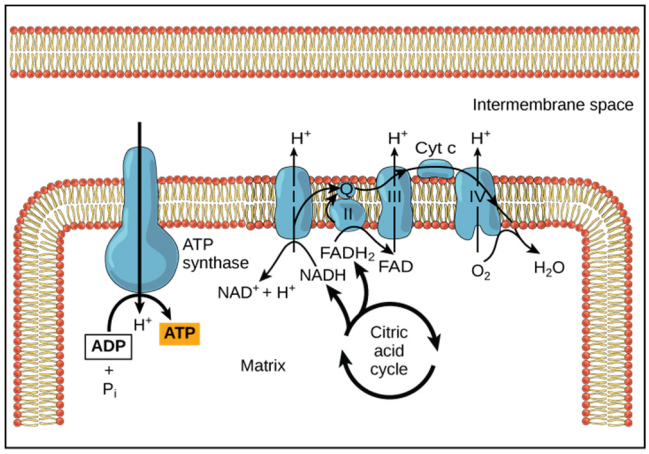

Figure 1.2 Oxidative Phosphorylation. *In cnx.org*

QH_2 and to regeneration of FAD. Unlike what happens in complex I, in complex II there is no proton ejection to IMS (Nelson and Cox, 2013). Thenoyltrifluoroacetone (Sun et al., 2005) or dimethyl malonate (DMM) (Dervartanian and Veeger, 1964, Mills et al., 2016) inhibit this complex. The electrons are then transferred to cytochrome c by complex III, and then transferred to complex IV and to molecular oxygen (O_2), which is the final electron acceptor of ETC, being reduced to water (H_2O). During this process, there is translocation of four protons to IMS in complex III and of two protons in complex IV (Nelson and Cox, 2013). Complex III is inhibited by antimycin A and complex IV is inhibited by cyanide (CN^-) (Kim et al., 1999, Berg et al., 2002, Nelson and Cox, 2013). In general, this transfer of electrons to the O_2 is highly exergonic, hence allowing the generation of the previously mentioned transmembrane electrochemical gradient (Nelson and Cox, 2013). Protonic gradient is then dissipated in complex V, with the energy of dissipation being used to synthetize ATP (Nakamoto et al., 2008, Nelson and Cox, 2013). Oligomycin, by blocking the F_O domain of this complex, inhibits ATP synthesis (Shchepina et al., 2002). Stoichiometrically, it is described that ejection of four protons is necessary to synthesize one molecule of ATP. Therefore, each NADH molecule gives rise to 10/4 = 2.5 ATP molecules and each succinate/$FADH_2$ gives rise to 6/4 = 1.5 ATP molecules (Hinkle et al., 1991, Nelson and Cox, 2013).

It is possible to measure several parameters associated with oxygen consumption rate (OCR) in mitochondria for cellular bioenergetic studies. For example, in the Seahorse™ Mito stress test, cellular OCR measured in the beginning of an experiment corresponds to the sum of basal OCR and non-mitochondrial OCR. Oligomycin addition, by inhibiting the component of oxygen consumption that fuels ATP synthesis by ATP synthase,

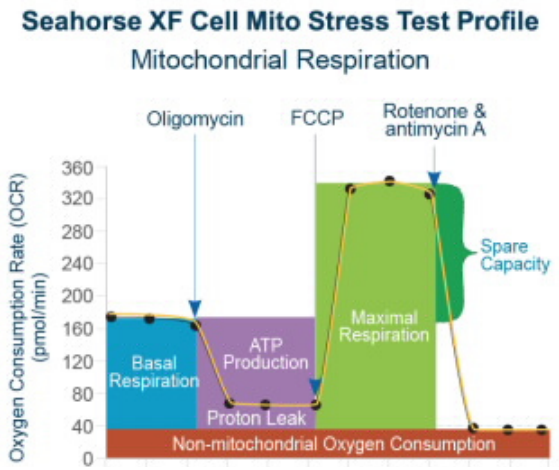

Figure 1.3 OCR-associated parameters measured in bioenergetic studies. *From agilent.com*

promotes a decrease in OCR, with the remaining OCR corresponding to the sum of proton leak dependent respiration and non-mitochondrial OCR. Moreover, the difference to the initial OCR corresponds to ATP production-linked respiration. Addition of carbonyl cyanide 4-(trifluoromethoxy)phenylhydrazone (FCCP), by dissipating the transmembrane electrical gradient, often leads to an increase in OCR, with the new value of OCR corresponding to the sum of non-mitochondrial OCR and maximal respiratory capacity (Aguer et al., 2011, Dott et al., 2014). FCCP is an uncoupling agent that transports H^+ through mitochondrial membrane, disrupting the proton gradient. Since mitochondrial transmembrane potential is essential for many mitochondrial functions, in the presence of reducing equivalents (ETC substrates), proton leak and FCCP stimulate the ETC to reestablish the transmembrane potential by pumping protons through complexes I, III and IV. Finally, addition of antimycin A and rotenone leads to full inhibition of ETC, allowing the determination of non-mitochondrial OCR (Aguer et al., 2011, Dott et al., 2014). Non-mitochondrial OCR may be due to other O_2-consuming sources such as the generation of reactive oxygen species (ROS) as described below, or other non-mitochondrial oxidases. All these parameters are shown in Figure 1.3.

Full oxidation of one glucose molecule into CO_2 is the most efficient way to produce ATP from glucose, since, in total, oxidation of one molecule of glucose has the potential to produce 32 ATP molecules. In comparison, the oxidation of glucose to lactate only leads to the production of two molecules of ATP, showing the importance of the mitochondria and the metabolic pathways that occur there (Nelson and Cox, 2013).

During OXPHOS, there is also generation of ROS. Electron transference from complex I to QH_2 and from QH_2 to complex III involve $^{\bullet}Q^-$ radical as intermediate, that can react with O_2 generating superoxide radical ($O_2^{\bullet -}$). This species is highly reactive and can generate hydroxyl radical ($^{\bullet}OH$), which is even more reactive. ROS can trigger serious cellular damage, by reacting with a high variety of biomolecules, such as proteins, nucleic acids or lipids (Nelson and Cox, 2013). One of most important

mechanism by which cells get rid of ROS makes use of superoxide dismutase (SOD), an enzyme that converts two $O_2^{\bullet -}$ molecules into hydrogen peroxide (H_2O_2) and O_2, with usage of two H^+. H_2O_2 is then degraded into H_2O, coupled with GSH oxidation into GSSG, by glutathione peroxidase. H_2O_2 can also be degraded by catalase, an enzyme that decomposes H_2O_2 into H_2O and O_2 (Nelson and Cox, 2013). For that reason, in a situation of mitochondrial dysfunction, a hallmark of several pathologies, there is an increase in cellular oxidative stress (Saada, 2014).

1.2 Cell culture conditions and drug toxicity

Nowadays, many pharmaceutical companies perform rapid and simple assays to predict mitochondrial toxicity in the earlier stages of drug development (Blomme and Will, 2016, Sanuki et al., 2017). Those assays consist generally in *in vitro* studies, since *in vivo* prediction is difficult, especially in rodents, given their high rates of xenobiotic metabolism and their large respiratory capacity (Sanuki et al., 2017). In addition, *in vitro* assays offer a higher throughput, avoiding, at the same time, the ethical questions associated with *in vivo* studies.

Primary cultures of cells, due to the fact of being obtained directly from tissues, are the best models for *in vitro* drug toxicology studies (Marroquin et al., 2007). It is believed that primary cell cultures retain *in vitro* some of their *in vivo* physiological characteristics (Wilson and Walker, 2009). However, there are several barriers that limit the utilization of this type of models, such as cost, difficulty of isolation and short survival time in culture (Marroquin et al., 2007, Wilson and Walker, 2009). Due to these limitations and to the fact that primary cell culture populations are very heterogeneous (Wilson and Walker, 2009), cell lines became the most used models in drug development studies (Marroquin et al., 2007), since they are easier and cheaper to maintain. However, they are not perfect models, since they lose some of their *in vivo* characteristics (Wilson and Walker, 2009).

Most of these cell lines are metabolically adapted to grow in acidic environments without O_2. Therefore, although OXPHOS is the most efficient way to obtain ATP,

these cell lines generate ATP mainly through glycolysis, even under aerobic conditions, in an effect known as the Crabtree effect (Rodriguez-Enriquez et al., 2001, Marroquin et al., 2007). Typically, cells are cultured in media containing 25 mM glucose (Marroquin et al., 2007), a much higher concentration compared to the physiological blood levels in healthy people (around 4 to 6 mM) (DeFronzo, 2004, Nelson and Cox, 2013), in order to allow proliferation at a higher rate. Under these conditions, most of the pyruvate generated is not directed to Krebs cycle. Instead, it is reduced to lactate, decreasing cytosolic pH, with lactate being then excreted by the cells (Leese and Bronk, 1975, Reitzer et al., 1979, Rodriguez-Enriquez et al., 2001). For that reason, one of the most used parameters to measure glycolytic rate is the extracellular acidification rate (ECAR) (Brand and Nicholls, 2011, Mookerjee and Brand, 2015). Cells favor this pyruvate fate because, in abundance of glucose, glycolysis and subsequent lactic fermentation allows to obtain ATP faster compared to other pyruvate-consuming metabolic pathways (Marroquin et al., 2007, Yu et al., 2017).

Given the glycolytic preference of these *in vitro* models, toxicants targeted to mitochondria have little effect, both in growth and in viability of these cells (Marroquin et al., 2007), and this is exacerbated by typically used cell culture methodology, since, in these *in vitro* studies, cells are usually cultured in media with much higher glucose levels compared to the physiological conditions, as mentioned before (Marroquin et al., 2007, Nelson and Cox, 2013). Also, taking into account that *in vivo* prediction of mitochondrial toxicity is sometimes difficult, the risk of a drug with mitochondrial liabilities to proceed to the market is large. In fact, clinical adverse drug reactions are the major cause of drug withdrawal from the market (Thompson et al., 2012), and there are many examples of withdrawn drugs that showed mitochondrial liabilities (Dykens et al., 2008a, Silva et al., 2016a).

So, upgrades to this methodology were developed in order to achieve higher mitochondrial effects after *in vitro* toxicant exposure and to predict and avoid posterior clinical adverse drug reactions associated to mitochondrial loss of function.

1.3 Alternatives to High Glucose Media

Necessity to unmask the effects of mitochondrial toxicants led to development of alternatives to these classical assays, by forcing cells to rely more on their oxidative energy metabolism.

Reitzer *et al.* (1979) presented some interesting results highlighting the importance of glutamine for cellular bioenergetics, showing that, in human cervical cancer derived HeLa cells, in the presence of glucose, oxidation of glutamine provided about 65% of the cell energy, in a process called glutaminolysis (Reitzer et al., 1979). Glutamine is first converted into glutamate by glutaminase (McKeehan, 1982, Moreadith and Lehninger, 1984, Yang et al., 2014). Glutamate is then converted α-ketoglutarate by alanine transaminase (ALT), in a reversible transamination reaction, in which there is transfer of an amine group from glutamate to pyruvate, generating α-ketoglutarate and alanine (Moreadith and Lehninger, 1984, Yang et al., 2014). α-ketoglutarate is an intermediate of the Krebs cycle, so, it is possible to say that glutamine is an anaplerotic substrate for Krebs cycle (Figure 1.4). In the absence of glucose and in the presence of fructose or galactose, Reitzer group showed the percentage of energy obtained from glutamine increased to more than 98%, concluding that glycolysis was dispensable for HeLa cells (Reitzer et al., 1979). There are several mechanisms by which glutamine can be uptaken by cells (Dall'Asta et al., 1990), with several types of transporters involved, such as the solute carrier 38 family of sodium-amino acid co-transporters, which is found in all cell types (Mackenzie and Erickson, 2004, Broer, 2014).

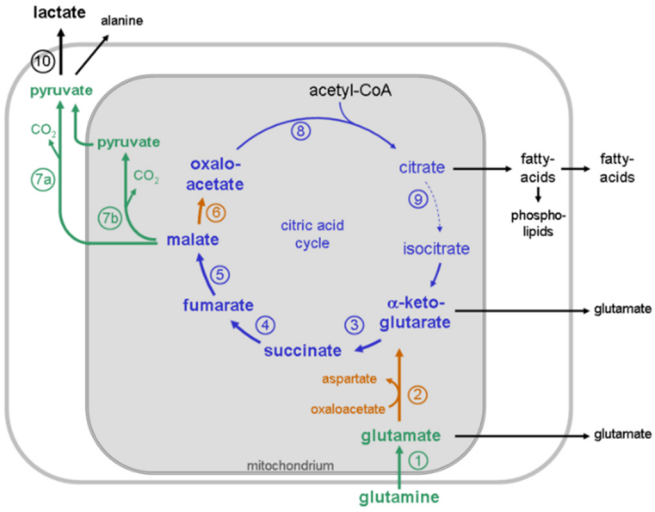

Figure 1.4 Glutamine as a source for Krebs Cycle. *In wikipedia.org*

Besides its role as a metabolic energy generating pathway, Krebs cycle is also important for the biosynthesis of several important biomolecules, such as heme

groups, pyrimidines, purines or some amino acids (Berg et al., 2002).

Alternatively, glutamate can be used instead of glutamine, with the advantage of decreasing ammonia accumulation in culture media (Altamirano et al., 2006).

In order to efficiently oxidize glutamine, cells need to perform OXPHOS (Rossignol et al., 2004), so several authors postulated that by culturing cells in absence of glucose, in media with galactose or fructose, they were stimulating OXPHOS. The presence of a carbohydrate is believed to be important as a carbon source for PPP (Reitzer et al., 1979). A study performed by Davit-Spraul and colleagues, in 1994, showed that the activity of G6PDH was increased in human liver cancer HepG2 cells cultured in 11 mM galactose media, when compared with cells cultured in 11 mM glucose, something that, although does not prove it, supports this postulation (Davit-Spraul et al., 1994).

Fructose can be phosphorylated by fructokinase into fructose-1-phosphate, which is then cleaved by fructose 1-phosphate aldolase into glyceraldehyde and into the glycolytic intermediate dihydroxyacetone phosphate. Then, glyceraldehyde is itself phosphorylated to form another glycolysis intermediate, glyceraldehyde 3-phosphate, by triose kinase, with consumption of another ATP (Figure 1.5). Summing up, conversion of fructose to dihydroxyacetone phosphate and glyceraldehyde 3-phosphate consumes two molecules of ATP, the same as the conversion of glucose into the same products (Berg et al., 2002, Nelson and Cox, 2013). However, fructokinase is not ubiquitous in the organism, being expressed only in the liver, intestine and kidney (Johnson et al., 2013, Fagerberg et al., 2014).

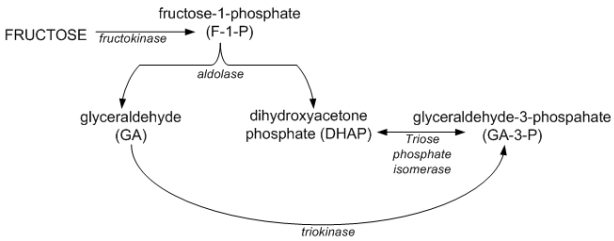

Figure 1.5 Fructose as a source for glycolysis. *In wikipedia.org*

Galactose can also be metabolized through glycolysis, although entering through a different way (Figure 1.6). First, it is phosphorylated by galactokinase (GALK) into galactose-1-phosphate, and this product then reacts with Uridine Diphosphate Glucose (UDP-Glucose), a reaction catalyzed by galactose-1-phosphate

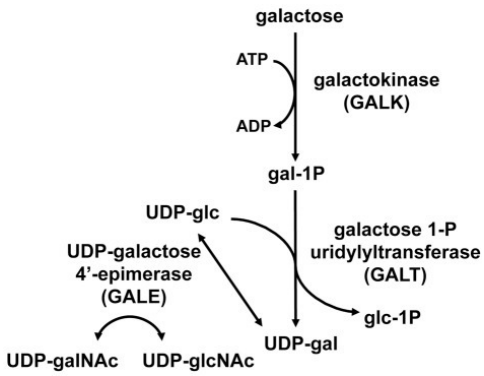

Figure 1.6 Galactose as a substrate for glycolysis. *In Daenzer et al. (2012).*

uridyltransferase (GALT) that originates Uridine Diphosphate Galactose (UDP-Galactose) and Glucose-1-phosphate, with the latter being easily converted into G-6-P by phosphoglucomutase (PGM) (Petry and Reichardt, 1998, Berg et al., 2002, Daenzer et al., 2012, Nelson and Cox, 2013). UDP-Galactose is then transformed into UDP-Glucose by UDP-glucose 4-epimerase (GALE) (Petry and Reichardt, 1998, Daenzer et al., 2012, Nelson and Cox, 2013). Both GALK, GALT and GALE are ubiquitous (Dobbing, 1989, Gibson et al., 1995, Petry and Reichardt, 1998, Fagerberg et al., 2014, Uhlen et al., 2015, Coelho et al., 2017). However, metabolization of galactose to glucose-1-phosphate is very slow, so, when galactose is the only carbohydrate source, cells cannot derive enough ATP from the glycolytic pathway and subsequent lactic fermentation, being forced to perform mitochondrial metabolic pathways to survive (Wagner et al., 1991, Robinson et al., 1992). In addition, some authors defend that oxidation of galactose to pyruvate produces no net ATP (Marroquin et al., 2007, Aguer et al., 2011, Elkalaf et al., 2013, Kase et al., 2013), probably considering UDP-glucose synthesis, that consumes the equivalent to two ATP molecules (Nelson and Cox, 2013), although this is a very controversial premise, due to the UDP-glucose recycling in each cycle. Moreover, several class I Glucose Transport proteins (GLUT), namely GLUT1, GLUT2 and GLUT3, by which there is galactose uptake into cells, have higher affinity for glucose than for galactose, so galactose uptake is slower than normal glucose uptake (Zhao and Keating, 2007, Cura and Carruthers, 2012, Nelson and Cox, 2013). Therefore, galactose is the most commonly chosen carbohydrate for these glutamine-based media, as described below.

In 2003, Ghelli and colleagues focused on Leber's hereditary optic neuropathy (LHON), a maternally inherited disease associated with mitochondrial DNA (mtDNA) point mutations that affect several complex I and III subunits (Brown et al., 1992, Ghelli et al., 2003). Cytoplasmic hybrids (cybrid) cell lines containing one of the most frequent

LHON pathogenic mutations showed lower cell viability when cells were cultured in glucose-free galactose-containing media. This was a first evidence that when galactose replaces glucose as main carbohydrate in culture medium, cells rely on OXPHOS to produce energy, since a mutation that compromises ETC normal flux promoted cell death in these galactose-cultured cells (Ghelli et al., 2003).

Several studies were made using glutamine and galactose media, and the hypothesis that culturing cells in these media forced cells to rely on mitochondrial metabolism was tested. Rossignol *et al.* (2004) cultured HeLa cells in media containing 25 mM glucose, without galactose and glutamine, called High-Glucose media, or in media containing 10 mM Galactose and 4 mM Glutamine, without glucose (OXPHOSm). They observed several interesting results. Firstly, they observed that cell population doubling time was three times lower in cells grown in High-Glucose media when compared with cells grown in OXPHOSm. In addition, they observed several evidences supporting the hypothesis of OXPHOS stimulation. The medium pH was more acidic in cells grown in High-Glucose media, a consequence of higher lactate production in the glycolytic pathway. In addition, complex IV activity, matrix redox state and mitochondrial proteins expression levels were increased in cells grown in OXPHOSm, without any increases in mtDNA content or in mitochondrial mass. Lastly, they observed several structural and internal organizational differences in mitochondria, observing a more interconnected and ramified mitochondrial reticulum and an increase in the number of mitochondrial cristae in OXPHOSm-grown cells. Authors speculated that there was a structural remodeling to adapt to a more oxidative metabolism in OXPHOSm-grown cells (Rossignol et al., 2004). Later, Marroquin *et al.* (2007) cultured HepG2 cells also in High-Glucose media or in OXPHOSm. Then, they measured oxygen consumption and observed that OCR of OXPHOSm-grown cells was significantly increased, supporting the hypothesis mentioned above (Marroquin et al., 2007). Similar results were obtained for rat cardiomyoblasts H9c2 cells (Deus et al., 2015).

These results are concordant with those observed when human primary myocytes

were used, since, when cultured in media with high glucose concentration, these cells were highly glycolytic, but by replacing glucose by galactose as the carbohydrate source, basal mitochondrial OCR and complex IV activity and expression were increased, so, this replacement forced cells to adapt to an energy metabolism more based on OXPHOS (Aguer et al., 2011).

As previously mentioned, in order to induce proliferation, cells are usually cultured in the presence of high glucose concentrations, but, before toxicity assays, cells need to be passaged to OXPHOSm. It is controversial whether this metabolic shift from glycolysis to OXPHOS requires an adaptation period or not. Methodology described by Marroquin *et al.* (2007) involves an adaptation of cells for some passages, in which, over time, the percentage of OXPHOSm components in media increases and the percentage of High-Glucose media components in media decreases. According to the authors, the adaptation period depends on the cell line used, depending if transcriptional events are necessary (Marroquin et al., 2007, Swiss and Will, 2011). However, new approaches have emerged. Sanuki *et al.* (2017) showed that adaptation is not necessary to stimulate OXPHOS in HepG2 cells, since switching cell medium directly from High-Glucose media to a media without glucose turned HepG2 cells immediately more oxidative, increasing their basal OCR and decreasing their ECAR (Sanuki et al., 2017). In this case, culture in OXPHOSm might be interpreted as a metabolic stress, as designated by Palmfeldt *et al.* (Palmfeldt et al., 2009). This adaptation-needless methodology has several inherent advantages, since it allows to spend less money in reagents, while allowing to reduce experiment time and to control the exposure time of the cells to OXPHOSm, standardizing the method (Sanuki et al., 2017).

Another substrate often used in cell culture media is pyruvate. Pyruvate is an α-ketoacid that is produced in glycolysis, as described above, which is reported to be also important as a scavenger of ROS (Wang et al., 2007, Babich et al., 2009, Lee et al., 2014, Wilkins et al., 2014) and as a substrate for Acetyl-CoA synthesis (Berg et al., 2002, Nelson and Cox, 2013). Pyruvate is, therefore, in theory, particularly necessary in

culture media without glucose, in which cells will have lower glycolytic rates, producing less pyruvate. However, usage of pyruvate in culture medium remains somewhat controversial, since, in media with carbohydrates, cells will produce pyruvate through glycolysis, and pyruvate supplementation can even inhibit the pathway.

In the same study quoted above, Davit-Spraul *et al.* (1994) also showed that the cell growth rate was higher in cells cultured in glucose media, when compared with cells cultured in galactose media, and that the presence of inosine nucleoside (a ribose donor for PPP) in culture media decreased the difference in growth rates (Davit-Spraul et al., 1994). In addition, cells depleted of mtDNA, called Rho zero (ρ0) cells, were found to be auxotrophic for uridine, another nucleoside, whose synthesis depends on mitochondrial correct function (Wilkins et al., 2014). It is also possible to theorize that uridine can perform a similar role to inosine as ribose donor. Further studies are necessary to understand if uridine can also be useful for the cells in culture as a component of OXPHOSm.

However, not all cell lines are capable of increasing their metabolism when cultured with galactose. Elkalaf *et al.* (2013) showed that, on murine myoblast line C2C12 cultured in OXPHOSm, there were no significant differences in basal or in ATP-linked OCR, suggesting that absence of glucose does not increase oxidative metabolism in these cells. Interestingly, they showed that a concentration of glucose in the culture medium similar to the physiological concentration is optimal to increase mitochondrial respiration in this cell line (Elkalaf et al., 2013). However, all culture media used this study were supplemented with glutamine, which is a possible limitation of the work (Elkalaf et al., 2013).

In conclusion, it is possible to turn some cell lines more dependent on mitochondrial metabolic pathways by growing them in OXPHOSm (Gohil et al., 2010). The effect of this methodology on cell growth rate and, therefore, in experiment duration, depends on the cell line used. Further work is required to optimize the culture conditions and to test the necessity of an adaptation protocol to maximize

mitochondrial usage by cells.

1.4 Effect of glucose absence in the susceptibility of cells to mitochondrial drugs

Given that absence of glucose in culture media forced cells to rely on mitochondria to obtain energy, several authors studied this effect in susceptibility of cells to mitochondrial toxicants, as shown in the flow chart of Figure 1.7. Just comparing drugs half maximal inhibitory concentration (IC50) on cell viability, it is possible to get some conclusions. If no differences in IC50 of a compound in cells cultured in High-Glucose media or OXPHOSm are seen, that compound does not impair neither glycolysis nor OXPHOS or, alternatively, it affects both pathways. If the IC50 of a compound is higher when cells are cultured in High-Glucose media, that compound affects mitochondrial function. If the opposite is seen, that compound predominantly affects glycolysis (Marroquin et al., 2007, Swiss and Will, 2011).

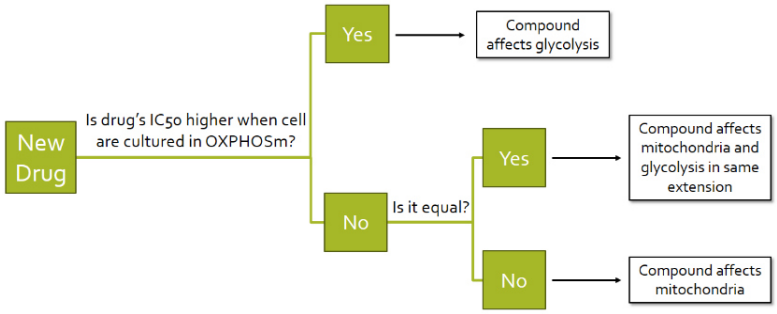

Figure 1.7 Flow chart for determination of a drug toxicity target based on its IC_{50} when cells are cultured in HGm or OXPHOSm.

The classically used mitochondrial toxicants, namely, rotenone, antimycin A, oligomycin and FCCP are among the commonly tested drugs. In HepG2 cells cultured in OXPHOSm, the effect of these compounds was significantly higher when compared to the effect of the same compounds in cells cultured in High-Glucose media (Marroquin et al., 2007, Swiss and Will, 2011). Similar results were obtained for antimycin A and oligomycin in K562 (human immortalized myelogenous leukemia cell line) (Swiss et al., 2013) and for rotenone in several strains of mouse embryonic fibroblasts (MEF) (Pereira et al., 2012). Also, using Sanuki's protocol, that is, the protocol without an adaptation period, similar results were obtained for oligomycin and rotenone (Sanuki et al., 2017).

Among mitochondria-disrupting drugs, one example are biguanidines, which are

guanine analogs that were identified in *Galega officinalis*. Several biguanidines were studied and developed for diabetes treatment, since they improve insulin sensitivity, such as phenformin, buformin and metformin. However, they are associated to lactic acidosis risk, considered a hallmark of mitochondrial impairment, which was related to the withdrawal of the first two drugs from the market (Dykens et al., 2008a), making this a good example in which this methodology would have been useful during the initial drug development phases. Troglitazone, another antidiabetic drug that decreases insulin resistance (Nolan et al., 1994), was also withdrawn from the market and was later shown to cause mitochondrial dysfunction (Masubuchi et al., 2006). Interestingly, HepG2 cells cultured in OXPHOSm also showed increased susceptibility for these compounds when compared to cells cultured in glucose (Luo et al., 2012), indicating that the toxicity of these drugs could have been predicted and their off-target effects could have been prevented.

Summing up, cells cultured in OXPHOSm show increased susceptibility when exposed to drugs whose toxicity is associated with mitochondria, when comparing with cells cultured in media containing the traditional high glucose concentrations. As mentioned before, it is also possible to make the inverse reasoning. As an example, in 2008, Will and colleagues studied the effects of several tyrosine kinase inhibitors, namely, imatinib, dasatinib, sunitinib and sorafenib, in H9c2 grown either in High-Glucose media or OXPHOSm. The objective was to test if these drugs promoted mitochondrial dysfunction. Indeed, sorafenib toxicity mechanism involved mitochondrial dysfunction, since cell susceptibility to sorafenib was higher in H9c2 cells cultured in OXPHOSm (Will et al., 2008).

Several other studies were performed using this methodology with the objective of testing or unmasking mitochondrial toxicity of drugs. Among many examples are studies using the antidepressant and complex I and IV inhibitor nefazodone (Marroquin et al., 2007, Dykens et al., 2008b, Luo et al., 2012, Pereira et al., 2012, Hynes et al., 2013, Swiss et al., 2013, Kamalian et al., 2015, Silva et al., 2016a), the antidepressant trazodone (Dykens et al., 2008b, Swiss et al., 2013), the anxiolytic and

antidepressant and complex I inhibitor buspirone (Dykens et al., 2008b, Luo et al., 2012, Swiss et al., 2013, Kamalian et al., 2015), the anticancer agent and complex I inhibitor flutamide (Marroquin et al., 2007, Rana et al., 2011, Luo et al., 2012, Pereira et al., 2012, Hynes et al., 2013, Swiss et al., 2013), the antilipidemic agent and complex I inhibitor fenofibrate (Brunmair et al., 2004, Marroquin et al., 2007, Swiss et al., 2013), the L-type Ca^{2+} channel antagonist nimodipine (Marroquin et al., 2007, Luo et al., 2012), the androgen receptor antagonist bicalutamide (Marroquin et al., 2007, Luo et al., 2012, Hynes et al., 2013, Swiss et al., 2013) and the antipsychotic and complex I inhibitor risperidone (Marroquin et al., 2007, Rana et al., 2011, Luo et al., 2012, Hynes et al., 2013).

1.5 Screening the effect of antioxidants

Natural aging (Bogdan Allemann and Baumann, 2008, Lapointe and Hekimi, 2010) and many pathologies, such as Alzheimer disease, Parkinson disease or amyotrophic lateral sclerosis, are associated with mitochondrial dysfunction and oxidative stress (Lin and Beal, 2006, Benfeito et al., 2013, Teixeira et al., 2013, Teixeira et al., 2017a).

Antioxidants are molecules that protect cells from oxidative stress and transition metals, through several mechanisms, which include chelation (of transition metals), reduction (acting as scavengers), among others (Benfeito et al., 2013). Cells have several endogenous antioxidant defenses, such as the already mentioned enzyme SOD, the glutathione system, catalase (Nelson and Cox, 2013), and also vitamin E, which contains a phenolic group that neutralizes free radicals by donating a proton, vitamin C, Q10, among others (Bogdan Allemann and Baumann, 2008, Teixeira et al., 2013). However, sometimes these defenses are inefficient against the high ROS levels, and exogenous antioxidant power is required, which is obtainable through the diet or through pharmacological sources, to protect cells from oxidative stress, preventing some ROS-associated pathologies (Benfeito et al., 2013, Teixeira et al., 2013, Teixeira et al., 2017a, Teixeira et al., 2018a).

Most traditional antioxidants, such as gallic acid or hydroxycinnamic acids, are

not very efficient, given their low bioavailability due to their hydrophilic properties (Teixeira et al., 2017a, Teixeira et al., 2018b). This problem is exacerbated by the difficulty of antioxidants reaching the relevant cellular locations, namely, mitochondria (Teixeira et al., 2017a), given that mitochondria play a vital role in ROS production (Teixeira et al., 2017b). Bearing this in mind, novel molecules, derived from the natural antioxidants, were developed to increase their accumulation in mitochondria, with the linkage of triphenylphosphonium (TPP) lipophilic cation being one of the most common approaches (Teixeira et al., 2012, Teixeira et al., 2017a, Teixeira et al., 2017b, Oliveira et al., 2018, Teixeira et al., 2018a, Teixeira et al., 2018b).

Mitochondria-targeted antioxidants, based on cinnamic acid and gallic acid can be a source of exogenous antioxidant power (Teixeira et al., 2012, Teixeira et al., 2017b), being accumulated up to five thousand times more than traditionally used antioxidants, according to the developers, being more effective against mitochondrial oxidation and rupture (Teixeira et al., 2018b). These antioxidants are being developed to counterattack different pathologies associated to mitochondrial dysfunction.

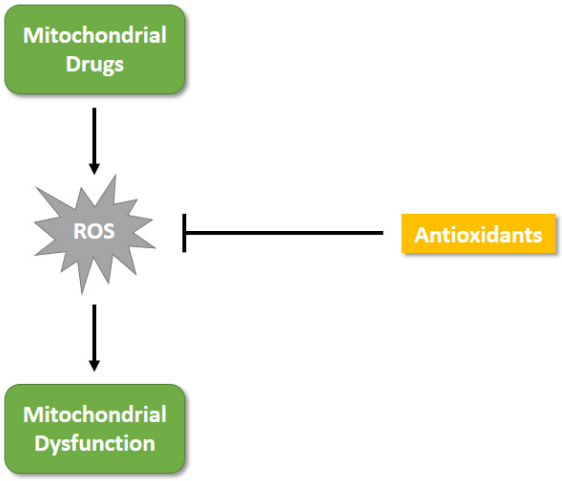

Figure 1.8 Hypothesis for the beneficial effect of antioxidants against mitochondrial dysfunction.

However, the development of new molecules with this objective requires an optimized efficient method to assess mitochondrial health in the presence of stressors (for example, mitochondrial drugs or oxidative stress inducers) and protectant

candidates, which is something that was not previously described. This new class of antioxidants is undergoing pre-clinical testing by the CNC and University of Porto spin-off *MitoTAG*.

1.6 Fibroblasts as an *in vitro* cell model

Fibroblasts are the most common cells in connective tissue, being present, among other body locations, in the dermis of the skin. Their major function is to synthetize extracellular matrix (ECM) proteins, such as collagen and elastin, but they also play a crucial role in wound healing (Grinnell, 1994, Chen et al., 2009, Driskell and Watt, 2015).

Naturally, as any other cell type, fibroblasts are also subjected to the ageing process. In the skin, the exposure to ultraviolet (UV) radiation increases ROS levels, with concomitant activation of several signaling pathways that, among other consequences, induce inflammatory mechanisms and upregulate matrix metalloproteinases (MMP), which degrade ECM (Rittie and Fisher, 2002, Rijken et al., 2004). Besides MMP upregulation and inflammation, ROS are also associated with mitochondrial aging (Bogdan Allemann and Baumann, 2008), inducing mutations in mtDNA, leading to synthesis of dysfunctional OXPHOS complexes, which, in turn, will produce even more ROS, in a vicious cycle known as the Mitochondrial Free Radical Theory of Aging (Sanz and Stefanatos, 2008). This theory is not fully accurate, since oxidative stress is not the only cause of aging, but it helps to explain mitochondrial aging (Lapointe and Hekimi, 2010). This makes fibroblasts a very good cell model for cosmetic studies, since, for example, anti-aging drugs can have fibroblasts as target and, therefore, mitochondrial toxicological studies should be previously made to predict drug toxicity. At the same time, testing antioxidant effects on fibroblasts is a way to understand their true effectiveness as anti-aging molecules.

Fibroblasts are also a good model for personalized medicine, to predict toxicity of drugs directed for an individual patient (Saada, 2014), or to treat neurodegenerative disorders in which there is a lot of variability between patients (Saada, 2014, Wang et

al., 2017), since they are easy to obtain from patients by a simple skin biopsy (Villegas and McPhaul, 2005). Their utility was already demonstrated in studies focused on diseases such as Parkinson or Alzheimer diseases (Auburger et al., 2012, Ambrosi et al., 2014, Hu et al., 2015, Wang et al., 2017, Pereira et al., 2018).

Since cosmetics and human health are two of the main target markets of mitochondria-targeted compounds, fibroblasts are the perfect model for our studies, being, therefore, an obvious candidate for the optimization of screening methodology.

There are several commercial human fibroblast cell lines available, such as Normal Human Dermal Fibroblast (NHDF) or BJ human foreskin fibroblasts. The first was the cell line used in this work. The latter was previously successfully adapted to OXPHOSm in our group (Pereira et al., 2018).

1.7 Objectives

The necessity to unmask *in vitro* toxicity of mitochondrial drugs led to the development of several alternative methodologies, involving different culture media compositions to increase OXPHOS reliance in cells. These methodologies have been very successful, being increasingly used by pharmaceutical companies and research groups.

However, the method is not standardized, so, there is a lot of variability in the protocols used across the scientific community. One of the main inconsistencies is the culture media composition, which compromises comparisons between different works found in the literature.

One of our main objectives is the standardization of the method for NHDF cell line, either in terms of the composition of culture media or in terms of the experimental protocol itself. It is essential to clarify the necessity of galactose and pyruvate in culture media and to understand whether Sanuki's rapid protocol (Sanuki et al., 2017), which was validated for HepG2 cells, can be also useful for NHDF cells. The final outcome of our method optimization, hopefully, can be extrapolated or slightly adapted for other cell lines, reducing the variability in the upcoming studies. Characterization of the

method, particularly by measuring several cellular parameters that might suffer alterations associated to the adoption of a more oxidative phenotype by the cells, is another objective of this work, in order to explain the differences in the metabolism of the cells cultured in different conditions.

After being optimized and characterized, this method will be useful for high-throughput applications to assess mitochondrial health in different physiological and pathological contexts, allowing not only much faster and simpler *in vitro* unmasking of mitochondrial drug toxicity but also *in vitro* prediction of the effectiveness of antioxidants as a therapeutic approach for ROS-associated mitochondrial dysfunction.

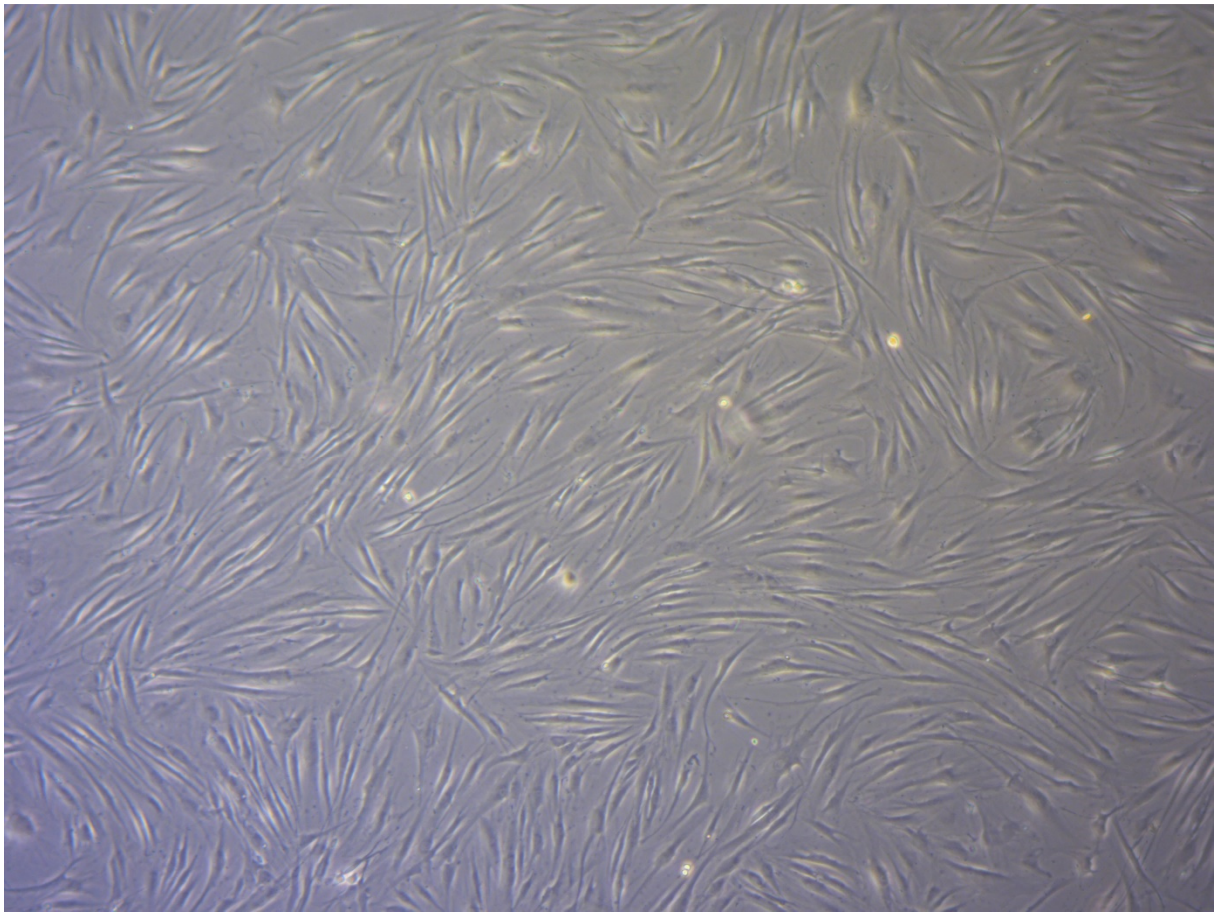

Figure 1.9 NHDF cells. Photo obtained using Zeiss Primovert microscope with an Axiocam ERc 5s camera and using ZEN 2.3 software and with a 4x ampliation.

Chapter II
Material and Methods

2.1 Reagents and Materials List

Table 2.1 Reagents list.

Reagent	Brand + Reference	Headquarters
3,3'-Diaminobenzidine (DAB) Tetrahydrochloride hydrate	Acros Organics 112090050	Waltham, Massachusetts, USA (Thermo Fisher Scientific)
40% Acrylamide/Bis Solution	Bio-Rad 161-0148	Hercules, California, USA
Absolute Ethanol	Fisher BP2818-500	Waltham, Massachusetts, USA (Thermo Fisher Scientific)
Adenosine 5'-diphosphate monopotassium salt dihydrate	Sigma-Aldrich A5285	St. Louis, Missouri, USA
Adenosine 5'-monophosphate sodium salt	Sigma-Aldrich A1752	St. Louis, Missouri, USA
Adenosine 5'-triphosphate disodium salt	Sigma-Aldrich A2383	St. Louis, Missouri, USA
Amersham™ ECL Select™ Western Blotting Detection Reagent	GE Healthcare RPN2235	Chicago, Illinois, EUA
Ammonium Persulfate (APS)	Gerbu 1708-0020	Heidelberg, Germany
Antibiotic-Antimycotic (Penicillin/Streptomycin/Amphotericin B)	Gibco 15240-062	Waltham, Massachusetts, USA (Thermo Fisher Scientific)
Antimycin A	Sigma-Aldrich A8674	St. Louis, Missouri, USA
Bio-Rad® Protein Assay Dye Reagent Concentrate	Bio-Rad 500-0006	Hercules, California, USA
Bisbenzimide Hoechst 33342 trihydrochloride	Sigma-Aldrich B2261	St. Louis, Missouri, USA
Blotting-Grade Blocker (nonfat dry milk)	Bio-Rad 170-6404	Hercules, California, USA
Bovine Serum Albumin (BSA)	Sigma-Aldrich A6003	St. Louis, Missouri, USA
Brilliant Blue G250	Sigma-Aldrich 27815	St. Louis, Missouri, USA
Bromophenol Blue sodium	Sigma-Aldrich B5525	St. Louis, Missouri, USA
CellTiter-Glo® Luminescent Cell Viability Assay Kit	Promega G7571	Madison, Wisconsin, USA
Chloroform	Sigma-Aldrich 650498	St. Louis, Missouri, USA
Cinnamic Acid	Sigma-Aldrich 133760	St. Louis, Missouri, USA
Cytochrome c	Sigma-Aldrich 30398	St. Louis, Missouri, USA
D-(+)-Glucose	Sigma-Aldrich G7021	St. Louis, Missouri, USA
D-Galactose	Sigma-Aldrich G5388	St. Louis, Missouri, USA

Digitonin	Calbiochem 300411	Kenilworth, New Jersey, USA
Dimethyl malonate	Sigma-Aldrich 136441	St. Louis, Missouri, USA
Dimethyl sulfoxide (DMSO)	Fisher D/4121/PB17	Waltham, Massachusetts, USA (Thermo Fisher Scientific)
Dithiothreitol (DTT)	Sigma-Aldrich D9779	St. Louis, Missouri, USA
DNase/RNase-free water	Qiagen 1017979	Hilden, Germany
Dulbecco's Modified Eagle's Medium (DMEM)	Sigma-Aldrich D5030	St. Louis, Missouri, USA
FCCP	Santa Cruz SC-203578	Dallas, Texas, USA
Fetal Bovine Serum	Gibco 15270-106	Waltham, Massachusetts, USA (Thermo Fisher Scientific)
Gallic Acid	Sigma-Aldrich G7384	St. Louis, Missouri, USA
Glacial Acetic acid	Sigma-Aldrich A6283	St. Louis, Missouri, USA
Glycerol	Sigma-Aldrich G5516	St. Louis, Missouri, USA
Glycine	Fisher BP381-1	Waltham, Massachusetts, USA (Thermo Fisher Scientific)
Hydrochloric Acid (HCl)	AppliChem 131020.1212	Barcelona, Spain
iScript™ cDNA Synthesis Kit	Bio-Rad 170-8891	Hercules, California, USA
L-Glutamine	Sigma-Aldrich G3126	St. Louis, Missouri, USA
Methanol	Fisher M/4056/17	Waltham, Massachusetts, USA (Thermo Fisher Scientific)
MitoBEN2	Kindly provided by Dr. Fernanda Borges	Porto, Portugal
MitoCIN4	Kindly provided by Dr. Fernanda Borges	Porto, Portugal
N,N,N′,N′-Tetramethylethylenediamine (TEMED)	NzyTech MB03501	Lisbon, Portugal
NativeMark™ Unstained Protein Standard	Invitrogen LC0725	Carlsbad, California, USA
NativePAGE™ Sample Buffer	Invitrogen BN2003	Carlsbad, California, USA
NativePAGE™ 3-12% Bis-Tris Gel	Invitrogen BN1001BOX	Carlsbad, California, USA
NativePAGE™ Cathode Additive	Invitrogen BN2002	Carlsbad, California, USA
NativePAGE™ Running Buffer	Invitrogen BN2001	Carlsbad, California, USA
n-Dodecyl-β-D-maltoside	Sigma-Aldrich D4641	St. Louis, Missouri, USA
NitroTetrazolium Blue chloride	Sigma-Aldrich N6876	St. Louis, Missouri, USA
Oligomycin	Santa Cruz SC-203342	Dallas, Texas, USA
Perchloric acid ($HClO_4$)	Fisher P/1280/PB15	Waltham, Massachusetts, USA (Thermo Fisher Scientific)
Phenylmethylsulfonyl fluoride (PMSF)	Sigma-Aldrich P7626	St. Louis, Missouri, USA

Pierce® Reversible Protein Stain Kit	Thermo Scientific 24585	Waltham, Massachusetts, USA
Pierce™ BCA Protein Assay Kit	Thermo Scientific 23227	Waltham, Massachusetts, USA
Potassium hydroxide (KOH)	Sigma-Aldrich P5958	St. Louis, Missouri, USA
Potassium phosphate monobasic	Sigma-Aldrich P0662	St. Louis, Missouri, USA
Precision Plus Protein™ Standard Dual Color	Bio-Rad 161-0374	Hercules, California, USA
PrimePCR™ RNA Control Kit	Bio-Rad 10025694	Hercules, California, USA
Propan-2-ol (Isopropanol)	Fisher P/7500/17	Waltham, Massachusetts, USA (Thermo Fisher Scientific)
Protease Inhibitor Cocktail	Sigma-Aldrich P8340	St. Louis, Missouri, USA
PureZOL™ RNA Isolation Reagent	Bio-Rad 732-6890	Hercules, California, USA
QIAamp® DNA Mini Kit	Qiagen 51304	Hilden, Germany
Resazurin sodium salt	Sigma-Aldrich R7017	St. Louis, Missouri, USA
Resolving Gel Buffer (1.5 M Tris-HCl)	Bio-Rad 161-0798	Hercules, California, USA
RIPA buffer	Thermo Scientific 89900	Waltham, Massachusetts, USA
RNase-free DNase Set	Qiagen 79254	Hilden, Germany
RNeasy® Mini Kit	Qiagen 74104	Hilden, Germany
Rotenone	Sigma-Aldrich R8875	St. Louis, Missouri, USA
Seahorse XF Calibrant Solution	Agilent 100840-000	Santa Clara, California, USA
Sodium Bicarbonate	Sigma-Aldrich S6014	St. Louis, Missouri, USA
Sodium chloride (NaCl)	Fisher S/3160/60	Waltham, Massachusetts, USA (Thermo Fisher Scientific)
Sodium Dodecyl Sulphate (SDS)	NzyTech MB01501	Lisbon, Portugal
Sodium hydroxide (NaOH)	Sigma-Aldrich S8045	St. Louis, Missouri, USA
Sodium phosphate dibasic	Sigma-Aldrich 255793	St. Louis, Missouri, USA
Sodium Pyruvate	Sigma-Aldrich P2256	St. Louis, Missouri, USA
SsoFast™ EvaGreen® supermix	Bio-Rad 172-5201	Hercules, California, USA
Stacking Gel Buffer (0.5 M Tris-HCl)	Bio-Rad 161-0799	Hercules, California, USA
Sulforhodamine B sodium salt	Sigma-Aldrich S9012	St. Louis, Missouri, USA
tert-Butyl hydroperoxide (tBHP)	Sigma-Aldrich B2633	St. Louis, Missouri, USA
Tetramethylrhodamine (TMRM), Methyl Ester, Perchlorate	Life Technologies T668	Carlsbad, California, USA
Trans-Blot® Turbo™ 5x Transfer Buffer	Bio-Rad 10026938	Hercules, California, USA

Trichloroacetic acid	Fisher 152130010	Waltham, Massachusetts, USA (Thermo Fisher Scientific)
Tris base	NZYTech MB01601	Lisbon, Portugal
Trypan Blue Stain	Gibco 15250-061	Waltham, Massachusetts, USA (Thermo Fisher Scientific)
Trypsin-EDTA	Gibco 25300-062	Waltham, Massachusetts, USA (Thermo Fisher Scientific)
Tween® 20	Fisher BP337-500	Waltham, Massachusetts, USA (Thermo Fisher Scientific)
Uridine	Sigma-Aldrich U3003	St. Louis, Missouri, USA
β-Mercaptoethanol	Sigma-Aldrich M3148	St. Louis, Missouri, USA
β-Nicotinamide adenine dinucleotide, disodium salt, reduced form	Acros Organics 271100010	Waltham, Massachusetts, USA (Thermo Fisher Scientific)

Table 2.2 Materials list.

Material	Brand + Reference	Headquarters
100 mm-diameter tissue culture dishes	VWR International 10062-880	Radnor, Pennsylvania, USA
75 cm2 Tissue Culture Flask	VWR International 10062-860	Radnor, Pennsylvania, USA
Counting Slides, Dual Chamber	Bio-Rad 145-0011	Hercules, California, USA
Hard-Shell® 96-Well PCR Plates	Bio-Rad HSP9601	Hercules, California, USA
Immobilon®-P Transfer Membranes (PVDF membranes)	Merck IPVH00010	Kenilworth, New Jersey, USA
Indicator Paper	Filtres Fioroni 1010F00021	Ingré, France
LiChrospher® 100 RP-18 (5 µm) LiChroCART® 125-4 column	Merck 1.50943.0001	Kenilworth, New Jersey, USA
LiChrospher® 100 RP-18 (5 µm) LiChroCART® 4-4 precolumn	Merck 1.50957.0001	Kenilworth, New Jersey, USA
Microseal® 'B' seals (for PCR)	Bio-Rad MSB1001	Hercules, California, USA
Mini-PROTEAN® Tetra cell	Bio-Rad	Hercules, California, USA
Nunclon™ Delta Surface F96 MicroWell™ Polystyrene White Plates	Thermo Scientific 136101	Waltham, Massachusetts, USA
Polyamide Membrane Filters 0.2 µm pore, 50 mm diameter	Whatman 10 414 014	Dassel, Germany
Polyethersulfone Membrane Filters	Sartorius 15407	Göttingen, Germany
Seahorse XF96 V3 PS Cell Culture Microplates	Agilent 101085-004	Santa Clara, California, USA
Tissue Culture 96-well plate	VWR International 10062-900	Radnor, Pennsylvania, USA
XCell SureLock™ Mini-Cell Electrophoresis System	Invitrogen EI0001	Carlsbad, California, USA
XFe96 sensor cartridges	Agilent 102418-000 B	Santa Clara, California, USA

2.2 Methods

2.2.1 Chapter 3

2.2.1.1 Culture Media Composition

- OXPHOS Medium: Dulbecco's Modified Eagle's Medium (DMEM) D5030, supplemented with 1.8016 g/L (10 mM) D-galactose, 0.976 g/L (6 mM) L-glutamine, 0.11 g/L (1 mM) sodium pyruvate, 3.7 g/L (44 mM) sodium bicarbonate, 100 U/ml penicillin, 100 μg/ml streptomycin, 250 ng/ml antifungal amphotericin B and 10% (v/v) fetal bovine serum (FBS). pH was adjusted to 7.2 using 1 M Sodium Hydroxide (NaOH) and/or 1 M Hydrogen Chloride (HCl).
- Low-Glucose Medium (LGm): Similar to OXPHOSm, but without galactose and supplemented with 0.9 g/L (5 mM) D-glucose.
- High-Glucose Medium (HGm): Similar to LGm, but supplemented with 4.5 g/L (25 mM) D-glucose instead of 0.9 g/L.

2.2.1.2 Cell Culture

The batch of NHDF cells used in this Chapter was available at the laboratory, but the initial number of passages was unknown, and no registry of the conditions under which the cells were previously cultured was available, which is important for the standardization of cell culture procedures. In our hands, NHDF cells were cultured in LGm in 100 mm-diameter tissue culture dishes at 37°C in a humidified atmosphere of 5% CO_2. Cells were always passaged by trypsinization when they reached a confluence of about 90%.

When appropriate, NHDF cells were adapted gradually to OXPHOSm or to HGm. Initially, cells were all routinely maintained in LGm in 100 mm-diameter tissue culture dishes at 37°C in a humidified atmosphere of 5% CO_2. When about 60% confluence was reached, culture media was replaced, without trypsinization, to a mixture of 75% LGm and 25% OXPHOSm, HGm or LGm. When cells reached about 90% confluence, they were passaged by trypsinization to a mixture of 50% LGm and 50% OXPHOSm, HGm or LGm. Later, when about 60% confluence was reached, culture media was

replaced, without trypsinization, to a mixture of 25% LGm and 75% OXPHOSm, HGm or LGm. Finally, when 90% of confluence was achieved, cells were passaged by trypsinization to 100% OXPHOSm, LGm or to HGm. Schematically, this methodology is represented in Figure 2.1.

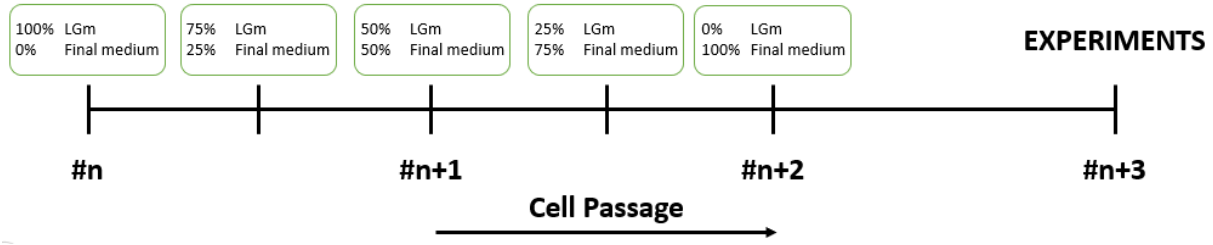

Figure 2.1 Schematic representation of adaptation protocol in two cell passages.

2.2.1.3 Cellular oxygen consumption and extracellular acidification measurements

Cellular oxygen consumption and extracellular acidification rates were measured in real time using a Seahorse XF^{e}96 Extracellular Flux Analyzer (Agilent, Santa Clara, California, United States of America (USA)), at 37°C, by performing XF Cell MitoStress Seahorse™ assays. Before measurements, all XF^{e}96 sensor cartridges were placed in a 96-well calibration plate containing 200 µl/well of Seahorse XF Calibrant Solution and left to hydrate overnight at 37°C.

NHDF cells were plated after trypsinization at cellular densities of 5000, 7500 or 8000 cells/well (as mentioned in Figure descriptions in Chapter 3) in 80 µl culture medium in Agilent Seahorse XF96 V3 PS Cell Culture Microplates. For cell counting, an aliquot of 10 µl of each cellular suspension was diluted in 0.4% (w/v) Trypan blue solution in a 1:1 ratio, and the new suspension was imaged in Bio-Rad® TC20™ Automated Cell Counter (Bio-Rad Laboratories, Hercules, California, USA).

NHDF cells acutely exposed to OXPHOSm (or to LGm) for 1 h were plated in LGm 24 h before the XF Cell MitoStress Seahorse™ assay. One hour before the assay, all wells were washed twice with DMEM D5030. Then, culture media was changed to OXPHOSm or to LGm without FBS, penicillin, streptomycin and sodium bicarbonate, with pH of both media (Seahorse OXPHOSm and Seahorse LGm) adjusted to 7.4, and

the plate was incubated for 1 h at 37°C. Oligomycin, antimycin A, rotenone and FCCP stock solutions were prepared in DMSO. Prior to the MitoStress assay, drug solutions were prepared by diluting stock solutions in Seahorse OXPHOSm or Seahorse LGm. Oligomycin concentrations were 4, 8, 16 and 24 μM, since these solutions were posteriorly diluted 8 times. Analogously, FCCP concentrations were 1.125 and 4.5 μM (diluted posteriorly 9 times) and 1.375 and 5.5 μM (diluted posteriorly 10 times) and the rotenone/antimycin A concentration was 11 μM for each drug (diluted posteriorly 11 times). Twenty five μl of oligomycin solutions were injected into XF^{e}96 sensor cartridge port A, 25 μl of 1.125 or 4.5 μM FCCP solutions were injected into XF^{e}96 sensor cartridge port B, 25 μl of 1.375 or 5.5 μM FCCP solutions were injected into XF^{e}96 sensor cartridge port C, and 25 μl of rotenone/antimycin A solutions were injected into XF^{e}96 sensor cartridge port D. Sensor XF^{e}96 cartridge was loaded with calibration plate into the XF^{e}96 Extracellular Flux Analyzer for calibration. When the calibration was complete, calibration plate was replaced by cell-containing plate and cells were subjected to XF Cell MitoStress Seahorse™ assay. Before drug injection, 3 baseline measurements of NHDF cells OCR and ECAR were obtained, after 3 cycles of 3 min mixing and 3 min continuous measuring. Drugs were then injected automatically, port by port, by the XF^{e}96 Analyzer into each well. Three baseline measurements of OCR and ECAR were obtained after each injection of port content, once again, after 3 cycles of 3 min mixing and 3 min continuous measuring.

NHDF cells that were previously adapted to OXPHOSm or to HGm (or to LGm) were plated in Agilent Seahorse XF96 V3 PS Cell Culture Microplates, with their respective culture medium 24 h before being subjected to XF Cell MitoStress Seahorse™ assay. One hour before the assay, all wells were washed twice with DMEM D5030 and, then, culture media was changed to Seahorse OXPHOSm, Seahorse LGm or to HGm without FBS, penicillin, streptomycin and sodium bicarbonate, with pH of media adjusted to 7.4 (Seahorse HGm), and the plate was incubated for 1 h at 37°C. Sixteen μM oligomycin, 9 μM FCCP and 10 μM antimycin A/rotenone were prepared by diluting the respective stock solutions in Seahorse OXPHOSm, Seahorse LGm or

Seahorse HGm. Twenty five µl of 16 µM oligomycin solutions were injected into XF^{e}96 sensor cartridge port A, 25 µl of 9 µM FCCP solutions were injected into XF^{e}96 sensor cartridge port B and 25 µl of 10 µM rotenone/antimycin A solutions were injected into XF^{e}96 sensor cartridge port C. Port D was left empty. The subsequent procedure was similar to the one described in the previous paragraph.

All data was normalized by cell mass, measured by sulforhodamine B (SRB) assay, as described in Subchapter 2.2.1.4.

2.2.1.4 Cell mass measurements

To normalize all data obtained in XF Cell MitoStress Seahorse™ assays, SRB assays were performed. Right after MitoStress assay, cells were fixed using 60% (w/v) trichloroacetic acid (final % of 10%), being incubated overnight at 4°C. Liquid was then discarded and cells were further incubated with 0.5% (w/v) SRB reagent dissolved in 1% (v/v) acetic acid for 1 h at 37°C. SRB excess was then removed using 1% (v/v) acetic acid. Cell-bound SRB was then extracted and dissolved using 10 mM Tris and absorbance was measured at 510 nm and 620 nm (background measurement), in BioTek® Cytation3™ UV–vis multi-well plate imaging reader (BioTek, Winooski, Vermont, USA). Absorbance is proportional to the amount of SRB in solution, which, in turn, is proportional to the cellular protein content (Lin et al., 1999, Vichai and Kirtikara, 2006).

2.2.1.5 Statistical analysis

All data was analyzed using GraphPad Prism 6.01 software (GraphPad Software, Inc., San Diego, California, USA). Results are expressed as mean ± standard error of the mean (SEM) for the number of experiments indicated in Figure legends. Data normality was tested with D'Agostino & Pearson omnibus normality test. Statistical tests used for each data analysis are indicated also in Figure legends. Values with $p < 0.05$ were considered statistically significant.

2.2.2 Chapter 4

2.2.2.1 Culture Media Composition

- Compositions of OXPHOSm, LGm and HGm were the same as described in Subchapter 2.2.1.1.
- Medium 1: Similar to OXPHOSm, but without pyruvate and galactose supplementation.
- Medium 2: Similar to OXPHOSm, but without pyruvate supplementation.
- Medium 3: Similar to OXPHOSm, but without pyruvate and galactose supplementation and with 0.02442 g/L (100 μM) uridine supplementation.
- Medium 4: Similar to OXPHOSm, but without galactose supplementation.
- Medium 6: Similar to OXPHOSm, but without galactose supplementation and with 0.02442 g/L (100 μM) uridine supplementation.
- Medium 7: Similar to OXPHOSm, but with 0.02442 g/L (100 μM) uridine supplementation.
- Medium 8: Similar to OXPHOSm, but without glutamine supplementation.

2.2.2.2 Cell Culture

NHDF cell line used in Chapter 4 was purchased from Lonza (Basel, Switzerland). NHDF cells were cultured in HGm in 100 mm-diameter tissue culture dishes at 37°C in a humidified atmosphere of 5% CO_2. All cells were passaged by trypsinization when at about 90% confluence.

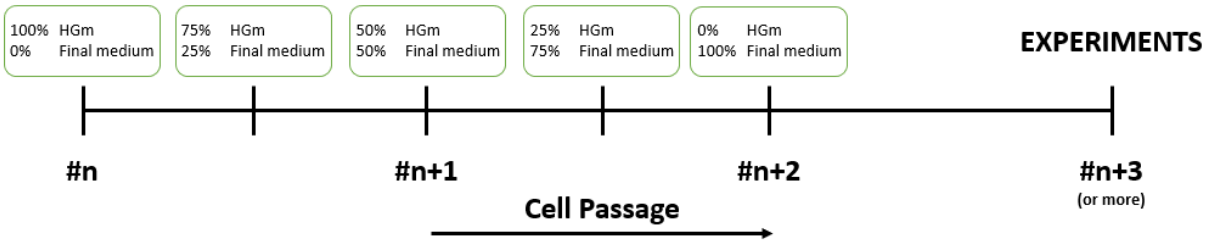

Figure 2.2 Schematic representation of adaptation protocol in two cell passages.

When appropriate, NHDF cells were adapted gradually to LGm or to Media 1 to

8. Two adaptation protocols were used, requiring either one or two cell passages. The adaptation protocol in two cell passages was similar to the one schematized in Figure 2.1, with one difference, which was the initial medium, which was HGm instead of LGm. The procedure is schematized in Figure 2.2.

In the adaptation protocol in one cell passage, cells were also initially cultured in a mixture of HGm and final medium, in a ratio of 75:25, in 100 mm-diameter tissue culture dishes at 37°C in a humidified atmosphere of 5% CO_2. When about 50-60% confluence was reached, culture media was replaced, without trypsinization, to a mixture of HGm and final medium, in a ratio of 50:50. When cells reached about 70-75% of confluence, culture media was replaced, without trypsinization, to a mixture of HGm and final medium, in a ratio of 25:75. Finally, when 90-100% of confluence was achieved, cells were passaged by trypsinization to 100% final medium. Schematically, this methodology is represented in Figure 2.3.

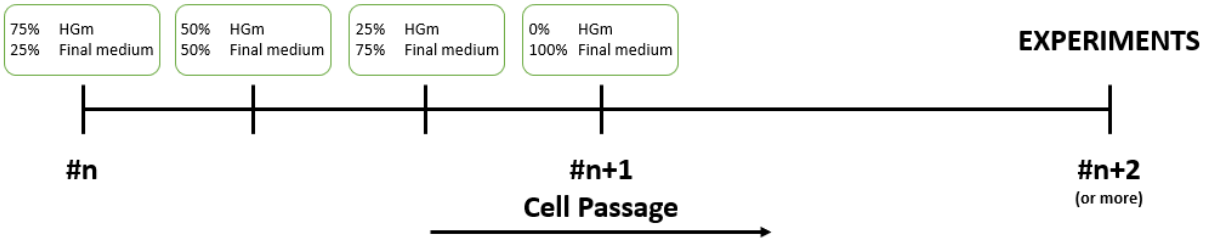

Figure 2.3 Schematic representation of adaptation protocol in one cell passage.

For cell counting, an aliquot of 10 µl of each cellular suspension was diluted in 0.4% (w/v) Trypan blue solution in an 1:1 ratio, and the new suspension was imaged in a Bio-Rad® TC20™ Automated Cell Counter (Bio-Rad Laboratories, Hercules, California, USA).

2.2.2.3 Cellular oxygen consumption and extracellular acidification measurements

Cellular oxygen consumption and extracellular acidification rates were measured using a Seahorse XF^{e}96 Extracellular Flux Analyzer (Agilent, Santa Clara, California, USA), at 37°C, by performing XF Cell MitoStress Seahorse™ assays. Before

measurements, all XF^{e}96 sensor cartridges were placed in a 96-well calibration plate containing 200 µl/well of Seahorse XF Calibrant Solution and left to hydrate overnight at 37°C.

NHDF cells were plated after trypsinization with cellular densities of 7500 or 8000 cells/well (as mentioned in figure descriptions in Chapter 4) in 80 µl of culture medium in Agilent Seahorse XF96 V3 PS Cell Culture Microplates.

NHDF cells acutely exposed to OXPHOSm or to LGm (or to HGm) for 1 h were plated in HGm 24 h before the XF Cell MitoStress Seahorse™ assay. One hour before the assay, all wells were washed twice with DMEM D5030. Then, culture media was changed to Seahorse OXPHOSm, Seahorse LGm or Seahorse HGm and the plate was incubated for 1 h at 37°C. The subsequent procedure was similar to what described in fourth paragraph of Subchapter 2.2.1.3.

NHDF cells that were previously adapted to LGm or to Media 1 to 8 were plated in Agilent Seahorse XF96 V3 PS Cell Culture Microplates, with their respective culture medium 24 h before being subjected to XF Cell MitoStress Seahorse™ assay. One hour before the assay, all wells were washed twice with DMEM D5030 and, then, culture media was changed to Seahorse LGm or to Seahorse HGm or to Seahorse Media 1 to 8 (Media 1 to 8 but without FBS, penicillin, streptomycin and sodium bicarbonate, with pH of adjusted to 7.4) and plate was incubated for 1 h at 37°C. The subsequent procedure was similar to what described in fourth paragraph of Subchapter 2.2.1.3.

All data was normalized by nuclei number. Cells were fixed with to Agilent Seahorse XF96 V3 PS Cell Culture Microplates using 60% (w/v) trichloroacetic acid (10% final concentration), being incubated overnight at 4°C. Liquid was then discarded and cells were incubated with 1 µg/ml Deoxyribonucleic Acid (DNA)-binding fluorescent dye Hoechst 33342 (Latt et al., 1975, Latt and Stetten, 1976) in Phosphate-buffered saline (PBS) 1x for 5 min and fluorescence was imaged in an InCell Analyzer 2200 (GE Healthcare, Chicago, Illinois, USA). Images were acquired for 16 fields per well at 10x magnification (Nikon 10x/0.45, Plan Apo, CFI/60) in combination with one fluorescent detection channels (DAPI). Image analysis, namely nuclei number

counting, was performed using the IN Cell Analyzer 1000 analysis program, Developer Toolbox. Results were analyzed by using the Software Version Wave Desktop 2.2 from Agilent (Agilent, Santa Clara, California, USA).

2.2.2.4 Gene expression measurements

Total cellular Ribonucleic Acid (RNA) was extracted using PureZOL™ RNA Isolation Reagent and chloroform. Cells were washed and 1000 µL of PureZOL™ reagent were added to the dishes where cells were growing. After 5 min of incubation at room temperature, cell suspensions were collected into tubes and 200 µL of chloroform were added. After 3 min of incubation at room temperature, tubes were centrifuged at 12000 g for 18 min, at 4°C. Three phases were generated after centrifugation. The aqueous phase containing the RNA (350 µL) was transferred into RNeasy® Mini Kit columns and the same amount of 100% ethanol was added. RNA was then purified according to RNeasy® Mini Kit Quick-start protocol, provided by QIAGEN® (Qiagen, Hilden, Germany). RNA quantity and purity were assessed using Thermo Scientific® NanoDrop 2000™ spectrophotometer (Thermo Fisher Scientific, Waltham, Massachusetts, USA). After quantification, and RNA was converted into complementary DNA (cDNA) using the iScript™ cDNA Synthesis Kit, using Bio-Rad® CFX96™ Real-Time PCR System (Bio-Rad Laboratories, Hercules, California, USA), and then samples were diluted in DNase/RNase-free water to a final concentration of 10 ng/µl. As a first negative control, one sample was subjected to the same conversion protocol but without the presence of reverse transcriptase enzyme (no-reverse transcriptase – NRT). Gene expression was then measured by quantitative Real Time Polymerase Chain Reaction (qRT-PCR) technique, using Bio-Rad® CFX96™ Real-Time PCR System (Bio-Rad Laboratories, Hercules, California, USA). DNA amplification was performed by using the SsoFast™ EvaGreen® supermix and its associated protocol recommended by the vendor (Bio-Rad), available at *www.bio-rad.com* website. DNA template amount was 12.5 ng per well and primers were at a final concentration of 500 nM each. Primer sequences are shown in Table 2.3. Annealing temperature used was

60°C. Each reaction was performed in duplicate. In addition, for each set of primers, a second negative control experiment (in which DNA sample was replaced by water in the well: no template control – NTC) and experiments with purified sample diluted with different dilution factors (denominated standards), to draw efficiency curves, were performed. Expression was calculated by Bio-Rad® CFX96 Manager software (version 3.1) (Bio-Rad Laboratories, Hercules, California, USA). RNA integrity was assessed using BioRad® PrimePCR™ RNA Control Kit. RNA of one sample was considered intact if |(RQ2 Cq)-(RQ1 Cq)| value (RQ ΔCq) was lower than 3.0. RNA of two samples was considered in a similar degree of integrity if the difference between their RQ ΔCq was lower than 1.0.

Table 2.3 Primer sequence list.

Gene	Designation	forward primer	reverse primer
ACTB	Actin beta	CGCCGCCAGCTCACCATG	CACATGCCGGAGCCGTTG
ATP5G1	ATP synthase, H+ transporting, mitochondrial Fo complex, subunit C1 (subunit 9), transcript variant 2	GGCTAAAGCTGGGAGACTGAAA	GTGGGAAGTTGCTGTAGGAAGG
ATP6	ATP synthase Fo subunit 6	GCGCCACCCTAGCAATATCA	GCTTGGATTAAGGCGACAGC
B2M	Beta-2-microglobulin	GGCTATCCAGCGTACTCCAA	AGTCAACTTCAATGTCGGATGG
COX3	Cytochrome c oxidase subunit 3	CCAATGATGGCGCGATG	CTTTTTGGACAGGTGGTGTGTG
COX4i1	Cytochrome c oxidase subunit IV isoform 1	GAGAAAGTCGAGTTGTATCGCA	GCTTCTGCCACATGATAACGA
CRLS1	Cardiolipin synthase 1, transcript variant 1	CACCCCCAGCCTGTATGAAAA	TTGGCCCAGTTTCGAGCAAT
CYB	Mitochondrial cytochrome b	CCACCCCATCCAACATCTCC	GCGTCTGGTGAGTAGTGCAT
CYCS	Cytochrome c, somatic	CGTTGAAAAGGGAGGCAAGC	TCCCCAGATGATGCCTTTGTTC
DLAT	Dihydrolipoamide S-acetyltransferase	CGCATCAGAAGGTTCCAT	GCCATATAACACTCCTCCAG
DLD	Dihydrolipoamide dehydrogenase, transcript variant 1	AGATGGCATGGTGAAGAT	TCTGATAAGGTCGGATGTG
GABPA	GA binding protein transcription factor, alpha subunit, transcript variant 1	GGAACAGAACAGGAAACAATG	CTCATAGTTCATCGTAGGCTTA
GABPB1	GA binding protein transcription factor, beta subunit 1, transcript variant beta-1	GCCACAGAAGAAGTAGTTAC	ACTGTTAATACTTGTTGTCCAT
GALE	UDP-galactose-4-epimerase, transcript variant 1	GGGCACAGGCTATTCAGT	ACCTTGTACGGGATCTTCTTC
GALK1	Galactokinase 1	TTCAGTGCAGTGGTGGTCAG	CTATTGTGCCCGAGTCTGGA
GALK2	Galactokinase 2, transcript variant 1	GCTTTGCTTAGACACTTGAA	ATGCTCTCCTATTATGTTGACT

GALT	Galactose-1-phosphate uridylyltransferase	CTGAGCGTGATG ATCTAGC	TGCCAATGGTTCC AGTTG
GAPDH	Glyceraldehyde 3-phosphate dehydrogenase	AAGGCTGGGGCT CATTTG	AGG CTGTTGTCATACTT CTCAT
GLS	Glutaminase	CCTGTGGCATGT ATGACTTC	CAGAGAAACAAG ATCGTGACAA
GLS2	Glutaminase 2	TCCACAACTATG ACAACCTGAG	GACCACAGTCTTG TTCCGAAT
HPRT1	Hypoxanthine phosphoribosyltransferase 1	CCCTGGCGTCGT GATTAGTG	CGAGCAAGACGTT CAGTCCT
ND2	NADH dehydrogenase subunit 2	AACCAAACCCA GCTACGCAA	AGCTTGTTTCAGGT GCGAGA
NDUFA9	NADH dehydrogenase (ubiquinone) 1 alpha subcomplex, 9, 39kDa	GCCTATCGATGG GTAGCAAGAG	TGAGTTCCAGTGG TGTTGCC
NRF1	Nuclear respiratory factor 1, transcript variant 1	TTGAGTCTAATC CATCTATCCG	TACTTACGCACCA CATTCTC
PDHA	Pyruvate dehydrogenase E1 alpha 1 subunit, transcript variant 1	TTGCTGCTGCCT ATTGTA	CGTGTACGGTAAC TGACT
PDK1	Pyruvate dehydrogenase kinase 1, transcript variant 1	CCAGGACAGCC AATACAA	CTCGGTCACTCAT CTTCAC
PGC1α	Peroxisome proliferator-activated receptor gamma, coactivator 1 alpha	GCGAAGAGTATT TGTCAACAG	TTGGTTTGGCTTGT AAGTGT
PKM	Pyruvate kinase M1/2, transcript variant 2	TCATCCGCAAGG CATCTG	TCATCAAACCTCC GAACCC
RNA18S	18S ribosomal RNA 5	TTGTCTGGTTAA TTCCGATA	AGACCTGTTATTG CTCAA
SDHA	Succinate dehydrogenase complex, subunit A, flavoprotein (Fp), transcript variant 1	CGGGTCCATCCA TCGCATAAG	TATATGCCTGTAG GGTGGAACTGAA
SLC2A1 (GLUT1)	Solute carrier family 2 member 1	ATCGTGGCTGAA CTCTTC	ACACAGTTGCTCC ACATAC
SOD2	Superoxide dismutase 2, mitochondrial, transcript variant 1	GAAGTTCAATGG TGGTGGTCAT	TTCCAGCAACTCC CCTTTGG
TFAM	Transcription factor A, mitochondrial, transcript variant 1	GTTTCTCCGAAG CATGTG	GGTAAATACACAA AACTGAAGG
UQCRC2	Ubiquinol-cytochrome c reductase core protein II	TTCAGCAATTTA GGAACCACCC	GGTCACACTTAAT TTGCCACCAA
YWHAZ	Tyrosine 3-monooxygenase/tryptophan 5-monooxygenase activation protein, zeta, transcript variant 1	TGTAGGAGCCCG TAGGTCATC	GTGAAGCATTGGG GATCAAGA

2.2.2.5 ATP levels measurements

Cellular ATP levels were measured using CellTiter-Glo® Luminescent Cell Viability Assay Kit, at room temperature and according to vendor's recommendations.

NHDF cells were plated after trypsinization with cellular densities of 7500 cells/well in 150 μl of culture medium in white 96-well plates. Twenty four hours after plating, drugs were added to the cells and 3 h later the culture media was removed, and kit solution was added to the cells. Plates were then subjected to orbital shaking for 2 min and incubated for 10 min in a BioTek® Cytation3™ UV–vis multi-well plate

imaging reader (BioTek, Winooski, Vermont, USA). After that, luminescence was read in the same apparatus.

2.2.2.6 Metabolic activity measurements

To measure metabolic activity in 96-well plates, as an indicator of cell viability, resazurin assay was performed, an assay which measures dehydrogenases activity based on the reduction of resazurin to resorufin (O'Brien et al., 2000).

NHDF cells were plated after trypsinization with cellular densities of 6500 or 7500 cells/well (as mentioned in Figure descriptions in Chapter 4) in 150 μl of culture medium in white 96-well plates.

When appropriate, after 24 h, *tert*-Butyl Hydroperoxide (tBHP) was added to the cells and, 3 h later, 10 μg/ml resazurin was added to the cells. After 1 h of incubation in the dark, at 37°C and with a 5% CO_2 atmosphere, metabolic activity was measured through fluorescence measurements, following the reduction of resazurin to resorufin, using excitation wavelength of 540 nm and emission wavelength of 590 nm, using BioTek® Cytation3™ UV–vis multi-well plate imaging reader (BioTek, Winooski, Vermont, USA) (Silva et al., 2016b).

When appropriate, 24 h after cell seeding, antioxidants were added to the cells, tBHP was added 24 h later and after 3 h, 10 μg/ml resazurin was added to the cells. Subsequent protocol was the same as described at the previous paragraph.

2.2.2.7 Protein levels quantification

Protein levels were measured by Western Blotting. NHDF cells were trypsinized and centrifuged at 250 g for 3 min. Cell pellet was then resuspended in RIPA buffer supplemented with 500 μM phenylmethylsulfonyl fluoride (PMSF), 2.5 μl/ml Protease Inhibitor Cocktail and 1 mM dithiothreitol (DTT). Then, protein solution was sonicated thrice for 10 s, with 30 s-long intervals in-between, using a Branson 5510® sonifier (Branson Sonic Power Company, Danbury, Connecticut, USA). Protein content was determined by bicinchoninic acid (BCA) method, using Pierce™ BCA Protein Assay

Kit and using Bovine Serum Albumin (BSA) solutions as standards (Smith et al., 1985). For OXPHOS complexes protein levels assessments, samples were initially denatured with Laemmli buffer-DTT at 55°C. For Heat Shock Protein 60 (HSP60), SOD2 and β-actin levels assessments, samples were initially denatured with Laemmli buffer-DTT at 95°C. Six μg of protein for each sample was separated by electrophoresis on 12% Sodium Dodecyl Sulfate (SDS)–polyacrylamide gel (SDS–PAGE), at 60 mA, using PowerPac™ Basic Power Supply (Bio-Rad Laboratories, Hercules, California, USA). Proteins were then transferred to a polyvinylidene difluoride (PVDF) membrane at 25 V, for 10 min, using Trans-Blot® Turbo™ Transfer System (Bio-Rad Laboratories, Hercules, California, USA). Total protein was then assessed by protein staining using Pierce® Reversible Protein Stain Kit. Image acquisition was performed using UVP BioSpectrum® 500 MultiSpectral Imaging System (Analytik Jena, Jena, Germany). Membranes were then washed and blocked with 5% milk in TBST (50 mM Tris–HCl, pH 8; 154 mM NaCl and 0.1% Tween 20) overnight at 4°C. Incubation of PVDF membranes with primary antibodies was also performed overnight at 4°C. List of the used primary antibodies is in Table 2.4. Membranes were further incubated with Horseradish Peroxidase (HRP)-conjugated horse anti-mouse Immunoglobulin G (IgG) secondary antibody (Cell Signaling 7076P2) (1:2500 dilution in 1% Milk in TBST) for 90 min at room temperature and incubated with GE Healthcare Amersham™ ECL Select™ Western Blotting detection kit. Image acquisition was performed using UVP BioSpectrum® 500 MultiSpectral Imaging System (Analytik Jena, Jena, Germany). Band densities were calculated with ImageJ 1.51u software.

Table 2.4 Primary antibodies list.

Designation	Reference	Origin	Dilution
Total OXPHOS Human Antibody Cocktail	ab110411	Mouse	1:1000 in 2% Milk in TBST
Anti-Actin Antibody, clone C4	MAB1501	Mouse	1:5000 in 5% Milk in TBST
HSP 60 Antibody	sc-13115	Mouse	1:200 in 1% Milk in TBST
SOD-2 Antibody	sc-130345	Mouse	1:200 in 1% Milk in TBST

2.2.2.8 In-Gel Activity

Complex I and IV activities were measured in-gel. NHDF cells were trypsinized

and centrifuged at 250 g for 3 min. Protein was then extracted from cell pellet using 1% (w/v) dodecyl-β-d-maltoside and 1% (w/v) digitonin. Protein content was then determined by BCA method, using Pierce™ BCA Protein Assay Kit and using BSA solutions as standards (Smith et al., 1985). Ninety five μg of protein of each sample was separated by NativePAGE electrophoresis, at 150 V, using an NativePAGE™ 3-12% Bis-Tris Gel.

For complex I activity determination, gels were incubated, at room temperature, with 2 mM Tris-HCl, 0.1 mg/ml NADH and 2.5 mg/ml NitroTetrazolium Blue (NTB), pH 7.4. Activity was measured by following the appearance of purple bands in the gel, correspondent to the oxidation of NADH by NTB.

For complex IV activity determination, gels were incubated with 0.5 mg/ml diamidobenzidine (DAB), 1 mg/ml cytochrome c and 45 mM phosphate buffer, pH 7.4. Activity was measured by following the appearance of brown bands in the gel, correspondent to the oxidation of cytochrome c by DAB.

Band densities were calculated with ImageJ 1.51u software.

2.2.2.9 mtDNA copy number assessment

Total cellular DNA was extracted and purified using QIAamp® DNA Mini Kit according to Appendix B of QIAamp® DNA Mini and Blood Mini Handbook, available at QIAGEN® website (*www.qiagen.com*). DNA quantity and purity were assessed using Thermo Scientific® NanoDrop 2000™ spectrophotometer (Thermo Fisher Scientific, Waltham, Massachusetts, USA). After quantification, DNA samples were sonicated thrice in 5 s-long pulses, with 5 s-long intervals in-between, using a Branson 5510® sonifier (Branson Sonic Power Company, Danbury, Connecticut, USA), and were diluted in DNase/RNase-free water to a final concentration of 10 ng/μl. mtDNA copy number was then assessed by measuring mitochondrial-encoded CYB gene copy number by qRT-PCR technique, using Bio-Rad® CFX96™ Real-Time PCR System (Bio-Rad Laboratories, Hercules, California, USA). For normalization purposes, copy number of nuclear-encoded ADP-ribosyltransferase polymerase-like 2 (RNAseP)

(Malik et al., 2011) was also measured. DNA amplification was performed similarly to what described in Subchapter 2.2.2.4, with some slight differences. The amount of DNA sample was of 25 ng per well and primer sequences are shown in Table 2.5. Data was analyzed using Bio-Rad® CFX96 Manager software (version 3.1) (Bio-Rad Laboratories, Hercules, California, USA), and mtDNA copy number was defined as the ratio between copy numbers of CYB gene and RNAseP gene.

Table 2.5 Primer sequence list.

Gene	Designation	forward primer	reverse primer
CYB	Mitochondrial cytochrome b	CCACCCCATCCAACATCTCC	GCGTCTGGTGAGTAGTGCAT
RNAseP	ADP-ribosyltransferase polymerase-like 2	CCCCGTTCTCTGGGAACTC	TGTATGAGACCACTCTTTCCCATA

2.2.2.10 Fluorescence microscopy imaging

NHDF cells were plated after trypsinization with cellular densities of 2000 cells/well in 150 µl of culture medium in 96-well plates. Twenty four hours after plating, cells were incubated with 100 nM Tetramethylrhodamine Methyl Ester (TMRM) probe and with 0.5 µg/ml Hoechst 33342 in media without FBS, for 15 min in the dark, at 37°C and with a 5% CO_2 atmosphere.

Mitochondrial network and nuclei number were then assessed using InCell Analyzer 2200 (GE Healthcare, Chicago, Illinois, USA). Images were acquired in 16 fields per well at 10x magnification (Nikon 10x/0.45, Plan Apo, CFI/60) in combination with two fluorescence detection channels (DAPI and CY3). Image processing was performed using ImageJ 1.51u software and image analysis, namely nuclei number counting and mitochondrial network area measurements, was performed using the IN Cell Analyzer 1000 analysis program, Developer Toolbox.

2.2.2.11 Adenine nucleotides levels measurements

Measurement of adenine nucleotide levels was performed by high performance liquid chromatography (HPLC). For nucleotide extraction, culture medium was aspirated from the dishes were cells were cultured and cells were washed with PBS 1x.

Then, 1 ml of ice-cold 0.6 M $HClO_4$ to each dish and content (lysates) was scraped to 2 ml tubes. All the procedure was performed on ice or at 4°C. Lysates were then centrifuged for 10 min at 14000 g, at 4°C. The resulting pellet was re-suspended in 500 µl of 1 M NaOH for posterior protein quantification, while the supernatant was neutralized with 3 M KOH/1.5 M Tris, and centrifuged again for 10 min at 14000 g, at 4°C. Resulting pellet was discarded and supernatant was collected and immediately analyzed by reverse-phase HPLC, using a LiChrospher® 100 RP-18 (5 µm) LiChroCART® 125-4 column. Isocratic elutions were performed with 100 mM phosphate buffer (KH_2PO_4), pH 6.5 and 1.2% (v/v) methanol, with a flow rate of 1 ml/min. Detection was made at 254 nm. The HPLC equipment used was a Waters® Breeze™ system (Waters Corporation, Milford, Massachusetts, USA). The pump was a Waters® 1525 Binary HPLC Pump, the injector was a Rheodyne™ 7725i (Thermo Scientific, Waltham, Massachusetts, USA) and the detector was a Waters® 2487 Dual Wavelength Absorbance Detector. Software used for data analysis was the Waters® Breeze™ HPLC software. To determine the nucleotide concentrations, standard curves of ATP, ADP and AMP were drawn.

Protein quantification was performed using the Bradford method (Bradford, 1976). Bio-Rad® Protein Assay Dye Reagent Concentrate was used and BSA solutions were used as standards. After 15 min of incubation in the dark, at 37°C, protein levels were measured by reading absorbance 595 nm, using BioTek® Cytation3™ UV–vis multi-well plate imaging reader (BioTek, Winooski, Vermont, USA).

2.2.2.12 Statistical analysis

All data was analyzed using GraphPad Prism 6.01 software (GraphPad Software, Inc., San Diego, California, USA).

Results are expressed as mean ± SEM for the number of experiments indicated in figure legends. Data normality was tested with D'Agostino & Pearson omnibus normality test. Statistical tests used for each data analysis are indicated also in figure legends. Values with $p < 0.05$ were considered statistically significant.

For IC50 interpolations, shown in Subchapter 4.4, non-linear regressions were used. For the results associated to cells adapted to OXPHOSm or to LGm, a log(dose) vs. response non-linear regression curve was used. For the results associated to cells adapted to HGm, a third order polynomial regression curve was used. Model equations are available at GraphPad website - *https://www.graphpad.com*.

Chapter III
Pilot Results and Discussion

This chapter describes our first experimental optimizations, which were obtained using NHDF cells that were previously available at the laboratory. The initial stock of these cells had an unknown number of passages and there was no registry of the conditions how the cells were previously cultured. Importantly, the suppliers only guarantee that this cell line retains its characteristics through fifteen population doublings when using recommended culture medium (information available at Lonza® website (accessed at August 16th) - *bioscience.lonza.com*) and, in some procedures, cells may have been used in a higher passage number.

Since our ultimate goal is to standardize cell culture procedures and we cannot have full confidence in the results obtained with these cells, the results described in this chapter are considered preliminary and serve only to show the reasoning that supported the first decisions taken in the work presented in the next chapter, and not to draw any final conclusions.

It is also important to note that, in this chapter, NHDF cells were initially grown in LGm and not in HGm, as described in literature (Marroquin et al., 2007, Sanuki et al., 2017), which is a common practice in our group, to better mimic physiological conditions for toxicological studies.

3.1 Optimization of XF Cell MitoStress Seahorse™ assay conditions.

Before performing the XF Cell MitoStress Seahorse™ assay, it was necessary to optimize assay conditions, both in terms of cell density to use in each well of the plate and in terms of drug concentrations. In this first assay, 4 concentrations of oligomycin (0.5, 1, 2 and 3 μM) were tested to determine the lowest drug concentration in the well at which complex V is inhibited. In addition, 4 concentrations of FCCP (0.125, 0.25, 0.5 and 1 μM) were also tested to determine the lowest drug concentration in the well at which maximal respiration was achieved and two cell densities (5000 and 8000

cells/well) to determine the cell density at which basal respiration was maximized. These conditions were tested in cells cultured in LGm, after acute exposure to Seahorse OXPHOSm or to Seahorse LGm for 1 h.

3.1.1 Selection of cell density.

Given that the objective was to select the cell density, exceptionally, results presented in this subchapter are not normalized.

As shown in Figure 3.1A, basal respiration was significantly higher at 8000 cells/well. Therefore, the lowest cell density was discarded. However, since the number of cells was a limiting factor in the first experiments performed, in most of the experiments, a slightly lower cell density was used.

For all the subsequent results presented in Subchapter 3.1, measurements at the density of 5000 cells/well were not considered.

3.1.2 Selection of drug concentrations.

Rotenone and antimycin A concentrations were defined at 1 μM, considering previous works performed in our laboratory (Deus et al., 2015).

Regarding oligomycin concentration, as shown in Figure 3.1B, only concentrations above 2 μM produced a significant effect on OCR, both in cells acutely exposed and not exposed to OXPHOSm. In addition, the percentage of OCR decrease in cells exposed to 2 μM oligomycin was not significantly different when compared to cells exposed to 3 μM oligomycin, so 2 μM was the selected concentration for the subsequent studies.

Regarding FCCP concentrations, as shown in Figure 3.1C, maximal effect on OCR was achieved when cells were exposed to concentrations above 0.5 μM FCCP in cells not exposed to OXPHOSm and above 1 μM in cells acutely exposed to OXPHOSm. Although there were no significant differences between maximal respiration values after exposure to 0.5 μM and 1 μM FCCP in non-exposed cells, over time, after exposure to 1 μM FCCP, OCR values stabilized near the maximal respiration value, an

effect that was not achieved after exposure to 0.5 μM FCCP (Figure 3.1D). Taking this into account, 1 μM FCCP was the selected concentration for the subsequent studies.

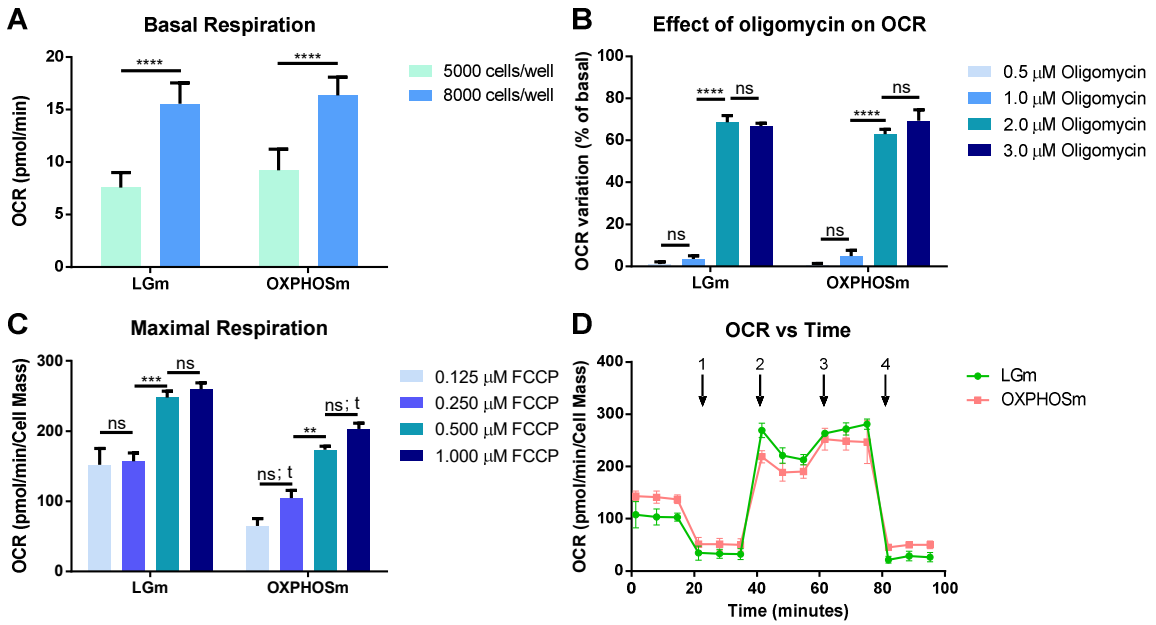

Figure 3.1 Optimization of XF Cell MitoStress Seahorse™ assay conditions. NHDF cells were cultured and plated on passage #12 in LGm, with a density of 5000 or 8000 cells/well. One hour before MitoStress assay, cells were acutely exposed to Seahorse OXPHOSm or to Seahorse LGm. **A** Basal respiration of NHDF cells plated at 5000 or 8000 cells/well and acutely exposed to Seahorse OXPHOSm or to Seahorse LGm. Data are expressed as mean ± SEM of 23–24 replicates. ****: p<0.0001, with p being calculated using two-tailed Mann-Whitney test. **B** Percentage of OCR decrease after addition of 0.5, 1, 2 or 3 μM oligomycin to NHDF cells acutely exposed to Seahorse OXPHOSm or to Seahorse LGm. Data are expressed as mean ± SEM of 5–6 replicates. ****: p<0.0001, ns: p≥0.05, with p being calculated using ordinary two-way ANOVA test with Sidak's multiple comparisons test. **C** Maximal respiration of NHDF cells acutely exposed to Seahorse OXPHOSm or to Seahorse LGm after exposure to 0.125, 0.25, 0.5 or 1 μM FCCP. Data are expressed as mean ± SEM of 3 replicates. ***: p<0.0001, **: p<0.01, ns: p≥0.05, with p being calculated using ordinary two-way ANOVA test with Sidak's multiple comparisons test; t: p<0.05, with p being calculated using one-tailed Mann-Whitney test. **D** OCR of NHDF cells acutely exposed to Seahorse OXPHOSm or to Seahorse LGm over time, with addition of 1 – oligomycin (final concentration: 2 μM) – , 2 and 3 – FCCP (final concentrations: 0.5 and 1 μM, respectively) – and 4 – antimycin A and rotenone (final concentrations: 1 μM for both drugs). Data are expressed as mean ± SEM of 3 replicates.

3.2 Exposure of NHDF cells to OXPHOSm for 1 h was not enough to promote OXPHOS.

Sanuki and colleagues showed that HepG2 cell line did not need a period of adaptation to the absence of glucose to switch from an essentially glycolytic phenotype

to an energy metabolism more based on OXPHOS. According to Sanuki *et al* (2017), cells only needed to be acutely exposed for 1 h to medium without glucose (Sanuki et al., 2017). However, there are no published studies focusing on whether the NHDF cell line also has this metabolic flexibility, which is the main focus of this subchapter.

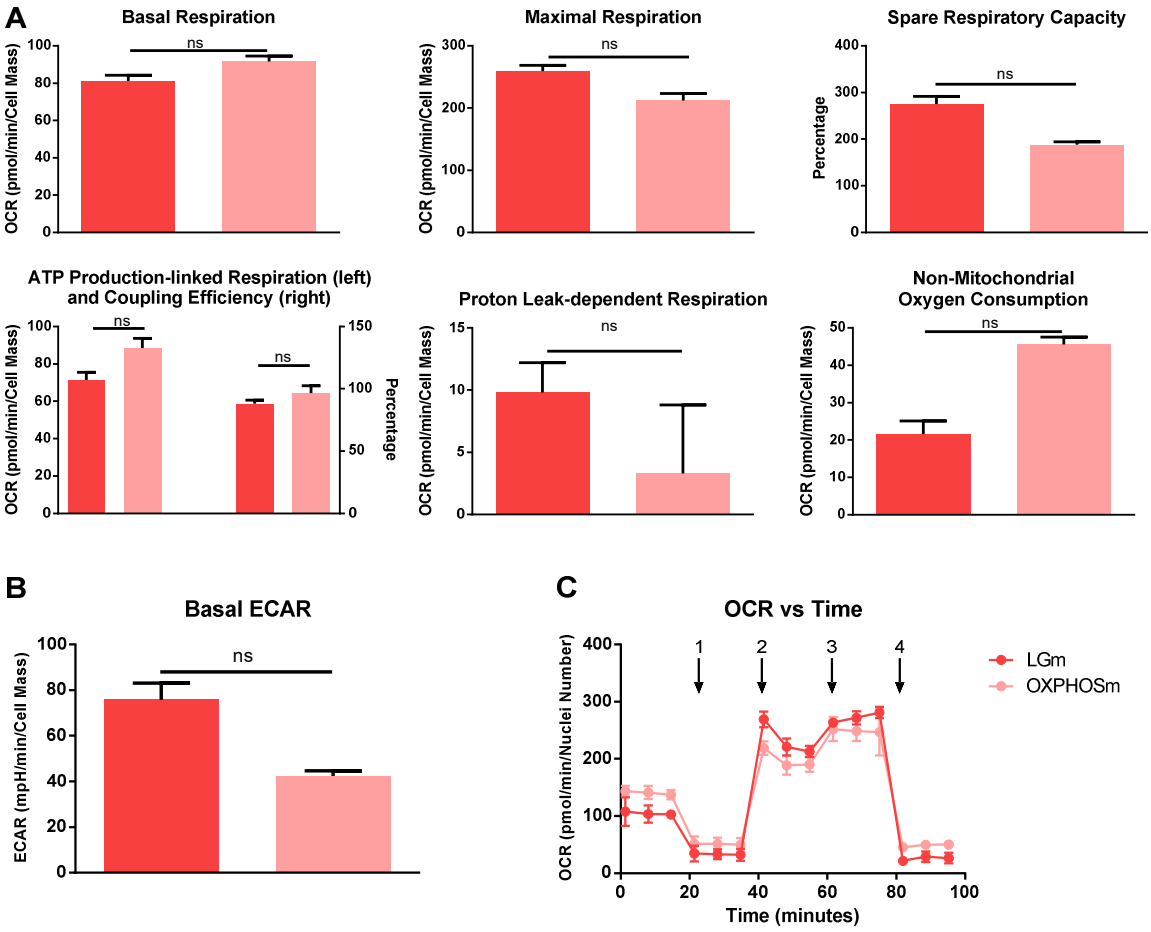

Figure 3.2 OCR-associated parameters and Basal ECAR of NHDF cells acutely exposed to OXPHOSm (pink) or grown in LGm (red). NHDF cells were plated on passage #12 in LGm, with a density of 8000 cells/well and 1h before MitoStress assay, cells were exposed to Seahorse OXPHOSm or to Seahorse LGm. **A** Basal respiration, maximal respiration, % spare respiratory capacity, ATP production-linked respiration and coupling efficiency, proton leak-dependent respiration and non-mitochondrial oxygen consumption. **B** Basal Extracellular Acidification Rate. **C** OCR over time of NHDF cells acutely exposed to OXPHOSm or to LGm, with addition of 1 – 2 μM oligomycin – , 2 – 0.5 μM FCCP – , 3 – 1 μM FCCP – and 4 – 1 μM antimycin A and 1 μM rotenone. Data are expressed as mean ± SEM of 3 replicates. ns: p≥0.05, with p being calculated using two-tailed Mann-Whitney test.

Considering values obtained in the optimization experiment, shown in Subchapter 3.1, it is possible to have clues on whether exposure of NHDF cells to OXPHOSm for

1 h is able to induce OXPHOS. Figure 3.2A represents basal respiration, ATP production-linked respiration, maximal respiration, spare respiration capacity, non-mitochondrial oxygen consumption and proton leak-associated respiration, measured in cells acutely exposed to OXPHOSm and in cells not exposed to this medium. It is possible to see in the figure that there were no significant differences in any of these parameters in cells exposed and in cells not exposed to OXPHOSm, suggesting that 1 h exposure to OXPHOSm was not enough to induce a more oxidative phenotype in NHDF cells. However, it is relevant to note that the *n* is very small. This has relevance considering that it is probable that most of the parameters would become significantly different if *n* was increased. Nevertheless, particularly in Basal Respiration, in ATP Production-linked Respiration and in Maximal Respiration, bigger differences are desirable, since differences observed were small compared to what is found on literature (Pereira et al., 2018). So, other protocols were tested.

3.3 Adaptation of NHDF cells to OXPHOSm promoted OXPHOS.

Given that Sanuki's rapid protocol (Sanuki et al., 2017) was not successful in inducing OXPHOS in NHDF cells, and since, as mentioned, BJ cell line was previously successfully adapted (Pereira et al., 2018), there were reasons to hypothesize that NHDF cells can also be adapted to OXPHOSm.

NHDF cell line, according to supplier recommendations, has a small passage work range. Therefore, traditional adaptation methods are too long because they require too many cell passages. For example, Marroquin *et al.*, before conducting any experiment, maintained cells in OXPHOSm for at least 10 passages (Marroquin et al., 2007). So, prior to subjecting the NHDF cells to these extensive protocols, cells were subjected to a shorter procedure, in which adaptation was made in only two cell passages and in which cells were maintained in OXPHOSm only during one passage before being used for experiments. Schematically, this process is represented in Figure 2.1.

After adaptation to OXPHOSm (and to HGm), NHDF cells were subjected to the XF Cell MitoStress Seahorse™ assay. OCR over time graph obtained in this assay is

represented in Figure 3.3C.

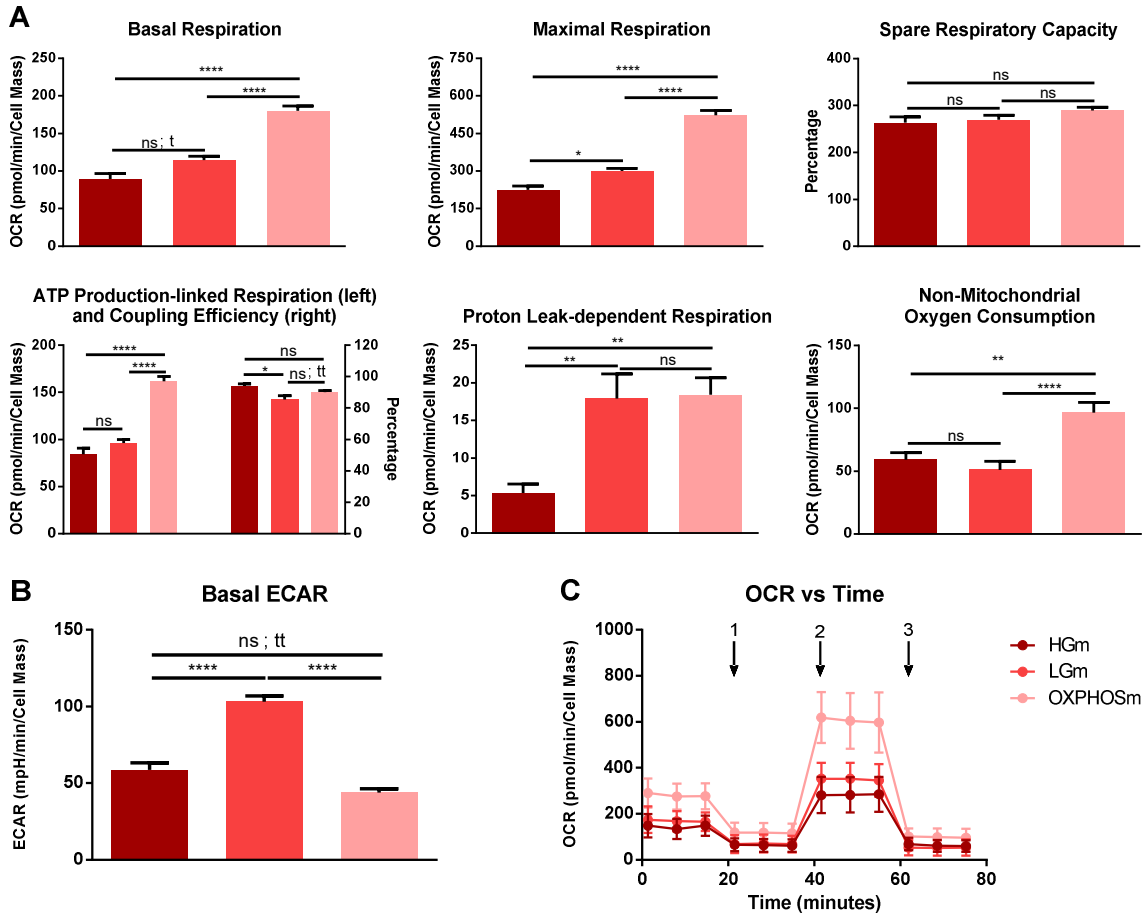

Figure 3.3 OCR-associated parameters and Basal ECAR of NHDF cells grown in LGm (red) and adapted to OXPHOSm (pink) or HGm (dark red). NHDF cells were plated on passage #22, with a density of 8000 cells/well. **A** Basal respiration, maximal respiration, % spare respiratory capacity, ATP production-linked respiration and coupling efficiency, proton leak-dependent respiration and non-mitochondrial oxygen consumption. **B** Basal extracellular acidification rate. **C** OCR of NHDF cells adapted to OXPHOSm, LGm or HGm over time, with addition of 1 – 2 μM oligomycin – , 2 – 1 μM FCCP – and 3 – 1 μM antimycin A and 1 μM rotenone. Data are expressed as mean ± SEM of 20-23 replicates. ****: p<0.0001, **: p<0.01, *: p<0.05, ns: p≥0.05, with p being calculated using Kruskal-Wallis test with Dunn's multiple comparisons test; tt: p<0.01, t: p<0.05, with p being calculated using two-tailed Mann-Whitney test.

As shown in Figure 3.3A, both basal, ATP production-linked, non-mitochondrial, proton leak-dependent and maximal respiration were significantly increased in NHDF cells adapted to OXPHOSm, leading to believe that this short protocol is enough to induce OXPHOS in NHDF cells. Moreover, ECAR was slightly decreased in the same cells, although not significantly, corroborating that thesis, as shown in Figure 3.3B.

In addition, % spare respiratory capacity was similar in LGm cultured cells and in cells adapted to OXPHOSm or to HGm, so all cells seemed to have similar respiratory potential, suggesting that, during this procedure, NHDF cells underwent some molecular changes that might have involved mitochondrial biogenesis or post-translational modifications in proteins.

3.4 Final considerations.

Although it is not possible to have full confidence in the results shown in this chapter, it is also true that these results may help to choose the best method to induce OXPHOS in NHDF cells.

Contrarily to the HepG2 cell line, it looks like that NHDF cell line is not so metabolically flexible that an adaptation period can be dismissed (Figure 3.2). However, these results suggest that the traditional extensive time-consuming methodology can be shortened into an adaptation protocol that takes about a week (Figure 3.3).

As mentioned, data presented in this chapter was considered as a starting point for all the subsequent work.

Chapter IV
Results and Discussion

All the data presented in this chapter was obtained using NHDF cells acquired directly from the supplier after the initial optimizations described in the previous chapter. All the procedures to which cells were subjected are known and registered by the members of MitoXT laboratory group, allowing us to control all the variables that can influence any result obtained with these cells.

In this chapter, unlike in the previous chapter, before being subjected to any procedures, cells were cultured in HGm, instead of LGm. Despite the argument favoring culture in LGm, mentioned in Chapter 3, in a first XF Cell MitoStress Seahorse™ assay, we observed that cells adapted from HGm to LGm not only became more glycolytic but also more oxidative, as shown in Energy Map of Figure 8.1C, in the supplementary data. However, it is important to note that this assay did not work as expected, as illustrated by the odd OCR values obtained. Nonetheless, based on these observations and in the fact that it is the most common procedure found in the literature (Marroquin et al., 2007), we decided to change initial culture medium to HGm. We plan to run another XF Cell MitoStress Seahorse™ assay to confirm the results shown in Figure 8.1C.

4.1 Selection of the protocol to induce OXPHOS in NHDF cell line.

Pilot results suggest that acute exposure of NHDF cells to media without glucose does not produce the desirable increase oxygen consumption as a consequence of increased mitochondrial respiration. Given that assumption and that adaptation in two cells passages was successful (Subchapter 3.3), longer protocols were not considered.

4.1.1 Adaptation of NHDF cells to OXPHOSm in two cell passages promoted OXPHOS.

The first step towards the selection of the protocol for induction of OXPHOS in NHDF cells was the validation of the results obtained in Subchapter 3.3. For this purpose, we tested whether cells adapted with a similar protocol, except the fact of being initially maintained in HGm, also presented a more oxidative metabolic phenotype.

After being adapted to OXPHOSm or to LGm (procedure shown in Figure 2.2), NHDF cells were subjected to the XF Cell MitoStress Seahorse™ assay. Data of OCR over time obtained in this assay is represented in Figure 4.1C and OCR-associated parameters and Basal ECAR are represented in Figures 4.1A and 4.1B, respectively.

OCR-associated parameters including basal, ATP production-linked, non-mitochondrial, proton leak-dependent and maximal respirations, as well as spare respiratory capacity were significantly increased in cells adapted to OXPHOSm, when compared with cells grown in HGm. These differences are indicative that, as expected, the absence of glucose in the culture medium caused a metabolic shift in the NHDF cells, making them more oxidative. Another evidence that supports this conclusion is the fact that, in contrast, basal ECAR was significantly decreased in the same cells, an indication that HGm-grown cells were more glycolytic, as expected. In addition, together, these findings show that this protocol was effective for adapting NHDF cells to grow in media containing 0 mM Glucose.

Interestingly, LGm-adapted cells seemed also more oxidative than HGm-grown cells, although the differences were not as high as those reported in the previous paragraph. In Figure 4.1A and B, it is possible to observe that these cells, grown in conditions closer to physiological conditions, were much less glycolytic, since basal ECAR was significantly decreased in these cells, and at the same time they were more oxidative, since both basal, ATP production-linked and proton leak-dependent respirations were increased, when compared with HGm-grown cells.

Between LGm and OXPHOSm-adapted cells, all the OCR-associated parameters

values, except proton leak-dependent respiration and coupling efficiency, were significantly different. In addition, basal ECAR was slightly, but not significantly, decreased in OXPHOSm-adapted cells.

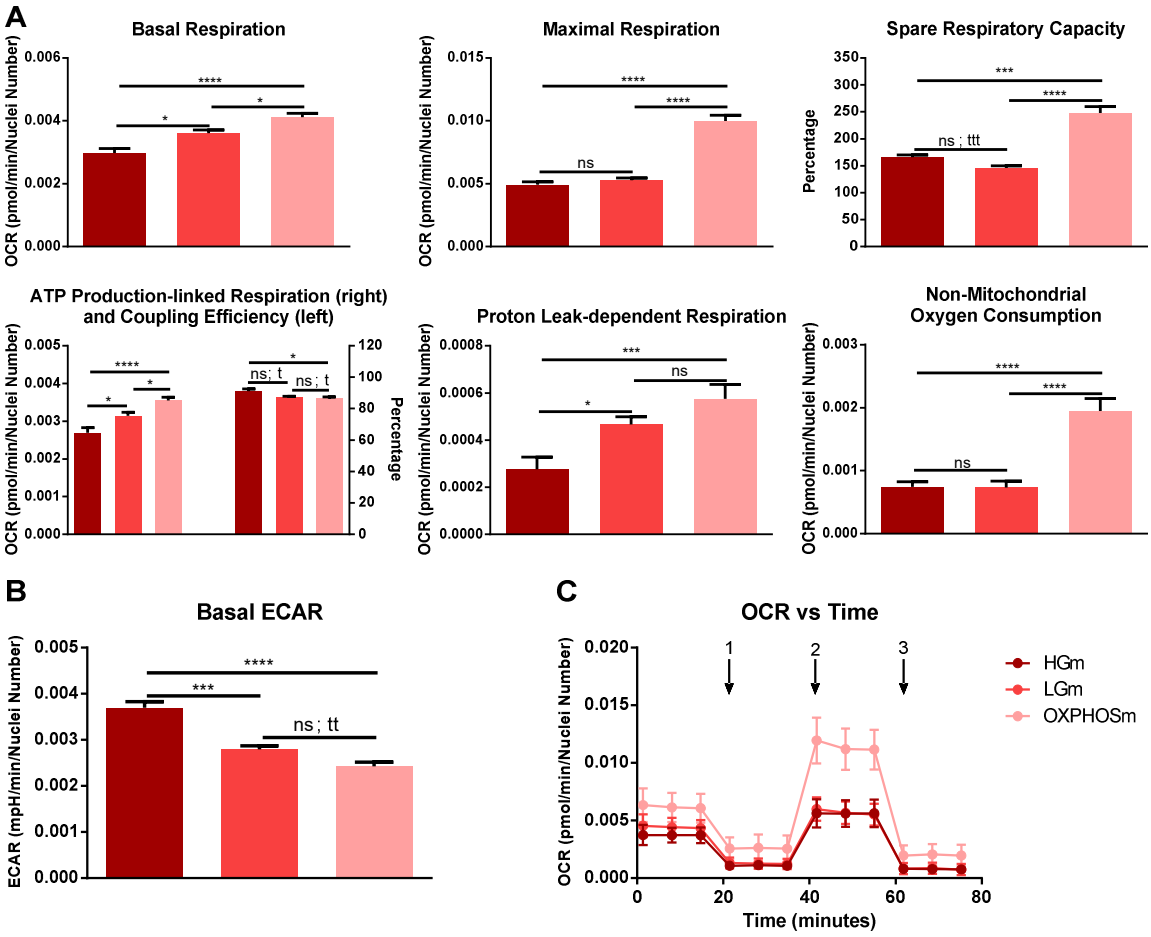

Figure 4.1 OCR-associated parameters and Basal ECAR of NHDF cells grown in HGm (dark red) and adapted to OXPHOSm (pink) or LGm (red). NHDF cells were plated on passage #9, with a density of 8000 cells/well. **A** Basal respiration, maximal respiration, % spare respiratory capacity, ATP production-linked respiration and coupling efficiency, proton leak-dependent respiration and non-mitochondrial oxygen consumption. **B** Basal extracellular acidification rate. **C** OCR of NHDF cells adapted to OXPHOSm, LGm or HGm over time, with addition of 1 – 2 µM oligomycin – , 2 – 1 µM FCCP – and 3 – 1 µM antimycin A and 1 µM rotenone. Data are expressed as mean ± SEM of 3 independent experiments performed 6-8 times. ****: p<0.0001, ***: p<0.001, *: p<0.05, ns: p≥0.05, with p being calculated using Kruskal-Wallis test with Dunn's multiple comparisons test; ttt: p<0.001, tt: p<0.01, t: p<0.05, with p being calculated using two-tailed Mann-Whitney test.

So, metabolically, cells adapted to LGm using this protocol seemed to be in a mid-term between cells grown in excess or in the absence of glucose. This suggests that

LGm cannot replace OXPHOSm as an inducer of OXPHOS for the practical applications of this methodology. This hypothesis will be further explored in the subsequent subchapters.

4.1.2 Adaptation of NHDF cells to OXPHOSm in one cell passage promoted OXPHOS.

The other adaptation protocol tested consisted in the adaptation of the cells in just one cell passage, as shown in Figure 2.3, being that the shortest adaptation protocol possible.

Once again, after being adapted to OXPHOSm or to LGm, NHDF cells were subjected to XF Cell MitoStress Seahorse™ assay. OCR-associated parameters and Basal ECAR are represented in Figures 4.2A and 4.2B, respectively. Data obtained for OCR over time is represented in Figure 4.2C.

Most of OCR-associated parameters, namely basal, non-mitochondrial, ATP production-linked and maximal respirations, were also significantly increased in OXPHOSm-adapted cells when compared with HGm-grown cells. Again, the values of these parameters allow us to conclude that cells adapted to OXPHOSm were more oxidative, as desirable. However, contrarily to what was described in Subchapter 4.1.1, basal ECAR values were not significantly different in this experiment, mainly due to the large SEM values observed, making it impossible to draw major conclusions about the glycolytic activity of cells grown under various conditions.

In this experiment, both OCR-associated parameters and basal ECAR values were similar between LGm-adapted cells and HGm-grown cells, since none of these parameters was significantly different in LGm-adapted cells. Results, therefore, suggest that cellular metabolism of cells grown in both conditions was similar.

Logically, if the differences between these cells were insignificant, the differences between LGm and OXPHOSm-adapted cells were in a similar extent to those observed between HGm-grown and OXPHOSm-adapted cells. So, the mid-term effect described in the previous subchapter was not observed in this situation.

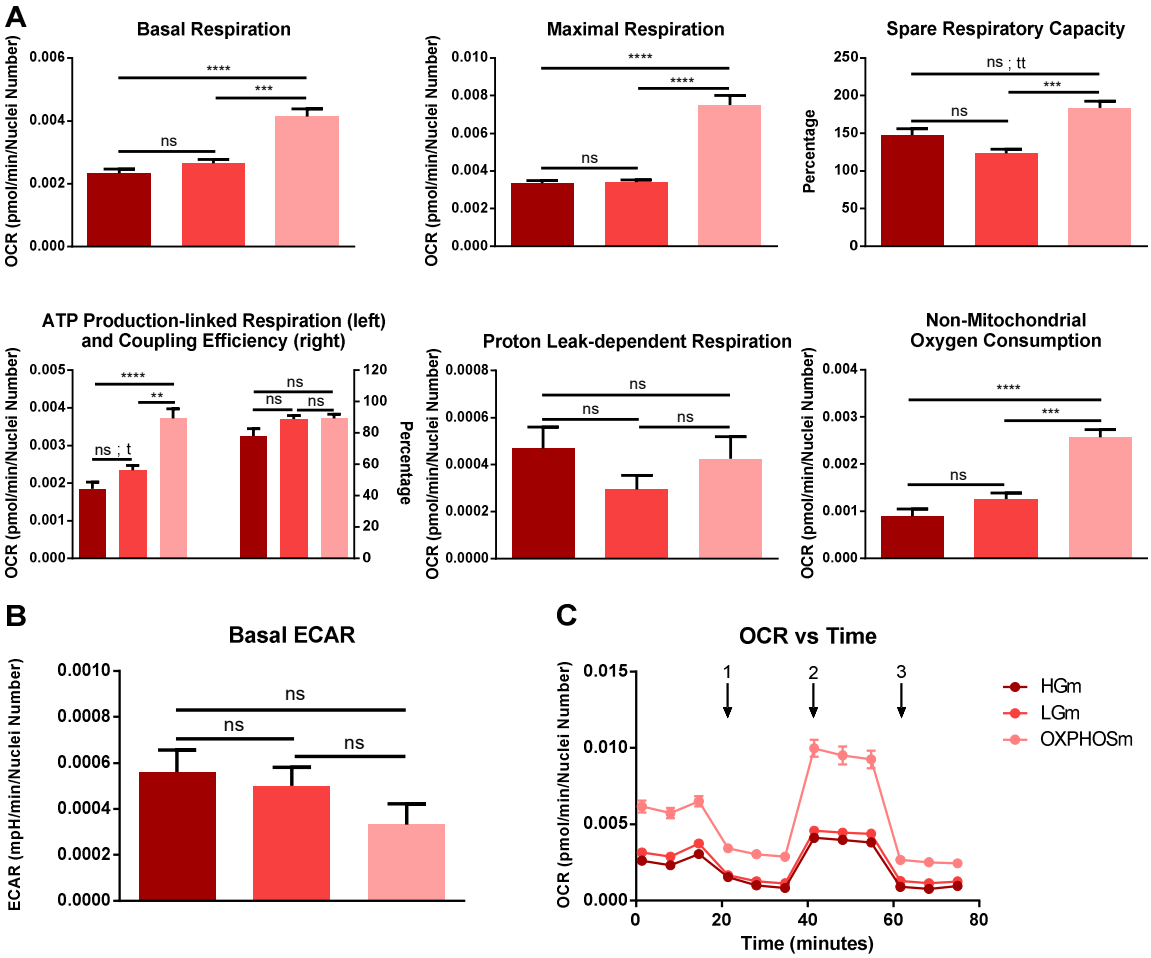

Figure 4.2 OCR-associated parameters and Basal ECAR of NHDF cells grown in HGm (dark red) and adapted to OXPHOSm (pink) or LGm (red). NHDF cells were plated on passage #10, with a density of 7500 cells/well. **A** Basal respiration, maximal respiration, % spare respiratory capacity, ATP production-linked respiration and coupling efficiency, proton leak-dependent respiration and non-mitochondrial oxygen consumption. **B** Basal extracellular acidification rate. **C** OCR of NHDF cells adapted to OXPHOSm, LGm or HGm over time, with addition of 1 – 2 μM oligomycin – , 2 – 1 μM FCCP – and 3 – 1 μM antimycin A and 1 μM rotenone. Data are expressed as mean ± SEM of 3 independent experiments performed 4-6 times. ****: p<0.0001, ***: p<0.001, **: p<0.01, ns: p≥0.05, with p being calculated using Kruskal-Wallis test with Dunn's multiple comparisons test; tt: p<0.01; t: p<0.05, with p being calculated using two-tailed Mann-Whitney test.

4.1.3 Comparison between different adaptation protocols.

Given that both protocols of adaptation in one or two cell passages were successful in the induction of OXPHOS in NHDF cells, it was necessary to choose one of them for the following studies.

Figure 4.3 shows the data obtained for basal respiration and ATP production-linked respiration values in cells adapted to OXPHOSm with both protocols,

normalized by the mean of the same parameters in HG-grown cells. It is possible to observe that the fold change in both parameters was higher in cells adapted to OXPHOSm in one passage.

These results and the fact that this protocol is shorter, constitute two arguments that support our choice by the protocol described in Figure 2.3.

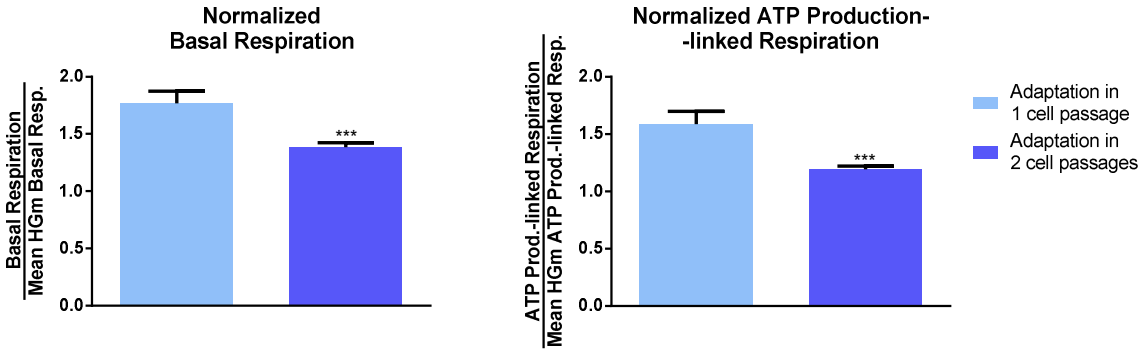

Figure 4.3 Basal and ATP Production-linked Respiration in cells adapted to OXPHOSm in one or in two cell passages, normalized with the mean values of the same parameters obtains in HGm-grown cells. Data are expressed as mean ± SEM of 3 independent experiments performed 5-8 times. ***: $p<0.001$, with p being calculated using two-tailed Mann-Whitney test.

4.1.4 Exposure of NHDF cells to OXPHOSm for 1 h was not enough to promote OXPHOS.

Lastly, it was necessary to validate that exposure for 1 h to OXPHOSm in NHDF cells previously grown in media containing glucose was not enough to induce significant differences in general cellular bioenergetics.

To do this, 1 h before XF Cell MitoStress Seahorse™ assay, part of the HGm-grown NHDF cells seeded for the experiment described in Subchapter 5.1.2, instead of being exposed to Seahorse HGm, were acutely exposed to Seahorse OXPHOSm. The other part of cells grown in HGm and the OXPHOSm-adapted cells were tested for comparison. Data obtained for OCR-associated parameters and basal ECAR values are shown in Figure 4.4.

The first interesting observation was that basal respiration value of OXPHOS-exposed cells was similar to the one observed in HGm-grown cells and significantly

lower than for OXPHOSm-adapted cells. In addition, the ECAR value of OXPHOSm-exposed cells was lower than of that of HGm-grown cells. So, these cells combined the metabolic deficits of both of the other conditions tested, being the most quiescent ones.

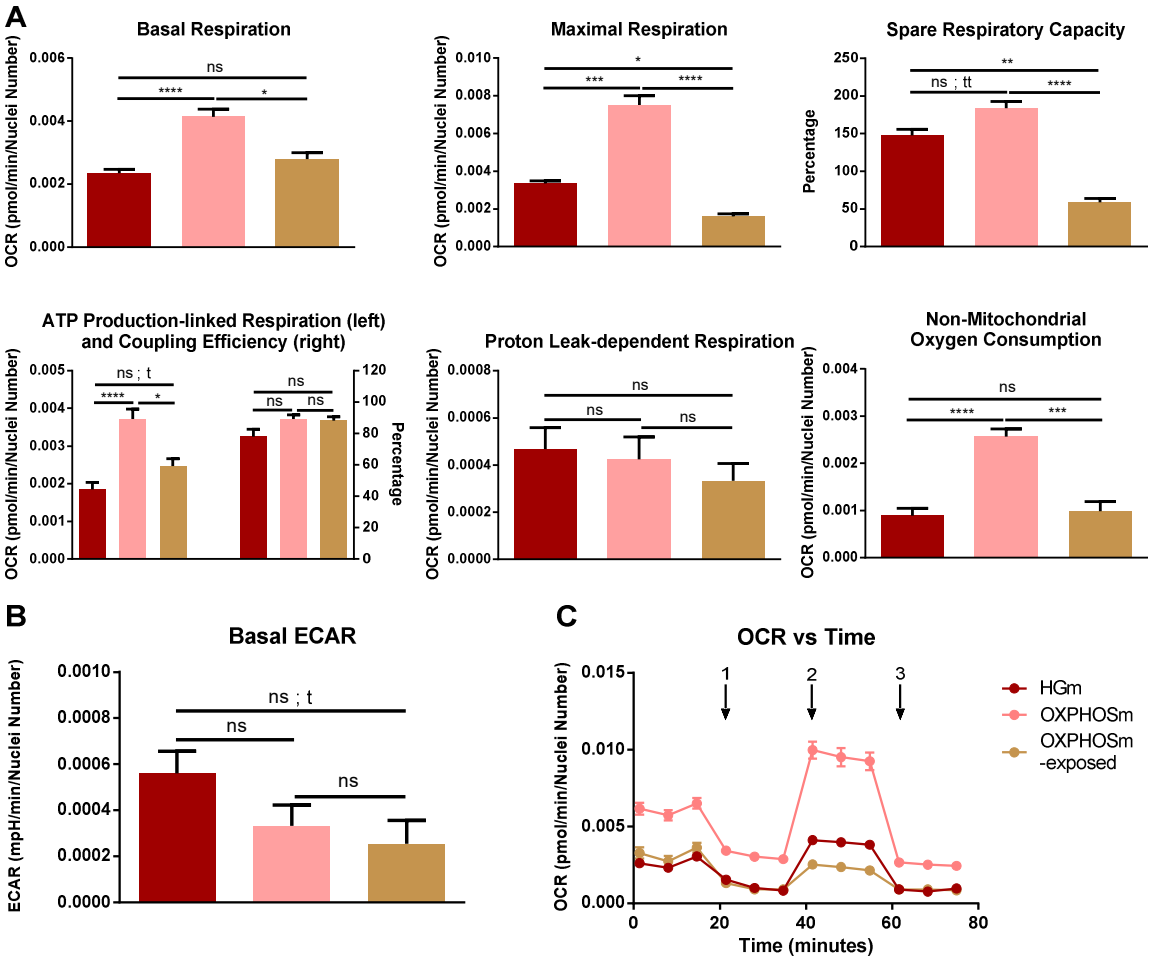

Figure 4.4 OCR-associated parameters and Basal ECAR of NHDF cells adapted to OXPHOSm (pink), acutely exposed to OXPHOSm (brown) or grown in HGm (dark red). NHDF cells were plated on passage #10, with a density of 7500 cells/well. **A** Basal respiration, maximal respiration, % spare respiratory capacity, ATP production-linked respiration and coupling efficiency, proton leak-dependent respiration and non-mitochondrial oxygen consumption. **B** Basal extracellular acidification rate. **C** OCR over time, with addition of 1 – 2 μM oligomycin – , 2 – 1 μM FCCP – and 3 – 1 μM antimycin A and 1 μM rotenone. Data are expressed as mean ± SEM of 3 independent experiments performed 1-6 times. ****: p<0.0001, ***: p<0.001, **: p<0.01, *: p<0.05, ns: p≥0.05, with p being calculated using Kruskal-Wallis test with Dunn's multiple comparisons test; tt: p<0.01, t: p<0.05, with p being calculated using two-tailed Mann-Whitney test.

The only parameter that was significantly increased, and only when Mann-Whitney test was used for p calculation, in OXPHOSm-exposed cells comparing with

HGm-grown cells was the ATP production-linked respiration, although this value was significantly lower compared to the value observed for the OXPHOSm-adapted cells. One explanation may lie in the effect reported by Sanuki and colleagues (Sanuki et al., 2017), which states that HepG2 cells shifted their metabolic preferences right after medium exchange. However, contrarily to the HepG2 cell line, in the NHDF cell line, metabolic alterations did not seem to be so instantaneous, since only ATP production-linked respiration was increased.

OXPHOSm-exposed cells also exhibited a strange behavior in response to the mitochondrial-modulator drugs, since they presented a maximal respiration value lower than the value of basal respiration, something easily observable by the value of the % spare respiratory capacity, which was around 59%. One possible cause might be a possible higher susceptibility of these cells to oligomycin due to the metabolic stress to which they were subjected.

Although these observations show some potential for the applications of our methodology in the area of toxicology, the induction of OXPHOS in NHDF cells was not achieved by exposure to OXPHOSm for 1 h, hence this protocol was abandoned.

4.2 Selection of OXPHOSm composition for OXPHOS induction in NHDF cell line.

One of the main goals of this work was to select a medium that maximized OXPHOS induction. Due to temporal restrictions, not all possible medium compositions could be tested. We decided to test eight combinations of glutamine, pyruvate, galactose and uridine, maintaining the concentration of these compounds constant in all the media tested. LGm and HGm were also tested for comparison. The candidate media compositions are shown in Table 4.1.

The choice of these concentration values was based on the literature. In fact, 10 mM and 1 mM are the concentrations of galactose and pyruvate, respectively, used in both the pioneering works about this subject, namely from Rossignol *et al.* and Marroquin *et al.* (Rossignol et al., 2004, Marroquin et al., 2007). In these studies, only glutamine concentration used was not the same, since Rossignol *et al.* used 4 mM and

Marroquin *et al.* used 6 mM. So, glutamine, pyruvate and galactose concentrations were based on the literature, even taking into account that these glutamine and pyruvate concentrations are higher than their physiological concentrations, which are reported to be 500 μM for glutamine (Stein and Moore, 1954, Schmidt et al., 2016) and 100 μM for pyruvate (Sullivan and Stern, 1983). Regarding uridine concentration, the literature did not offer a value that could serve as a benchmark. Uridine physiological blood concentration was reported to be around 3 to 5 μM (Traut, 1994, Dudzinska et al., 2010). However, in cells, uridine also exists in its phosphorylated forms, in higher concentrations (Traut, 1994), which is something to take into consideration, so uridine physiological concentration is probably not ideal for our purposes. In 2007, when uridine was used to promote wound healing on rabbit cornea, it was shown that, *in vitro*, 100 μM uridine had no cellular toxicity in keratinocytes nor in epithelial cells, which are cell types that coexist with fibroblasts in the skin (Oh et al., 2007). So, 100 μM was the chosen uridine concentration for this work.

Table 4.1 Composition of the candidate media to induce OXPHOS in NHDF cell line.

Medium	6 mM Glutamine	10 mM Galactose	1 mM Pyruvate	100 μM Uridine
1	X			
2	X	X		
3	X			X
4	X		X	
5 (traditional OXPHOSm)	X	X	X	
6	X		X	X
7	X	X	X	X
8		X	X	

In this subchapter, NHDF cells were routinely grown in HGm and were adapted as schematized in Figure 2.3 to the candidate media or to LGm. Then, OCR-associated parameters and basal ECAR were measured by subjecting cells to the XF Cell MitoStress Seahorse™ assay.

Results are summarized in the Energy Map shown in Figure 4.5 and scrutinized in the following subchapters.

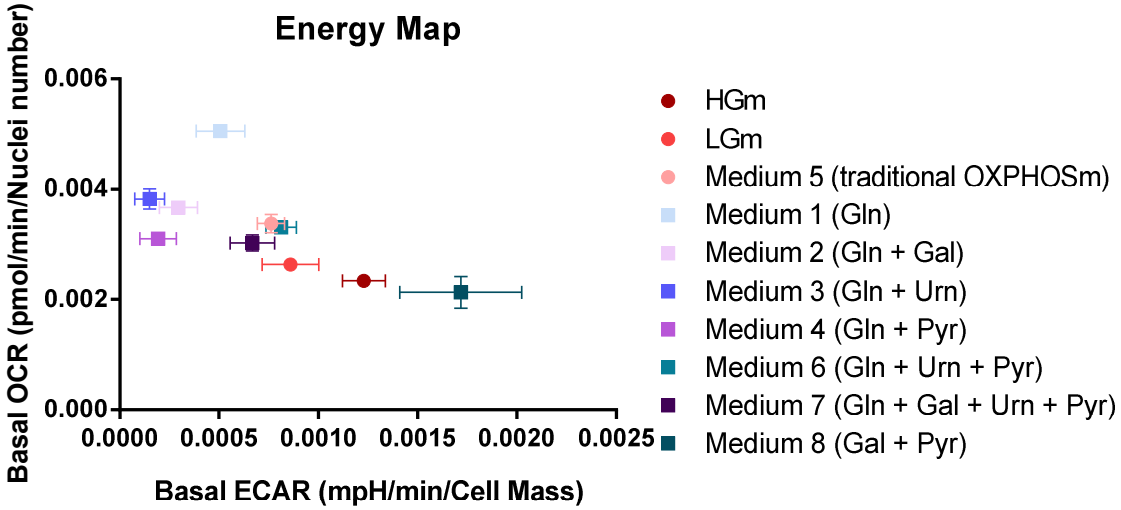

Figure 4.5 Energy Map of NHDF cells grown in HGm and adapted to LGm or to Media 1 to 8. Gal, Gln, Pyr and Urn mean Galactose, Glutamine, Pyruvate and Uridine, respectively. NHDF cells were plated on passage #11, with a density of 7500 cells/well. Data are expressed as mean ± SEM of 5-9 replicates.

4.2.1 Glutamine is essential for OXPHOS induction in NHDF cells grown in absence of glucose.

Glutamine is an indirect fuel of Krebs Cycle (Moreadith and Lehninger, 1984, Yang et al., 2014) and was described to be the main energy fuel in HeLa cells (Reitzer et al., 1979). Without its presence in glucose-free culture medium, it is difficult to predict cellular metabolism of NHDF cells. As mentioned in Chapter 1, there is some discussion on whether galactose can generate ATP through glycolysis or not. Independently of that, its metabolization generates two NADH molecules, which can be oxidized in mitochondria through OXPHOS (Berg et al., 2002, Nelson and Cox, 2013). Also, as pyruvate can be converted into acetyl-CoA and enter the Krebs Cycle, it can be an energy source for cells (Berg et al., 2002, Yu et al., 2017), although probably only in short-term if it is the only source of energy, because there would be no source to maintain the pool of Krebs Cycle intermediates (that are used in other metabolic pathways (Nelson and Cox, 2013)), as opposed to what happens when glutamine is

the main fuel.

Figures 4.6A and 4.6B show OCR-associated parameters and basal ECAR, respectively, measured in HGm-grown NHDF cells and in NHDF cells adapted to OXPHOSm, LGm or to Medium 8, whose composition is similar to OXPHOSm, with the only difference being the absence of glutamine.

In most parameters, including basal respiration and ATP production-linked respiration, the values obtained for cells adapted to Medium 8 were significantly decreased when compared to the homologous values measured in OXPHOSm-adapted cells, which suggests that glutamine is essential for the stimulation of OXPHOS in NHDF cells adapted to glucose-free media. Given that basal respiration and ATP production-linked respiration were similar in Medium 8-adapted cells and in HGm-grown cells, it is also possible to postulate that OXPHOS activity was similar in both cells. However, the cells showed different potentials to rely on OXPHOS in stress situations, as observed in maximal respiration and in spare respiratory capacity values. In fact, in cells adapted to Medium 8, OXPHOS was working near their maximal potential, since % spare respiratory capacity was slightly higher than 115%, far from the ~200% observed for cells grown in HGm or adapted to LGm or to OXPHOSm.

Regarding ECAR values, basal ECAR observed for Medium 8-adapted cells was much higher than in all the other conditions. This reflects the fact that galactose might be metabolized by these cells in a higher extent, since their oxidative metabolism is repressed due to the absence of glutamine.

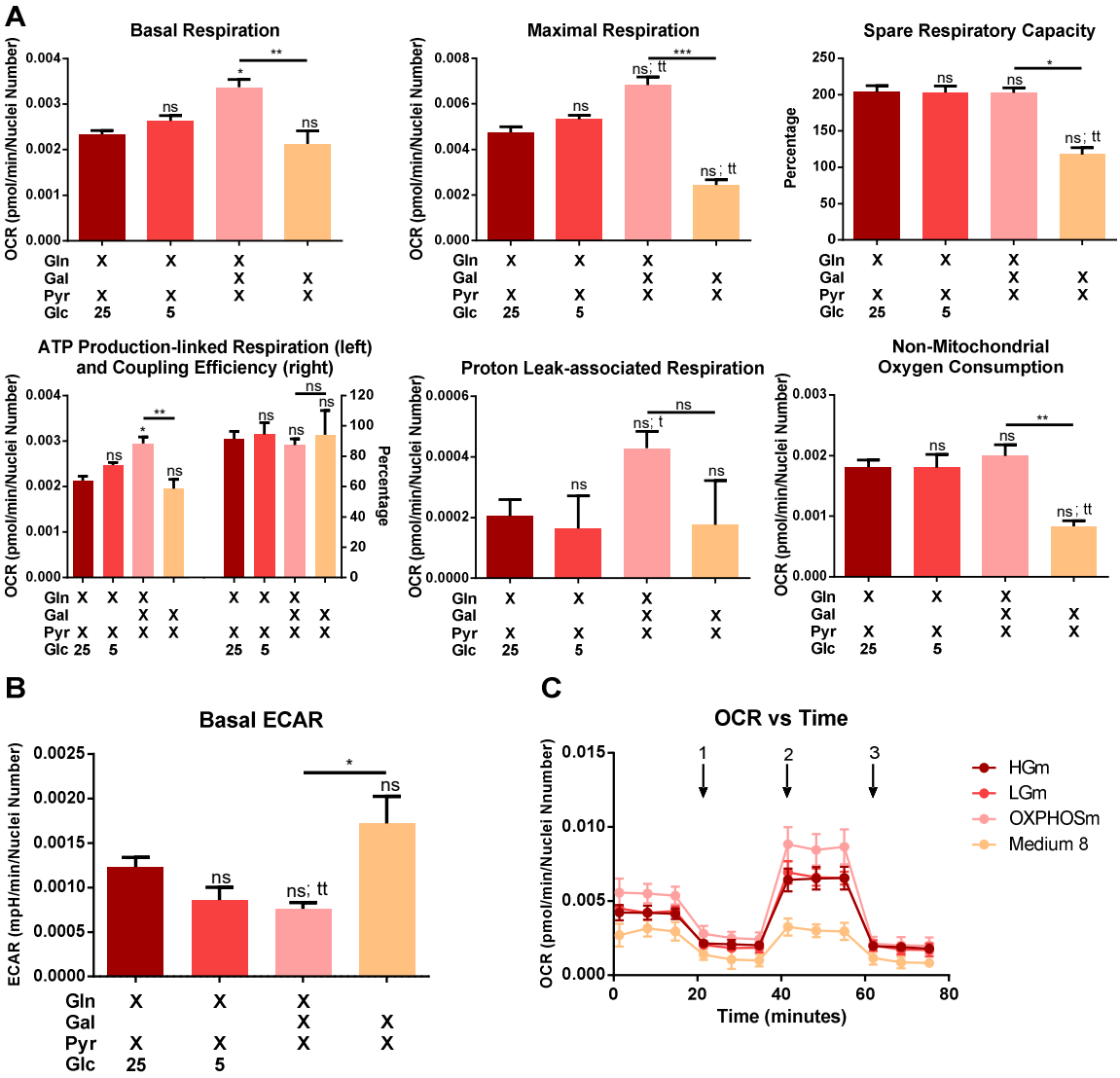

Figure 4.6 OCR-associated parameters and Basal ECAR of NHDF cells grown in HGm (dark red) and adapted to Medium 8 (light orange), OXPHOSm (pink) or LGm (red). NHDF cells were plated on passage #11, with a density of 7500 cells/well. **A** Basal respiration, maximal respiration, % spare respiratory capacity, ATP production-linked respiration and coupling efficiency, proton leak-dependent respiration and non-mitochondrial oxygen consumption. **B** Basal extracellular acidification rate. **C** OCR of NHDF cells adapted to Medium 8, OXPHOSm, LGm or HGm over time, with addition of 1 – 2 μM oligomycin – , 2 – 1 μM FCCP – and 3 – 1 μM antimycin A and 1 μM rotenone. Data are expressed as mean ± SEM of 5-9 replicates. ***: p<0.001, **: p<0.01, *: p<0.05, ns: p≥0.05, with p being calculated using Kruskal-Wallis test with Dunn's multiple comparisons test vs OXPHOSm, when identified with an horizontal line, or vs HGm, when not identified; tt: p<0.01, t: p<0.05, with p being calculated using two-tailed Mann-Whitney test vs OXPHOSm, when identified with an horizontal line, or vs HGm, when not identified.

4.2.2 Galactose seems to contribute for OXPHOS induction in NHDF cells adapted to OXPHOSm.

For HeLa cells, it was shown that glycolysis was dispensable for ATP production in cells grown in glutamine-containing media (Reitzer et al., 1979). With this conclusion in mind, this subchapter focuses on the need of sugar in the culture medium for NHDF cell line.

Figure 4.7 shows OCR-associated parameters and basal ECAR measured in HGm-grown NHDF cells and in NHDF cells adapted to OXPHOSm or to Medium 4, which lacks galactose.

In Figure 4.7A, it is possible to observe that basal and proton leak-dependent respirations were significantly increased in Medium 4-adapted cells when compared with HGm-grown cells. Using Mann-Whitney test, also ATP production-linked and maximal respirations are significantly increased. This suggests that cells adopted an energy phenotype more based on OXPHOS, even in absence of galactose, since they still had pyruvate and glutamine as substrates. Interestingly, as expected, the biggest difference was in basal ECAR, which was roughly six times lower in the cells adapted to the Medium 4. This was an expectable result because, in the absence of a sugar, given that there was no pyruvate generated through glycolysis, the only major contributor to extracellular acidification was the exogenous pyruvate. We believe that the exogenous pyruvate was directed largely to mitochondria and to the Krebs Cycle and therefore only a small part was converted into lactate.

Making the same comparisons for the case of cells adapted to OXPHOSm, it was also possible to draw some conclusions. Firstly, basal ECAR was also decreased in Medium 4-adapted cells, as expected. The cause was already explained in previous paragraph, but it was also an evidence that an important part of galactose was metabolized in the glycolytic pathway, producing pyruvate. Results also seem to suggest that galactose is somehow important for OXPHOS induction in NHDF cells, since ATP production-linked and maximal respiration of cells adapted to Medium 4 were tendentially decreased compared to cells adapted to the traditional OXPHOSm,

reaching statistical significance when using the Mann-Whitney test. At first sight, this result might appear senseless, since galactose contribution for OXHPOS would be small, given the presence of exogenous pyruvate and glutamine, according to the findings of Reitzer and colleagues (Reitzer et al., 1979). However, in the absence of sugars in the culture medium, there is no carbon source for PPP, which is probably another fate of galactose (Reitzer et al., 1979). Hence, without galactose, many biosynthetic reactions are compromised, including those that produce NADH or ATP, which have PPP intermediates as precursors (Nelson and Cox, 2013). In some cell types, it is possible to speculate that this absence of sugar could eventually be compensated by stimulating gluconeogenesis.

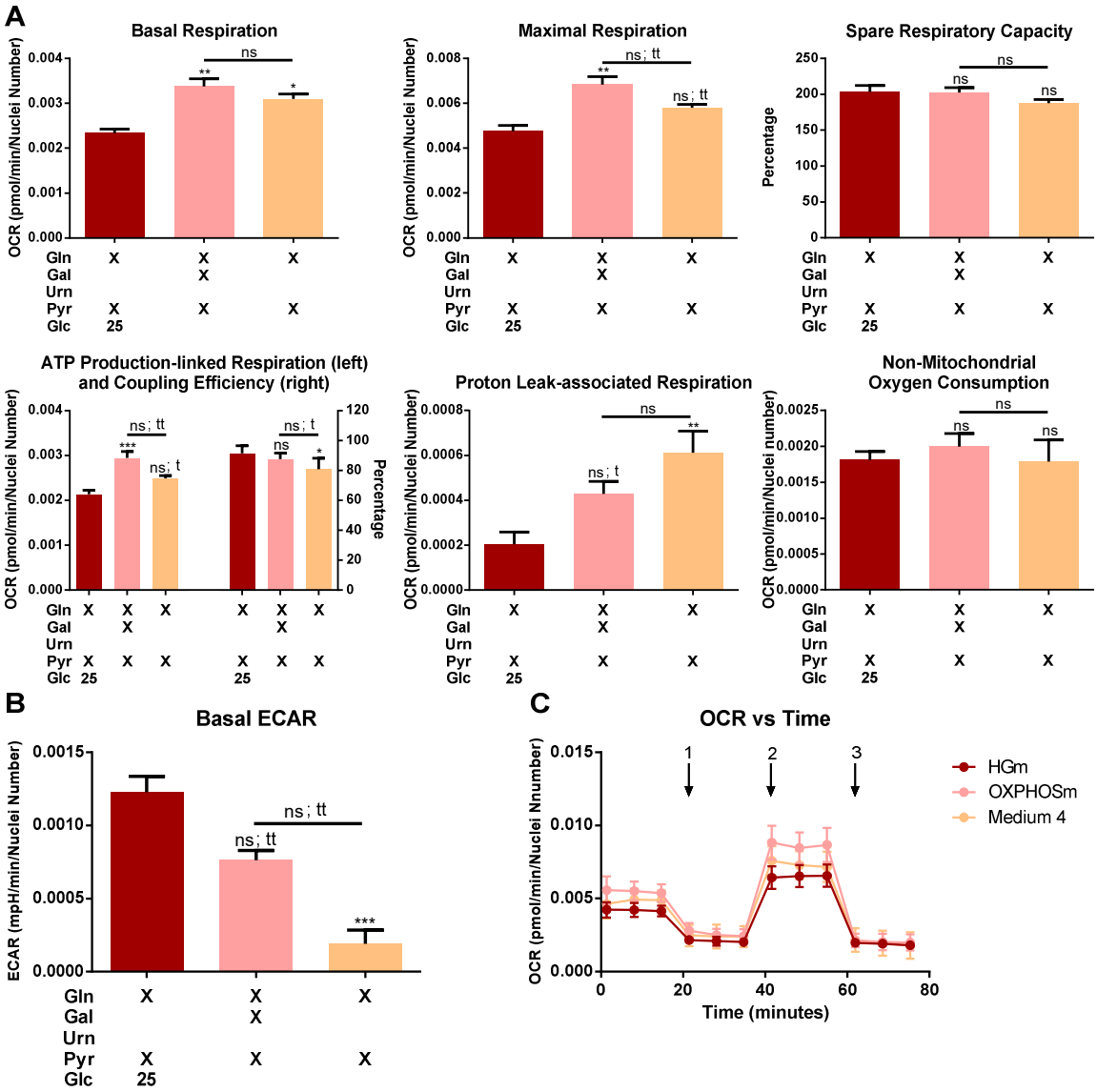

Figure 4.7 OCR-associated parameters and Basal ECAR of NHDF cells grown in HGm (dark red) and adapted to Medium 4 (light orange) or OXPHOSm (pink). NHDF cells were plated on passage #11, with a density of 7500 cells/well. **A** Basal respiration, maximal respiration, % spare respiratory capacity, ATP production-linked respiration and coupling efficiency, proton leak-dependent respiration and non-mitochondrial oxygen consumption. **B** Basal extracellular acidification rate. **C** OCR of NHDF cells adapted to Medium 4, OXPHOSm or HGm over time, with addition of 1 – 2 μM oligomycin – , 2 – 1 μM FCCP – and 3 – 1 μM antimycin A and 1 μM rotenone. Data are expressed as mean ± SEM of 5-9 replicates. ***: $p<0.001$, **: $p<0.01$, *: $p<0.05$, ns: $p\geq0.05$, with p being calculated using Kruskal-Wallis test with Dunn's multiple comparisons test vs OXPHOSm, when identified with an horizontal line, or vs HGm, when not identified; tt: $p<0.01$, t: $p<0.05$, with p being calculated using two-tailed Mann-Whitney test vs OXPHOSm, when identified with an horizontal line, or vs HGm, when not identified.

That postulation, however, cannot be applied to the NHDF cell line, since gluconeogenesis key enzyme phosphoenolpyruvate carboxykinase-C (PEPCK-C) is reported not to be expressed in the skin (Fagerberg et al., 2014), underlining the importance of the presence of galactose for NHDF cells grown in media without glucose. It is worth to highlight that this hypothesis cannot be extrapolated to other cell lines, particularly cell lines derived from liver, kidney or small intestine, such as HepG2, human embryonic kidney 293 (HEK) or human duodenum adenocarcinoma HuTu-80 cell lines, since PEPCK-C gene is highly expressed in these tissues (Fagerberg et al., 2014). Further metabolomic analyses are required to understand the exact role of galactose for NHDF cell metabolism grown in these conditions.

4.2.3 Pyruvate is not critical for OXPHOS induction in cells grown without glucose and with galactose supplementation.

Pyruvate supplementation in culture media without glucose is not entirely consensual, despite its known roles for cells. As mentioned in the Introduction section, pyruvate is not only a carbon source for Krebs Cycle, and therefore for the synthesis of metabolites that feed ETC (Berg et al., 2002, Nelson and Cox, 2013), but also an important ROS scavenger (Wang et al., 2007, Babich et al., 2009, Lee et al., 2014, Wilkins et al., 2014), contributing to a lower degradation of the mitochondrial proteins and hence to a possible greater enzymatic activity of the ETC complexes. Nevertheless, supplementation of the culture medium with pyruvate, in addition to a sugar, is often

considered redundant, since the metabolism of sugars through glycolysis produces pyruvate (Berg et al., 2002, Nelson and Cox, 2013). This hypothesis is supported by the data shown in Figure 4.7B and explained in Subchapter 4.2.2.

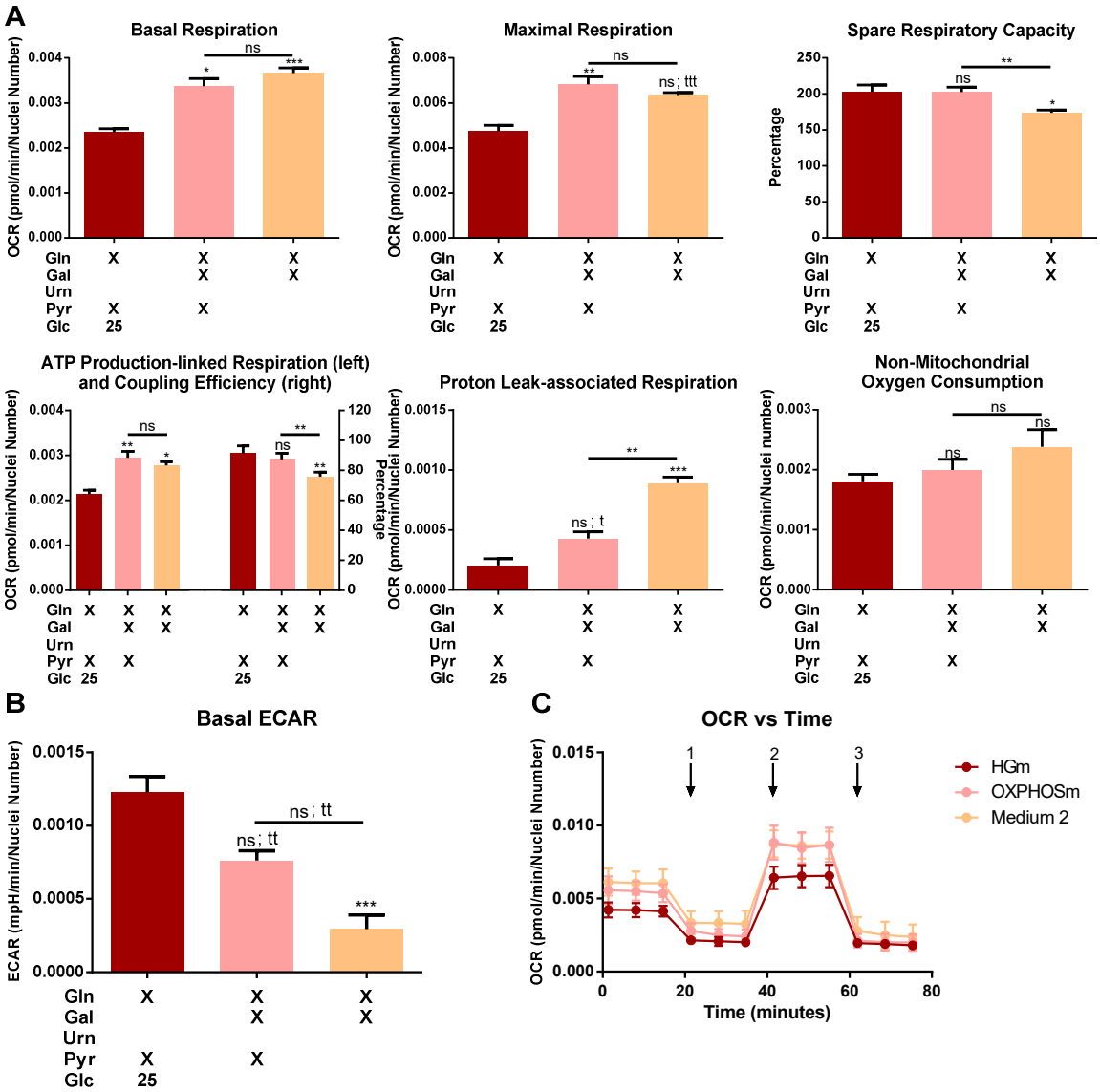

Figure 4.8 OCR-associated parameters and Basal ECAR of NHDF cells grown in HGm (dark red) and adapted to Medium 2 (light orange), or OXPHOSm (pink). NHDF cells were plated on passage #11, with a density of 7500 cells/well. **A** Basal respiration, maximal respiration, % spare respiratory capacity, ATP production-linked respiration and coupling efficiency, proton leak-dependent respiration and non-mitochondrial oxygen consumption. **B** Basal extracellular acidification rate. **C** OCR of NHDF cells adapted to Medium 2, OXPHOSm or HGm over time, with addition of 1 – 2 µM oligomycin – , 2 – 1 µM FCCP – and 3 – 1 µM antimycin A and 1 µM rotenone. Data are expressed as mean ± SEM of 5-9 replicates. ***: p<0.001, **: p<0.01, *: p<0.05, ns: p≥0.05, with p being calculated using Kruskal-Wallis test with Dunn's multiple comparisons test vs OXPHOSm, when identified with an horizontal line, or vs HGm, when not identified; ttt: p<0.001, tt: p<0.01, t: p<0.05, with p being calculated

using two-tailed Mann-Whitney test vs OXPHOSm, when identified with an horizontal line, or vs HGm, when not identified.

Results shown in Figure 4.8A seem to indicate that pyruvate supplementation has indeed a small influence in OXPHOS induction, since its absence in culture Medium 2 did not lead to a decrease in several OCR-associated parameters, such as basal, ATP production-linked, maximal and non-mitochondrial respirations. These results are probably explained by the redundant effect mentioned before. In the following subchapter, it is shown that uridine has some potential as a substitute for galactose to induce OXPHOS. However, at least directly, uridine cannot generate pyruvate, as does galactose. The results for Medium 3 (which lacks galactose and pyruvate but contains uridine), shown in Figure 4.9A, support the idea of the redundancy of pyruvate supplementation, given the significantly lower value of ATP production-linked and maximal respiration in cells adapted to this medium, when compared with cells adapted to OXPHOSm, which, as shown in Figure 4.8A, was not observed when cells were adapted to Medium 2.

The removal of pyruvate also led to a decrease in ECAR. Although, as explained, pyruvate supplementation is unnecessary for OXPHOS stimulation, its removal led to a big decrease in its pool, which was only originated by galactose metabolization. Thus, given the decrease and the demand of pyruvate for the Krebs Cycle, the amount of pyruvate metabolized into lactate was lower, driving a decrease in medium acidification, as shown in Figure 4.8B.

4.2.4 Uridine has the potential to replace galactose in OXPHOSm composition.

Since ρ0 cells are auxotrophic for uridine (Wilkins et al., 2014) and since another nucleoside (inosine) was found to be important for cellular growth as ribose donor (Davit-Spraul et al., 1994), uridine could eventually perform a useful role as an OXPHOSm component.

Figure 4.9 shows OCR-associated parameters and basal ECAR measured in cells grown in HGm or adapted to OXPHOSm, to Medium 6 (composition similar to

OXPHOSm, only with uridine instead of galactose), to Medium 3 (supplemented only with glutamine and uridine), or to Medium 7 (supplemented as OXPHOSm and with uridine).

In what concerns cells adapted to Medium 3, although basal respiration was increased compared to cells grown in HGm, ATP production-linked and maximal respirations were not increased, suggesting that this medium was not effective in inducing OXPHOS in NHDF cells, probably due to the lack of pyruvate, either exogenous or endogenous (since there was no carbohydrate supplementation to generate it through glycolysis). Moreover, the absence of carbohydrates also contributes to the low value of basal ECAR, observed in Figure 4.9B.

The most interesting results are the ones relative to Medium 6. In Figure 4.9A, it is possible to see that all OCR-associated parameters measured were similar in both OXPHOSm-adapted and Medium 6-adapted cells, which suggests that, ensuring the maintenance of the pyruvate pool, uridine may replace galactose in the OXPHOS inducing culture medium. The strangest result, however, was the similar value of basal ECAR on both media (Figure 4.9B). This was not expected, since the glycolytic rate in Medium 6-adapted cells should be presumably lower, due to the lack of carbohydrate supplementation. Further experiments are necessary to explain this observation.

Finally, it seems that there was no advantage in adapting cells to a medium containing both galactose and uridine, instead of adapting them to media with only one of these compounds. Most OCR-associated parameters, including basal, ATP production-linked and proton leak-associated respirations and also coupling efficiency and non-mitochondrial oxygen consumption were similar in cells adapted to OXPHOSm or to Medium 7, and maximal respiration and spare respiratory capacity were even tendentially decreased, supporting this conclusion.

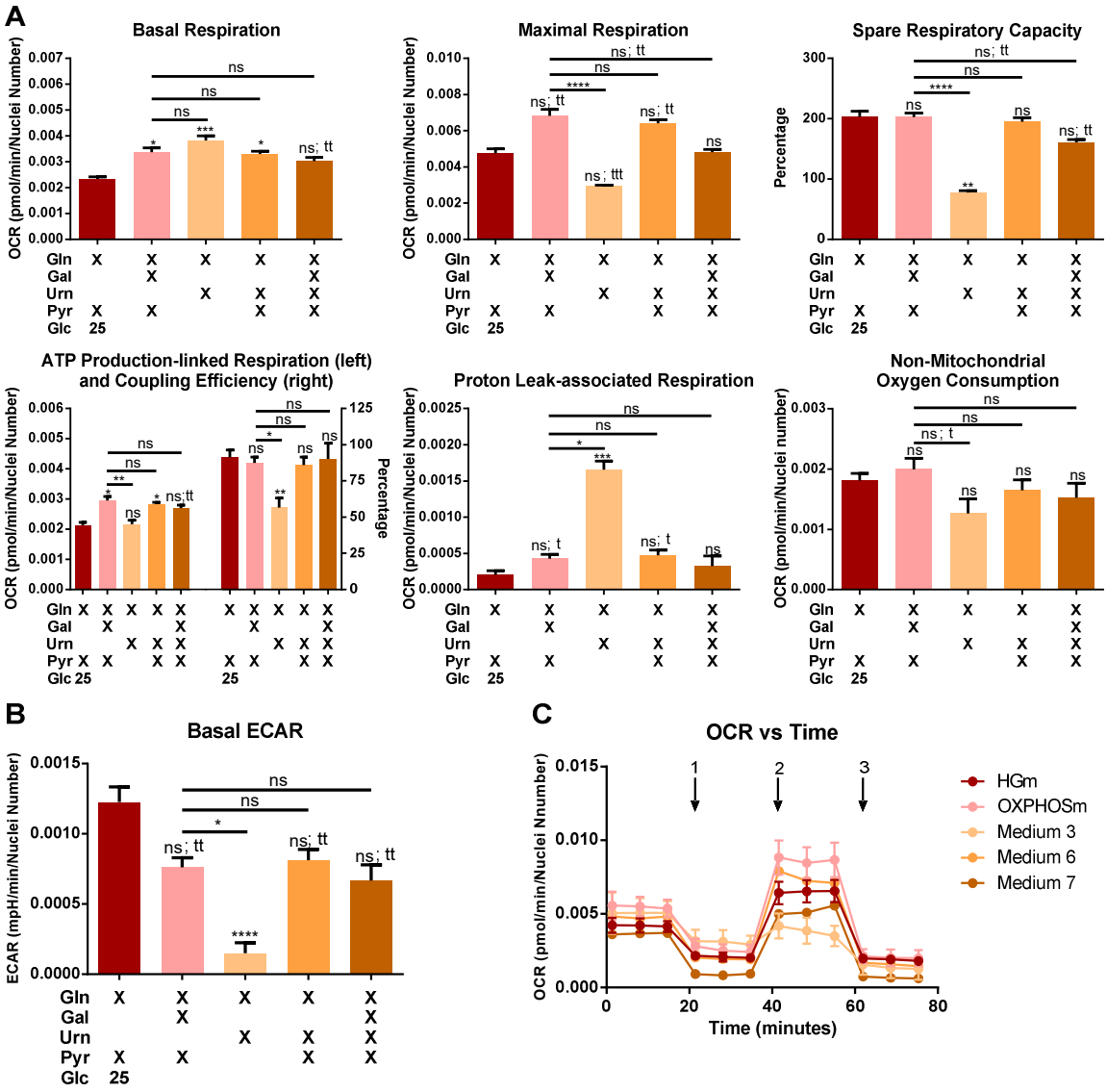

Figure 4.9 OCR-associated parameters and Basal ECAR of NHDF cells grown in HGm (dark red) and adapted to Medium 3 (light orange), 6 (orange), 7 (dark orange) or OXPHOSm (pink). NHDF cells were plated on passage #11, with a density of 7500 cells/well. **A** Basal respiration, maximal respiration, % spare respiratory capacity, ATP production-linked respiration and coupling efficiency, proton leak-dependent respiration and non-mitochondrial oxygen consumption. **B** Basal extracellular acidification rate. **C** OCR of NHDF cells adapted to Medium 3, 6, 7, OXPHOSm or HGm over time, with addition of 1 – 2 μM oligomycin – , 2 – 1 μM FCCP – and 3 – 1 μM antimycin A and 1 μM rotenone. Data are expressed as mean ± SEM of 5-9 replicates. ****: p<0.0001, ***: p<0.001, **: p<0.01, *: p<0.05, ns: p≥0.05, with p being calculated using Kruskal-Wallis test with Dunn's multiple comparisons test vs OXPHOSm, when identified with an horizontal line, or vs HGm, when not identified; tt: p<0.01, t: p<0.05, with p being calculated using two-tailed Mann-Whitney test vs OXPHOSm, when identified with an horizontal line, or vs HGm, when not identified.

4.2.5 Supplementation only with glutamine has potential for toxicology applications.

Medium 1 was the simplest medium tested, since it was supplemented only with glutamine, in the hope that the metabolism of NHDF cells adapted to this medium was almost exclusively oxidative.

During the XF Cell MitoStress Seahorse™ assay, cells adapted to Medium 1 presented a behavior that led us to hypothesize that this medium can eventually have potential for toxicological assays. These cells presented the highest basal respiration value between the ten conditions analyzed, and their ATP production-linked OCR value was similar to the value observed for cells adapted to OXPHOSm (Figure 4.10). These values indicate that, indeed, these are probably the most oxidative cells analyzed. However, these cells did not react to FCCP, since their maximal respiration was lower than their basal respiration, as shown in Figure 4.10. In addition to the possibility of an experimental error, this strange behavior may also be due the induction of necrosis after oligomycin addition. Interestingly, nuclei number was lower in the wells where were plated cells adapted to Medium 8 (data not shown), which supports this idea. Further studies are required to understand this behavior and to test the hypothesis mentioned in the title of this subchapter.

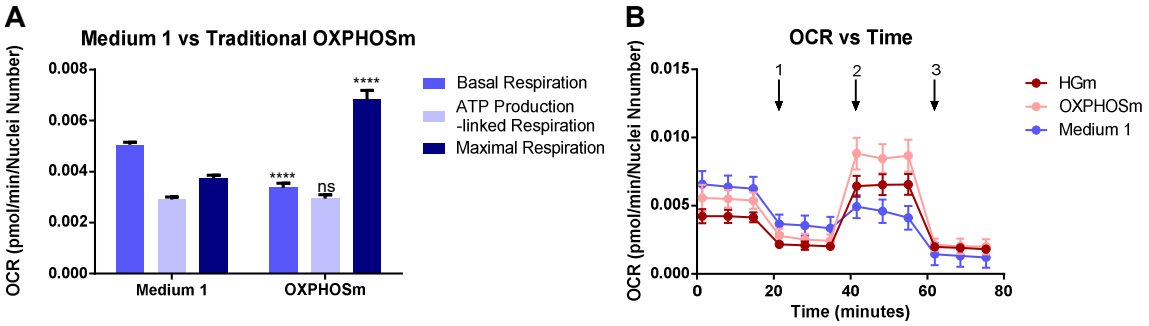

Figure 4.10 NHDF cells were plated on passage #11, with a density of 7500 cells/well. **A** Basal Respiration, ATP Production-linked Respiration and Maximal Respiration of cells adapted to medium 1 or to OXPHOSm. **B** OCR of NHDF cells grown in HGm and adapted to Medium 1 or to OXPHOSm over time, with addition of 1 – 2 μM oligomycin – , 2 – 1 μM FCCP – and 3 – 1 μM antimycin A and 1 μM rotenone. Data are expressed as mean ± SEM of 5-9 replicates. ****: $p<0.0001$, ns: $p\geq0.05$, with p being calculated using two-tailed Mann-Whitney test.

Considering these results, and although Medium 1 seems to have potential for toxicology, given the unpredictable behavior of these cells, Medium 1 was abandoned.

4.2.6 Selection of OXPHOSm composition: final considerations.

Several conclusions can be drawn from the data presented in the Subchapter 4.2.

Firstly, as explained in Subchapter 4.2.1, it is possible to conclude that glutamine is essential for OXPHOS induction. Eventually, given that its main role is to feed Krebs Cycle, glutamine could be replaced by glutamate or α-ketoglutarate, which are the molecules to which it is metabolized (McKeehan, 1982, Moreadith and Lehninger, 1984, Yang et al., 2014). The uptake of both compounds is described to be possible in fibroblasts (Dall'Asta et al., 1983, Aussel et al., 1996). In contrast, the use of media supplemented exclusively with glutamine might have some potential for toxicology applications, since the cells appeared more oxidative and at the same time more sensitive to mitochondrial toxicants.

In regard to pyruvate, another of the traditionally used components, results seem to suggest that its supplementation is not necessary, provided that a precursor compound is supplied to cells. The most obvious example is galactose, as shown in Subchapter 4.2.3. Other possibilities include lactate, which can be converted in pyruvate by LDH (Berg et al., 2002, Yu et al., 2017), and alanine, which can be converted in pyruvate by ALT (Moreadith and Lehninger, 1984, Yang et al., 2014). Acetyl-CoA can also be an alternative to pyruvate, since, although it cannot be directly converted into pyruvate, its generation is one of the main fates of pyruvate (Berg et al., 2002, Yu et al., 2017).

The results also suggested that galactose plays an important role in OXPHOS induction. However, uridine and possibly other nucleosides, such as inosine, seem to have potential to replace galactose, as far as the pyruvate pool is guaranteed.

Considering our results, the traditional OXPHOSm was the medium selected for the subsequent experiments, because, among all the media tested, no other presented evident advantages, although there were some that also did not present major

disadvantages. The fact that this is the widely used medium also weighed on the choice.

4.3 NHDF cells presented the oxidative phenotype after two cell passages in OXPHOSm.

There are no published studies that focus on how immediate the molecular changes are in cells adapted to OXPHOSm, once that they become more oxidative. In fact, Swiss *et al.* (2011) alerted to the fact that the adaptation period depends on the cell type used, recommending to assess the oxidative state of OXPHOSm-grown cells to check for the metabolic switch (Swiss and Will, 2011). In the results shown in the previous subchapters, one of the consequences of this metabolic shift was described, namely, the OCR increase, which was also the key parameter to demonstrate the success of the adaptation.

There may be several molecular causes for increased OCR. However, to determine the number of cell passages in OXPHOSm needed until these changes were observable, we focused on only one parameter, namely, the expression of the mtDNA-encoded CYB gene, which encodes a subunit of complex III. The choice of this gene was due to the fact that it may also be used to assess the copy number of mtDNA (Deus et al., 2015). Also, it is described that the expression of this gene is sensitive to the culture medium in which BJ cell line, another fibroblast cell line, is cultured (Pereira et al., 2018). Lastly, assessment of mitochondrial genes by PCR is one of the parameters recommended by Swiss *et al.* (2011), in the work where OXPHOSm adaptation was first explained (Swiss and Will, 2011).

To assess the timecourse of molecular adaptations induced by OXPHOSm adaptation, cells were adapted to OXPHOSm using the adaptation protocol chosen in the previous experiments, and RNA was extracted and purified after one, two, four and six cell passages in 100% OXPHOSm. Results, shown in Figure 4.11, indicate that changes in CYB expression are visible after 2 passages in OXPHOSm. Extrapolating, it is possible to speculate that the same is true for other genes and other molecular

markers. This will be explored in later subchapters. From this data, the decision taken was to initiate experimental procedures in adapted cells only after two passages in 100% OXPHOSm.

It is important to note that the variance in this experiment was relatively large, so even though some differences are significant, it is necessary to clarify them in the future, for example by increasing the *n*.

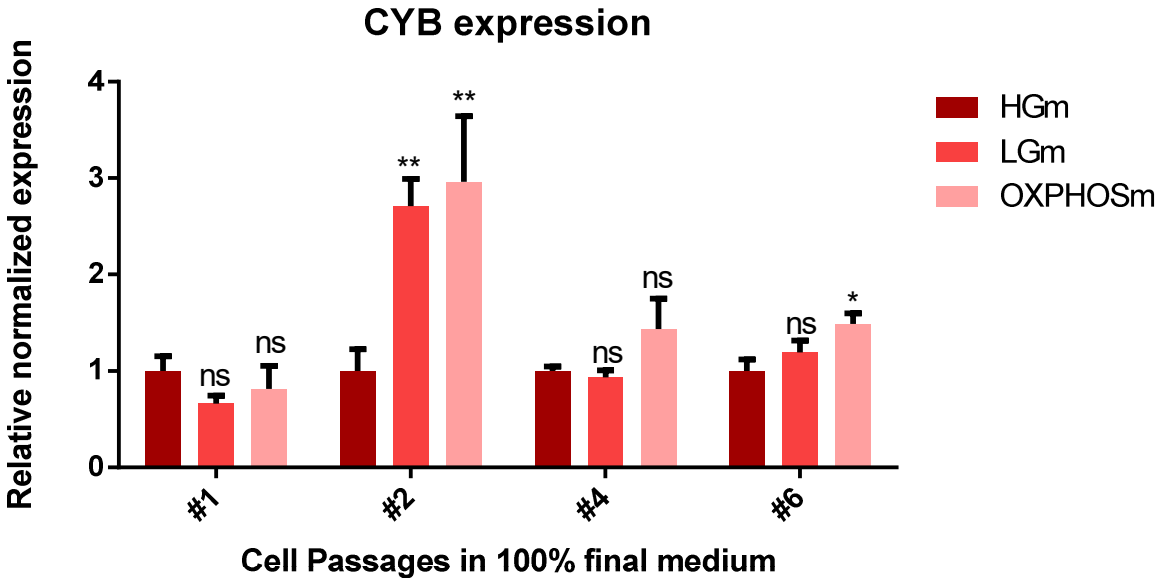

Figure 4.11 CYB gene expression in cells grown in HGm or adapted to LGm or OXPHOSm after 1, 2, 4 or 6 cells passages in 100% final medium. Total RNA was extracted, purified, converted into cDNA, and amplified by qRT-PCR. Gene expression was measured and normalized to YWHAZ levels and divided by the mean of the values obtained for HGm-grown cells. Data are expressed as mean ± SEM of 4-5 independent experiments. **: $p<0.01$, *: $p<0.05$, ns: $p\geq0.05$, with p being calculated using ordinary two-way ANOVA test with Tukey's multiple comparisons test.

4.4 Adaptation of NHDF cells to OXPHOSm increased their sensitivity to several mitochondrial poisons.

One of the applications of this methodology are toxicological assays. There are many published works that use glucose-free media to increase the effect of mitochondrial toxicants, as discussed in Subchapter 1.4. Among those toxicants are complex I inhibitor rotenone, complex III inhibitor antimycin A and complex V inhibitor oligomycin (Marroquin et al., 2007, Swiss and Will, 2011, Pereira et al., 2012,

Swiss et al., 2013). In the NHDF cell line, we tested these three poisons, the complex II inhibitor DMM and the oxidative stress inducer tBHP (Kennedy et al., 1992, Kucera et al., 2014). Cells were adapted to OXPHOSm or to LGm and seeded in 96-well plates. Twenty four hours later, cells were exposed to different concentrations of each poison for 3 h and then ATP levels or metabolic activity were measured.

Figure 4.12A shows the ATP levels measured in HGm-grown and in LGm or OXPHOSm-adapted NHDF cells exposed to rotenone. It is easily observable that cells adapted to OXPHOS were much more susceptible to rotenone than their glucose-containing media-cultured counterparts, being that consistent with the quoted works found in literature and proving that our methodology has applications for toxicological studies.

Interestingly, it is also possible to observe that NHDF cells adapted to LGm, when exposed to the lowest tested concentrations, seemed to present a mitohormetic behavior, something not observable for HGm-grown cells. One possible explanation might rely on the fact that HGm-grown cells do not need OXPHOS to survive, and, thus, rotenone does not affect their ATP levels at all. In contrast, LGm-adapted cells seem to be slightly more reliant on OXPHOS for ATP production, which is unbalanced by rotenone, leading them to compensate that by increasing glycolysis. This may lead to the small increase in total ATP levels in these cells, in the presence of low concentrations of rotenone.

Similar results were observed for oligomycin-exposed NHDF cells (Figure 4.12D).

Regarding antimycin A, the major difference was the non-hormetic behavior of cells adapted to LGm, as shown in Figure 4.12C. It is also interesting that the effect of this drug in cells adapted to OXPHOSm also appeared to be slightly higher than the effects of oligomycin and rotenone. Together, these observations seem to suggest that antimycin is slightly more toxic than rotenone and oligomycin.

Contrarily to what was expected, DMM toxicity was not unmasked by our methodology for concentrations up to 7.4 mM (Figure 4.12B). According to the reasoning explained in the first paragraph of Subchapter 1.4, it is not possible to

conclude anything about the mechanism of action of DMM, although, as stated, it is described to be an inhibitor of complex II. One possible explanation relies in the fact that ETC can still be active, since electrons can flow from complex I to complex III, although this explanation can be counter-argued with the fact that an analogous reasoning should be applied for rotenone. However, complex II might be less essential for OXPHOS in NHDF cells where complex I is functional, since it contributes in a lower extension to membrane potential generation and, consequently, to ATP synthesis. Another possibility for the lack of effect promoted by DMM is an eventual low bioavailability of the compound in mitochondria. To achieve greater toxicity, increasing the concentration of DMM used could be a solution.

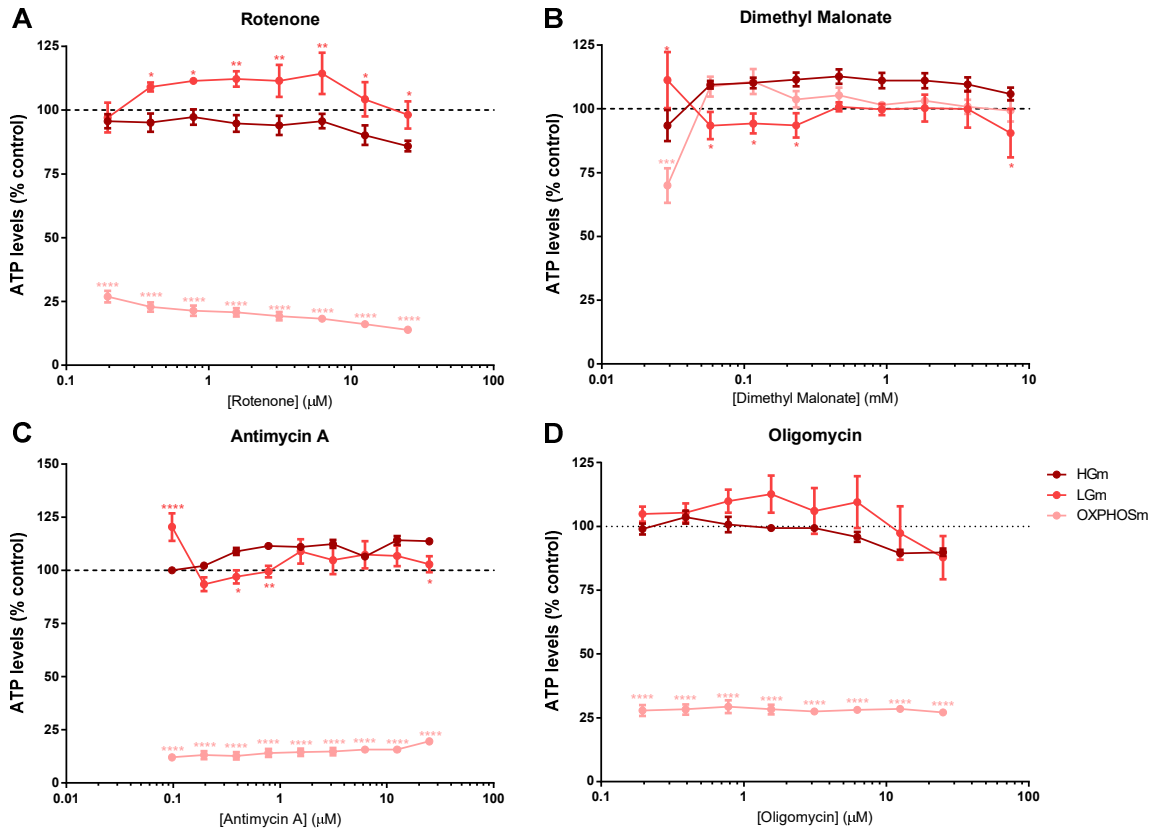

Figure 4.12 ATP levels in cells grown in HGm or adapted to LGm or OXPHOSm after 3 h of exposure to **A** rotenone, **B** DMM, **C** antimycin A or **D** oligomycin. NHDF cells were plated on passage #8, with a density of 7500 cells/well. After 24 h, toxicant was added to the cells and, 3 h later, ATP levels were measured using CellTiter-Glo® Luminescent Cell Viability Assay Kit. Data are expressed as mean ± SEM of 4 independent experiments. ****: $p<0.0001$, ***: $p<0.001$, **: $p<0.01$, *: $p<0.05$, with p being calculated using ordinary two-way ANOVA test with Dunnett's multiple comparisons test.

The effect of oxidative stress inducer tBHP was also measured in HGm-grown and in LGm or OXPHOSm-adapted cells. Besides ROS induction in mitochondria, tBHP increases mitochondrial Ca^{2+} levels (Byrne et al., 1999), contributing, therefore, to mitochondrial permeability transition (Nieminen et al., 1995, Fedotcheva and Mokhova, 2013). In addition, α-ketoglutarate and pyruvate oxidation by mitochondrial NAD-dependent dehydrogenases and complex I were found to be inhibited after tBHP treatment (Drahota et al., 2005, Endlicher et al., 2009). Results shown in Figure 4.13A correspond to NHDF cells grown in HGm or adapted to LGm or OXPHOSm and exposed to tBHP for 3 h. After drug exposure, resazurin assay was performed to measure metabolic activity, as an indicator of cell viability.

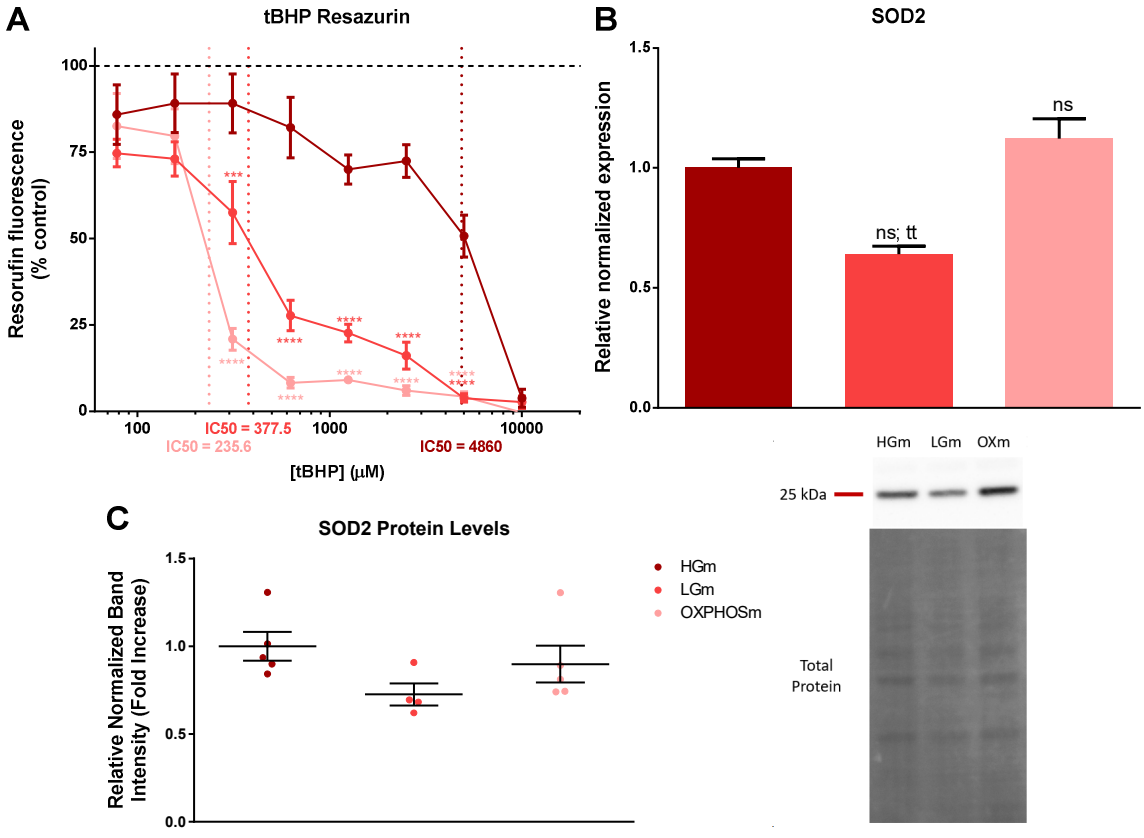

Figure 4.13 A Metabolic activity of in cells grown in HGm or adapted to LGm or OXPHOSm after 3 h of exposure to tBHP. NHDF cells were plated on passage #13, with a density of 6500 cells/well. After 24 h, tBHP was added to the cells and, 3 h later, 10 µg/ml resazurin was added to the cells. After 1 h incubation, metabolic activity was measured following the reduction of resazurin to resorufin. Control wells are wells in which cells were not exposed to tBHP. Data are expressed as mean ± SEM of 3 independent experiments performed 2 times. ****: p<0.0001, ***:

p<0.001, with p being calculated using ordinary two-way ANOVA test with Dunnett's multiple comparisons test. **B** SOD2 gene expression in cells grown in HGm or adapted to LGm or OXPHOSm. Total RNA was extracted, purified, converted into cDNA, and amplified by qRT-PCR. Gene expression was measured and normalized to B2M, HPRT1 and RNA18S levels, and divided by the mean of the values obtained for HGm-grown cells. Data are expressed as mean ± SEM of 5 independent experiments. ns: p≥0.05, with p being calculated using Kruskal-Wallis test with Dunn's multiple comparisons test vs HGm; tt: p<0.01, with p being calculated using two-tailed Mann-Whitney test vs HGm. **C** SOD2 Protein Levels in cells grown in HGm or adapted to LGm or OXPHOSm. SOD2 protein levels were measured by Western Blot and normalized to total protein levels. Images at right show representative blots. Data are expressed as mean ± SEM of 4-5 independent experiments. Dots represent individual measurements.

Contrarily to the results shown in Figure 4.12, we were able to calculate the IC50 for cells grown in the different conditions. In the figure, it is possible to observe that tBHP effect of NHDF cells was exacerbated in cells cultured in OXPHOSm, given that the IC50 for these cells was the lower than in the other conditions.

Also, in contrast to what was observed in CellTiter-Glo® Luminescent Cell Viability Assay, the effect of tBHP was also very pronounced in LGm-adapted cells (Figure 4.13A). Interestingly, mitochondrial SOD2 transcript levels were significantly decreased in the same cells when Mann-Whitney test was applied, as shown in Figure 4.13B, which helps to explain this result. This result was confirmed by western blot, although without statistical significance, given that protein levels were slightly decreased in cells adapted to LGm, as shown in Figure 4.13C. Evaluation of other endogenous antioxidant defenses can strengthen these postulations.

4.5 Preconditioning with mitochondria-directed antioxidants protected NHDF cells against tBHP only in OXPHOSm-adapted cells.

Considering the effect of mitochondria-directed antioxidants mentioned in Subchapter 1.5, in this chapter we aimed to test the applicability of OXPHOSm also to cell protection assays, in comparison with LGm and HGm. Here, oxidative stress inducer tBHP, whose effect was evaluated in HGm and adapted or not to LGm or to OXPHOSm in the previous subchapter, was used as a stressor, in concentrations near

the IC50 for each medium.

Four antioxidants were tested, namely, MitoBEN2 and its parent antioxidant Gallic Acid and MitoCIN4 and its parent antioxidant Cinnamic Acid, whose structures are represented in Figure 4.14A to D. MitoBEN2 synthesis and properties were published by Teixeira *et al.* (Teixeira et al., 2017b). MitoCIN4 synthesis and properties were published by Teixeira *et al.* (Teixeira et al., 2012).

NHDF cells were preconditioned with antioxidants and 24 h later were exposed to tBHP for further 3 h. Figure 4.14E shows the metabolic activities of these cells, as an indicator of cell viability.

The first conclusion to take is that we were not able to replicate tBHP effect, since its toxicity was much higher than 50% in this assay in cells grown with glucose. This did not allow us to accomplish the major objective of the chapter, since it was not possible to compare the percentages of protection in cells grown in the different media when cell death values were so different. However, it is worth to note that, for OXPHOSm-adapted cells, tBHP toxicity results were much more reproducible, what might constitute an advantage for this methodology.

Results also show that our methodology allowed to detect cell protection when cells were preconditioned with MitoBEN2, MitoCIN4 or Cinnamic Acid, but it seems that Gallic Acid preconditioning did not protect the cells at the concentrations used. This conclusion was drawn because we are able to prevent metabolic activity decrease or even increase that value in tBHP-exposed cells preconditioned with the antioxidants when compared to control condition and to non-preconditioned condition.

Considering the results of metabolic activity, 780 nM and 195 nM were the lower values that induced cell protection, for MitoBEN2 and MitoCIN4, respectively (as highlighted with an arrow in Figure 4.14E). At these concentrations, the % of protection of both mitochondria-directed antioxidants is higher than the value observed for the respective parent antioxidant (Figure 4.14F), underlining the potential of these molecules for cell protection against oxidative stress insults.

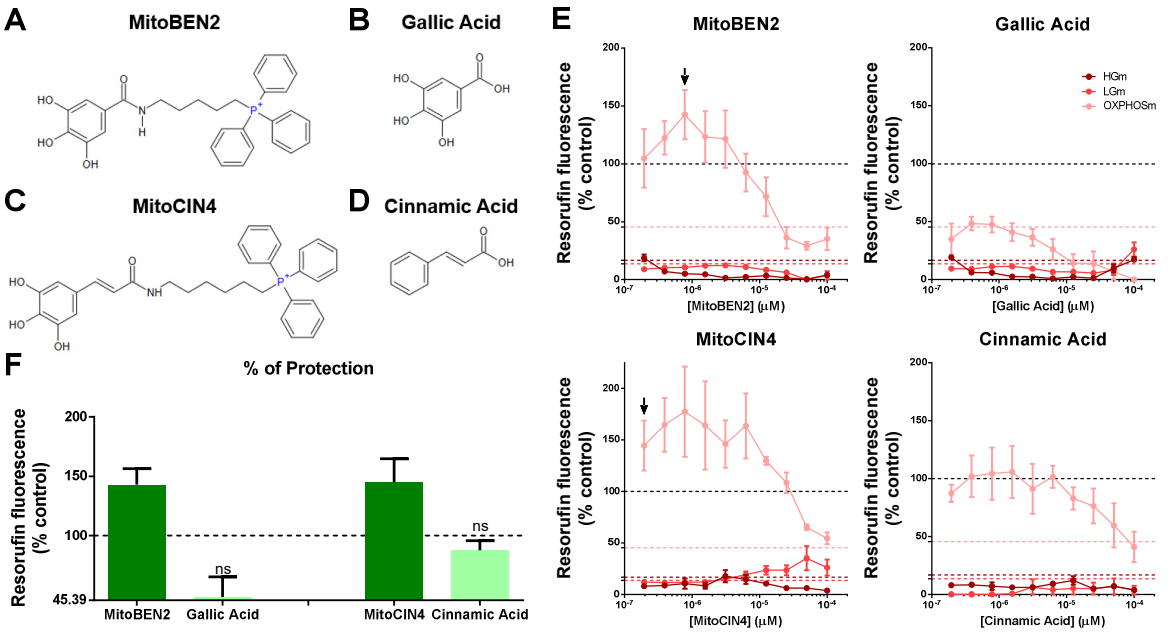

Figure 4.14 A to D Molecular structures of MitoBEN2 (**A**), Gallic Acid (**B**), MitoCIN4 (**C**) and Cinnamic Acid (**D**). **E** Metabolic activity of cells grown in HGm or adapted to LGm or OXPHOSm, preconditioned with MitoBEN2, Gallic Acid, MitoCIN4 or Cinnamic Acid and exposed to tBHP. NHDF cells were plated on passage #9, with a density of 7500 cells/well. After 24 h, antioxidants were added to the cells, in concentrations between 195 nM and 100 µM. After another 24 h, cells plated in OXPHOSm, LGm and HGm were exposed for 3 h to 250 µM, 500 µM or 6 mM tBHP, respectively, and, 3 h later, 10 µg/ml resazurin was added to the cells. After 1 h of incubation, metabolic activity was measured following the reduction of resazurin to resorufin. Control wells are wells in which cells were not exposed to tBHP nor preconditioned with antioxidants. Horizontal lines in pink, red or dark red correspond to tBHP effect in cells not preconditioned with antioxidants. Data are expressed as mean ± SEM of 3 independent experiments. **F** Percentage of improvement of metabolic activity of cells of 780 nM MitoBEN2 or Gallic Acid or 195 nM MitoCIN4 or Cinnamic Acid preconditioning against stress induced by tBHP in NHDF cells adapted to OXPHOSm. 0 in the graph correspond to tBHP effect, while horizontal line corresponds to control wells % metabolic activity (100% in Figure 4.14E graphs). Data are expressed as mean ± SEM of 3 independent experiments. ns: $p \geq 0.05$, with p being calculated using two-tailed Mann-Whitney test.

4.6 Changes in NHDF metabolism after adaptation to OXPHOSm were not accompanied by changes in cellular energetic state.

Results shown in the previous chapters corroborate several studies found in the literature, which show that cultivating cells without glucose leads to a metabolic shift to a more oxidative phenotype (Rossignol et al., 2004, Gohil et al., 2010, Sanuki et al., 2017, Pereira et al., 2018), since, in Subchapters 3.3 and 4.1, it is shown that this approach increases several OCR-associated parameters. In this subchapter, the main

objective was to explore the molecular causes behind these alterations in a metabolic point of view.

4.6.1 Adaptation to OXPHOSm increased the expression and/or the levels of several OXPHOS complexes subunits, accompanied by an increase in complex I activity.

Considering that, in the cells, most oxygen is consumed in the OXPHOS system, parameters related to OXPHOS complexes are obvious candidates to be altered in response to the metabolic remodeling caused by adaptation to OXPHOSm. In fact, previous studies have already described an increased gene expression of several mtDNA-encoded OXPHOS complexes subunits after adaptation to OXPHOSm (Pereira et al., 2018) and also in protein levels of some subunits (Rossignol et al., 2004, Pereira et al., 2018).

Our results show that adaptation to OXPHOSm promoted an increase in the expression of mtDNA-encoded ND2 (complex I), CYB (complex III), COX3 (complex IV) and ATP6 (complex V) genes (Figures 4.15A to D), as well as in nuclear DNA-encoded NDUFA9 (complex I), SDHA (complex II), UQCRC2 (complex III), COX4i1 (complex IV) and ATP5G1 (complex V) genes (Figures 4.15E to I), most with statistical significance, when compared to the expression of these genes in HGm-grown cells. In addition, also CYCS (cytochrome c) gene expression was increased, although without statistical significance, as shown in Figure 4.15J.

However, these results were not confirmed by the protein levels, in accordance to what described in HeLa and in human lung fibroblast MRC5 cells (Rossignol et al., 2004) and for BJ cells (Pereira et al., 2018), since, with exception of complex I, in which seems to be more abundant in OXPHOSm-adapted cells, although not significantly, all the differences are modest, as represented in Figure 4.15K.

Considering these data, evaluation of the activity of mitochondrial complexes and of mitochondrial potential gained relevance, since complexes could be more active without an increase in their levels. Figure 4.15L shows complex I activity, measured in-gel after blue native electrophoresis. Evaluation of the activity of other complexes

is also important but was not yet optimized in the laboratory. In the figure, it is possible to observe a statistically non-significant increase in complex I activity. Several molecular factors altered by this metabolic remodeling can lead to this increase in complex I activity without affecting its protein levels. For example, NAD-dependent deacetylase Sirtuin-3 (SIRT3) reversibly binds to NDUFA9 complex I subunit, regulating its deacetylation and enhancing its activity (Ahn et al., 2008, Duong et al., 2016). PTEN-induced putative kinase 1 (PINK1), a kinase that phosphorylates complex I and helps complex I assembly, being essential for its activity (Morais et al., 2014, Pogson et al., 2014), might be involved in this increased activity. Also, Cyclic Adenosine Monophosphate (cAMP)/Protein Kinase A (PKA) pathway arises as a candidate for this increased activity, since there are evidences that PKA phosphorylates NDUFS4 subunit (Papa et al., 2001, Papa et al., 2012). De Rasmo *et al.* proposed that cAMP/PKA pathway drives the import of newly synthesized NDUFS4 subunit into mitochondria, in order to replace subunits damaged by ROS and, therefore, increasing complex activity (De Rasmo et al., 2015). Another candidate, although less obvious and less probable is protein deglycase (DJ-1), an important molecule for redox equilibrium maintenance in cells, particularly in neurons (Zhou et al., 2006), that has been described to bind NDUFA4 and ND1 complex I subunits, being important to maintain complex activity and integrity (Hayashi et al., 2009, Duong et al., 2016). In the future, all these molecular factors should be explored to give clues about the molecular mechanism behind these results.

Complex IV activity was also measured, but due to lack of optimization, results are not trustable and are shown in supplementary Chapter 8.2.

These differences were not observed in LGm-adapted NHDF cells, which helps to explain the similar OCR-associated parameters values in these cells compared with HGm-grown cells.

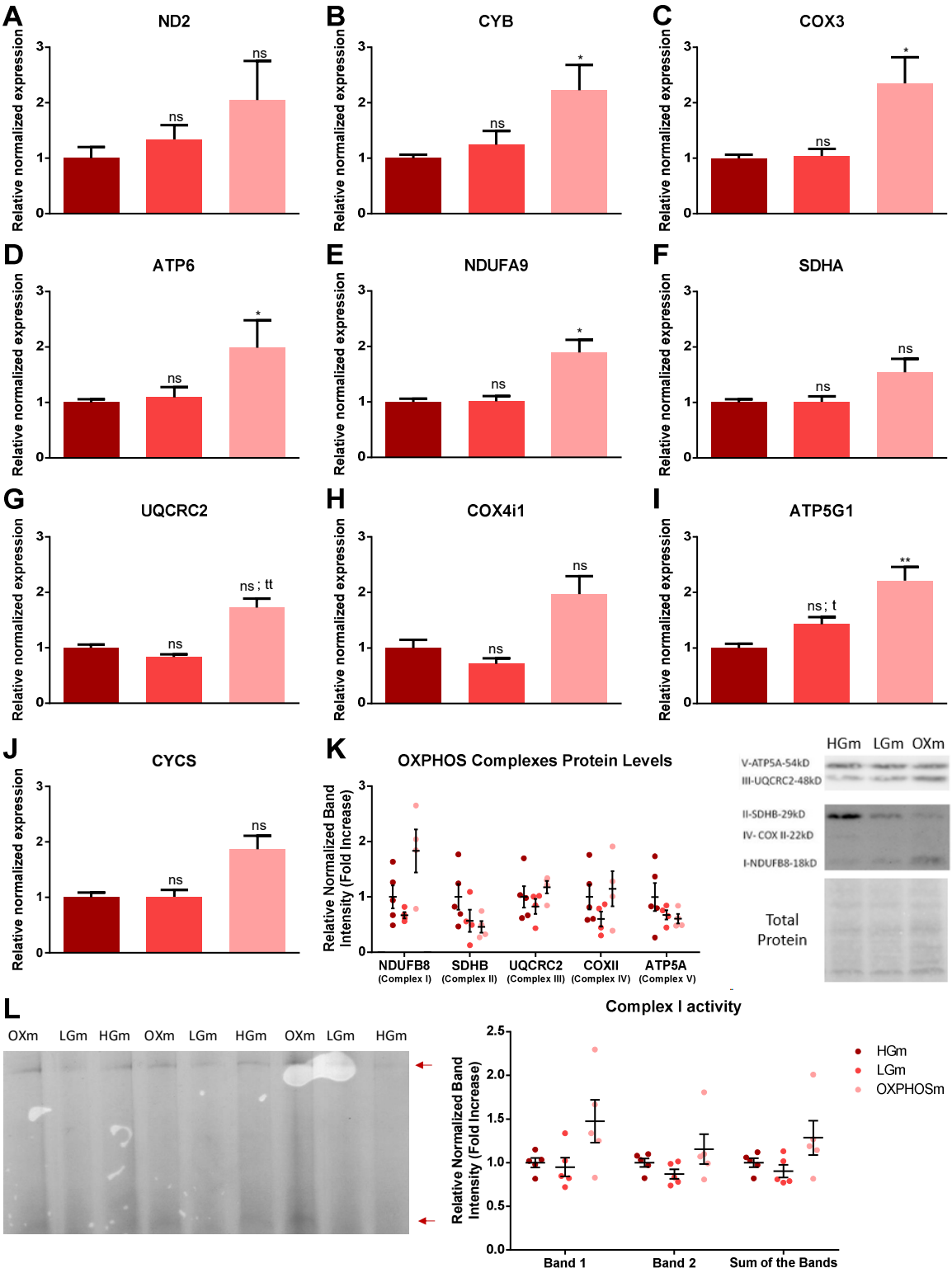

Figure 4.15 A to J ND2, CYB, COX3, ATP6, NDUFA9, SDHA, UQCRC2, COX4i1, ATP5G1 and CYCS gene expression in cells grown in HGm or adapted to LGm or OXPHOSm. Total RNA was extracted, purified, converted into cDNA, and amplified by qRT-PCR. Gene expression was measured and normalized to B2M, HPRT1 and RNA18S levels, and divided by the mean of the values obtained for HGm-grown cells. Data are expressed as mean ± SEM of 5 independent experiments. **: p<0.01, *: p<0.05, ns: p≥0.05, with p being calculated using Kruskal-Wallis

test with Dunn's multiple comparisons test vs HGm; tt: $p<0.01$, t: $p<0.05$, with p being calculated using two-tailed Mann-Whitney test vs HGm. **K** OXPHOS complexes Protein Levels in cells grown in HGm or adapted to LGm or OXPHOSm. Protein levels were measured by Western Blot and normalized to total protein levels. Images at right show representative blots. Data are expressed as mean ± SEM of 4-5 independent experiments. Dots represent individual measurements. **L** Complex I activity in cells grown in HGm or adapted to LGm or OXPHOSm. Activity was measured in-gel, through the appearance of purple bands, correspondent to the oxidation of NADH by NTB. Image at left shows representative gel. Arrows indicate the location of the two bands. Data are expressed as mean ± SEM of 5 independent experiments. Dots represent individual measurements.

4.6.2 Adaptation to OXPHOSm led to increased expression of several genes related to cell general metabolism.

Given the most oxidative phenotype of OXPHOSm-adapted cells, we evaluated several metabolism-related transcripts expression, namely, glycolytic enzymes glyceraldehyde 3-phosphate dehydrogenase (GAPDH) and pyruvate kinase (PKM), galactose metabolism enzymes GALK1, GALK2, GALE and GALT, pyruvate dehydrogenase complex subunits PDHA1, DLD and DLAT, as well as pyruvate dehydrogenase kinase 1 (PDK1), glutaminase (GLS) and GLS2 and GLUT1.

In Figure 4.16A to D, it is possible to observe that both GALK1, GALE and GALT were highly upregulated in cells adapted to OXPHOSm, emphasizing the importance of galactose metabolization in cells that cannot use glucose due to its absence. This is consistent to what was published by Pereira *et al.* (2018), which showed increases in GALE and GALK1 expression (Pereira et al., 2018). It is worth to note, however, that our data should be confirmed with protein levels and with enzymatic activities.

Interestingly, in what regards glycolytic enzymes, we saw a significant increase in GAPDH gene expression, as well as a tendency (significant when Mann-Whitney test was used) for increased PKM expression (Figure 4.16E and F). Although these results are contrary to what would be expected, they can be somehow linked to the data shown by Rossignol *et al.* (2004), which showed that the glycolytic system was similar in HeLa cells grown with or without glucose (Rossignol et al., 2004). Rossignol used Hexokinase (HK) I and II protein levels to draw this conclusion, which are not important for galactose metabolization, and postulated that these similar HK protein

levels were a characteristic of the cell line used, which was cancer-derived. This postulation cannot be applied to our data but can support one possible reason for the increases observed by us, which is the need to achieve higher glycolytic efficiency, given the lack of glucose in medium. Another result that might support this is the small, non-significant, increase in gene expression of GLUT1 transporter in OXPHOSm-adapted cells (Figure 4.16G), responsible not only for glucose but also for galactose uptake (Zhao and Keating, 2007, Cura and Carruthers, 2012, Nelson and Cox, 2013). Given that galactose uptake through this transporter is slower, this increase might be associated with the mentioned need. For the record, in HeLa cells, this increase was not observed (Rossignol et al., 2004). Evaluation of protein levels and enzymatic activity of these proteins, and also of the remaining glycolytic enzymes, is very important to draw stronger conclusions.

We evaluated also the metabolism of the other OXPHOSm compounds, namely, glutamine and pyruvate, as shown in Figures 4.16H to L. As shown in Figure 4.16H, we observed no differences in GLS gene expression in OXPHOSm-adapted and in HGm-grown cells, although a small tendency was observed, while we were not able to detect GLS2 expression. In what regards PDH complex, PDHA1 transcript levels were significantly increased (Figure 4.16I), suggesting an increase in the forwarding of pyruvate to the Krebs cycle. This result is supported by the observations of Rossignol *et al.* (2004), which showed that, in cells grown without glucose, PDH protein levels were increased (Rossignol et al., 2004) and also by the ECAR values measured in both conditions in the previous subchapters. Interestingly, gene expression of PDH negative regulator PDK1 was also increased, although statistical significance was only obtained when Mann-Whitney test was used, as shown in Figure 4.16L. This overexpression, by itself, does not mean a bigger inhibition of PDH. That assumption can only be made after the evaluation of pyruvate dehydrogenase enzymatic activity or protein phosphorylation levels. Once again, all these results of gene expression should be confirmed by evaluating the levels of the respective proteins and their activities.

All the differences mentioned in this subchapter were not observed in LGm-adapted NHDF cells when compared to HGm-grown cells, with the only exception being GLS expression (Figure 4.16H), and only when Mann-Whitney test was used. This similarity is another argument favoring the fact that, metabolically, cells cultured in LGm or HGm are very similar.

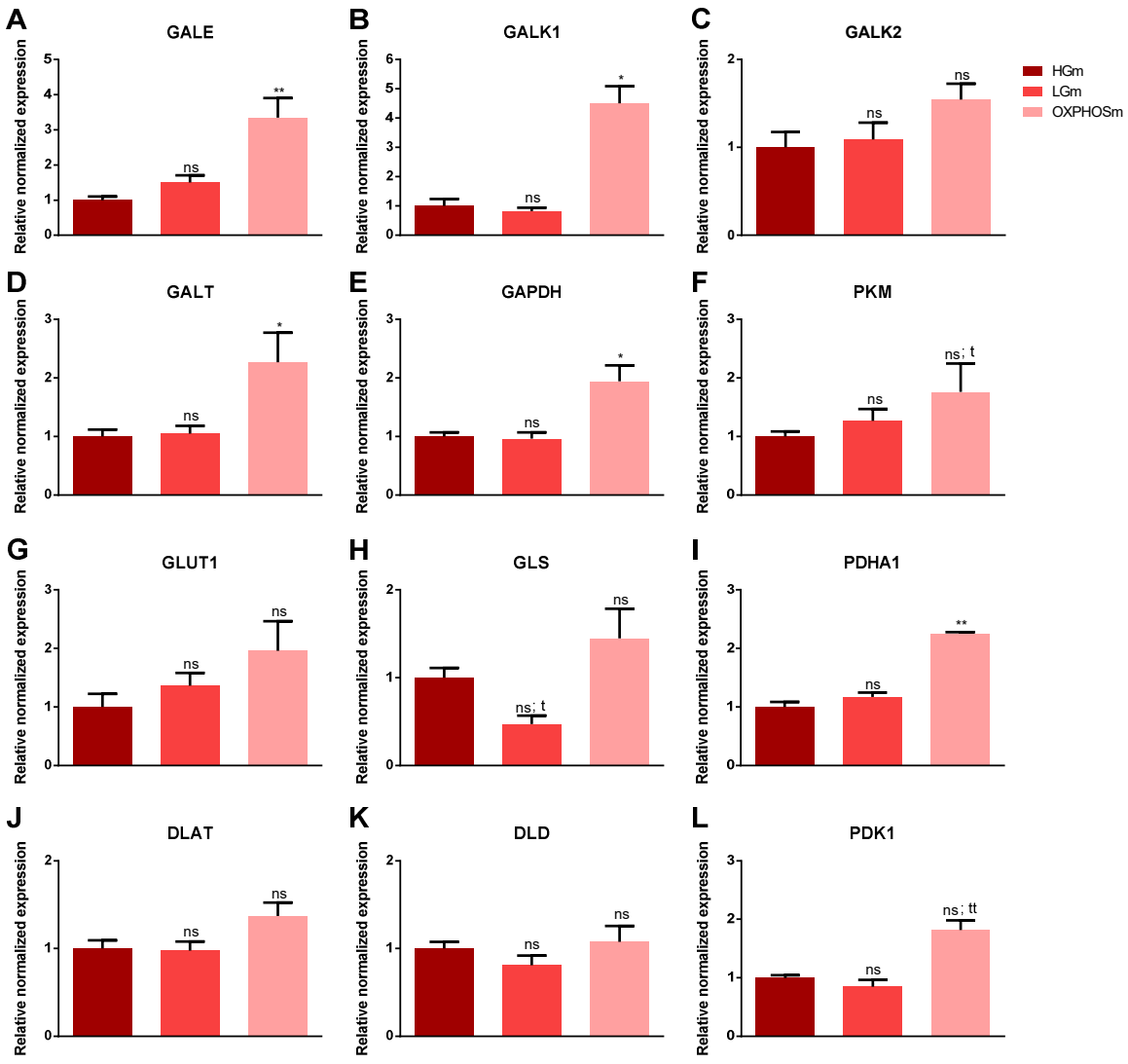

Figure 4.16 GALE, GALK1, GALK2, GALT, GAPDH, PKM, GLUT1, GLS, PDHA1, DLAT, DLD and PDK1 gene expression in cells grown in HGm or adapted to LGm or OXPHOSm. Total RNA was extracted, purified, converted into cDNA, and amplified by qRT-PCR. Gene expression was measured and normalized to B2M, HPRT1 and RNA18S levels, and divided by the mean of the values obtained for HGm-grown cells. Data are expressed as mean ± SEM of 5 independent experiments. **: $p<0.01$, *: $p<0.05$, ns: $p\geq0.05$, with p being calculated using Kruskal-Wallis test with Dunn's multiple comparisons test vs HGm; tt: $p<0.01$, t: $p<0.05$, with p being calculated using two-tailed Mann-Whitney test vs HGm.

4.6.3 Adaptation to OXPHOSm seemed to increase mitochondrial content.

Oxidative capacity of cells can be assessed using quantitative indicators such as mitochondrial content (Larsen et al., 2012). Thus, given the increased maximal respiration in OXPHOSm-adapted cells (Subchapter 4.1) and given the results presented in Subchapter 4.6.1, mitochondrial content should be also increased.

That hypothesis was tested using two mitochondrial content markers, namely, the commonly used mtDNA copy number (Malik and Czajka, 2013) and also mitochondrial chaperonin Heat Shock Protein (HSP60) protein levels.

Results are shown in Figure 4.17, and, indeed, seem to show that mitochondrial content was increased, given the increase in mtDNA copy number, although statistical significance was observed only when Mann-Whitney test used. These results support the findings of Pereira *et al*. (2018) in the BJ cell line (Pereira et al., 2018), while contradicting the results shown by Rossignol *et al*. (2004) in HeLa cell line (Rossignol et al., 2004). Confirmation of these results with other mitochondrial content markers, such as TOM20 or citrate synthase protein levels (Pereira et al., 2018) or cardiolipin content (Larsen et al., 2012) would confer more confidence to these results.

To explain these results, we hypothesize that mitochondrial biogenesis occurred. As already mentioned, adaptation to OXPHOSm can be considered a stress situation (Palmfeldt et al., 2009). Presumably, initially, the AMP/ATP and NAD^+/NADH ratios increase. If this happens, it may lead to the activation of AMP-activated protein kinase (AMPK) and Sirtuin-1 (SIRT1), which in turn activate peroxisome proliferator-activated receptor gamma coactivator-1α (PGC1α) (Nirwane and Majumdar, 2018, Picca et al., 2018). Activation of PGC1α unleashes a signaling pathway that culminates in mitochondrial biogenesis (Nirwane and Majumdar, 2018, Picca et al., 2018). Although we consider this hypothesis, we do not yet have data to support it. In Subchapter 8.3, measurements of the gene expression of several factors involved in the process are shown. However, these measurements were performed with RNA extracted in already adapted cells, so they give little information. More useful will be measure the expression of some genes and proteins in cells undergoing adaptation, or

immediately after the adaptation process, given that, according to the results shown in Figure 4.11, it takes some time before cells are fully adapted. Among the genes and/or proteins of interest are the mentioned phospho-AMPK (activated form of AMPK), SIRT1 and PGC1α, the phosphorylated fork head box O3 (FoxO3) (activated form), which is a transcriptional factor activated by AMPK that is involved in the activation of PGC1α (Nirwane and Majumdar, 2018), nuclear respiratory factors 1 and 2 (NRF1 and NRF2) and peroxisome proliferator-activated receptor-α (PPARα), which are transcriptional factors involved in mitochondrial transcription factor A (TFAM) synthesis (Nirwane and Majumdar, 2018), and TFAM, which is involved in mtDNA transcription, replication and maintenance (Nirwane and Majumdar, 2018, Picca et al., 2018). In addition, evaluation of cardiolipin content and of cardiolipin synthase gene expression and protein levels might be also interesting.

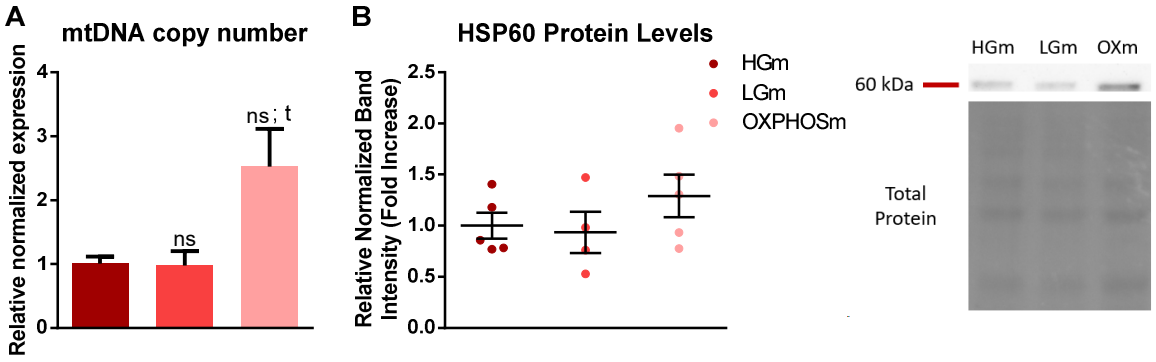

Figure 4.17 A mtDNA copy number in cells grown in HGm or adapted to LGm or OXPHOSm. Total DNA was extracted,purified, and amplified by qRT-PCR. mtDNA copy number was measured by quantifying CYB expression, normalized to RNAseP levels, and divided by the mean of the values obtained for HGm-grown cells. Data are expressed as mean ± SEM of 5-7 independent experiments. ns: $p \geq 0.05$, with p being calculated using Kruskal-Wallis test with Dunn's multiple comparisons test vs HGm; t: $p < 0.05$, with p being calculated using two-tailed Mann-Whitney test vs HGm. **B** HSP60 Protein Levels in cells grown in HGm or adapted to LGm or OXPHOSm. HSP60 protein levels were measured by Western Blot and normalized to total protein levels. Images at right show representative blots. Data are expressed as mean ± SEM of 4-5 independent experiments. Dots represent individual measurements.

4.6.4 Adaptation to OXPHOSm did not affect general cellular energetic state.

In the previous chapters, we have demonstrated that, associated to the metabolic

remodeling of NHDF cells after adaptation to OXPHOSm, there are several molecular changes, not only metabolic but also structural. Having that in consideration, an important question arises: do these changes affect general cellular energetic state?

To answer that question, adenine nucleotides were extracted from cells grown in HGm and adapted or not to OXPHOSm or to LGm and quantified, by HPLC, in order to calculate ATP/ADP ratio and Energy Charge (Equation 1), which may elucidate about the cellular energy levels (Atkinson and Walton, 1967, Khlyntseva et al., 2009, Maldonado and Lemasters, 2014, Will and Dykens, 2018). Results are shown in Figure 4.18.

$$\text{Energy Charge} = \frac{[\text{ATP}]+\frac{1}{2}[\text{ADP}]}{[\text{ATP}]+[\text{ADP}]+[\text{AMP}]} \qquad \text{(Equation 1) (Atkinson and Walton, 1967)}$$

As shown in the figure, both ATP/ADP ratio and energy charge values are similar in all the conditions tested, indicating that, whatever are the components available for metabolization, cells adapt to produce ATP from them, with the energetic state being maintained independently of those sources. To address this with more precision and to confirm the shift in ATP production pathways, new Seahorse real-time ATP rate assay kit can be used or, alternatively, measurements of ATP/ADP ratios in the present of inhibitors of OXPHOS or glycolysis can be performed.

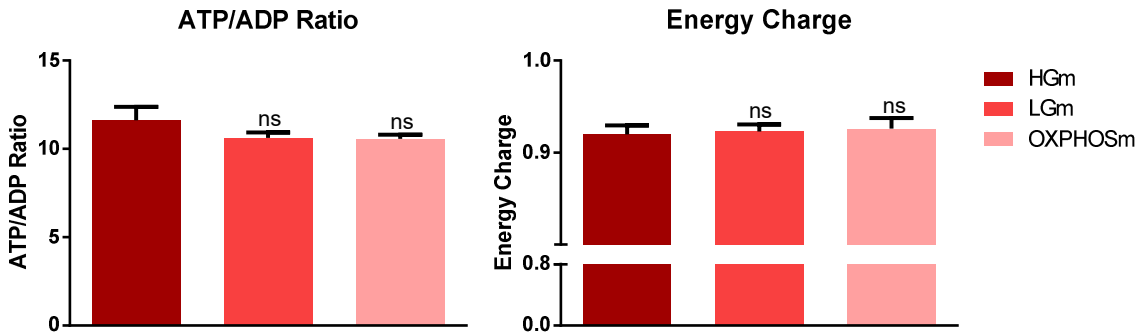

Figure 4.18 ATP/ADP ratio and Energy Charge in NHDF cells grown in HGm or adapted to LGm or OXPHOSm. ATP, ADP and AMP were measured by HPLC. Data are expressed as mean ± SEM of 4-5 independent experiments. ns: p≥0.05, with p being calculated using Kruskal-Wallis test with Dunn's multiple comparisons test.

4.7 Adaptation to OXPHOSm promoted some structural changes in NHDF cell line.

In the previous chapters, we showed that NHDF cells grown without glucose, in presence of galactose, glutamine and pyruvate, become more oxidative. In this chapter, several structural parameters were evaluated, in order to characterize the cells adapted to OXPHOSm.

4.7.1 Adaptation to OXPHOSm led to an increase in β-actin gene expression but did not lead to increased actin protein levels.

Actin is a highly conserved protein found in eukaryotic cells, being the most abundant protein and the most important protein for protein-protein interactions (Dominguez and Holmes, 2011). One of the most important functions of actin in cells is to be part of cytoskeleton, being important for cell dynamics and other functions (Lodish, 2000).

Cells express several actin isoforms. One of the main ones is the ubiquitous β-actin (Dominguez and Holmes, 2011). β-actin gene is often used as a housekeeping gene for qRT-PCR (Lin and Redies, 2012). However, there are data pointing out some limitations of normalization of gene expression by β-actin messenger RNA (mRNA), given that its expression depends on cell type (Lin and Redies, 2012). In addition, given the dynamic instability of cytoskeleton, cell size might suffer alterations in response to stress situations, and, in that case, also actin expression might change.

Having this idea in mind, β-actin (ACTB) gene expression was evaluated, and the results are shown in Figure 4.19A. This data indicates that adaptation of NHDF cells to OXPHOSm increased ACTB gene expression, which suggests an increased cell size or, alternatively, a structural remodeling in response to the metabolic remodeling promoted by adaptation to OXPHOSm. These results were not confirmed by changes in actin protein levels, which seemed to be similar is all conditions tested (Figure 4.19B). However, it is possible to postulate that the results of Western Blot experiment might not be correctly normalized, because, in an empirical reasoning, an alleged increase in cell size accompanied by an increase in actin levels would also be

accompanied by an increase in total protein levels, which is the normalizing parameter used in this experiment.

To test the hypothesis that adaptation to OXPHOSm leads to an increase in cell size, a more accurate evaluation is required, for example, by fluorescence microscopy, using probes such as CellTracker™ Green dye.

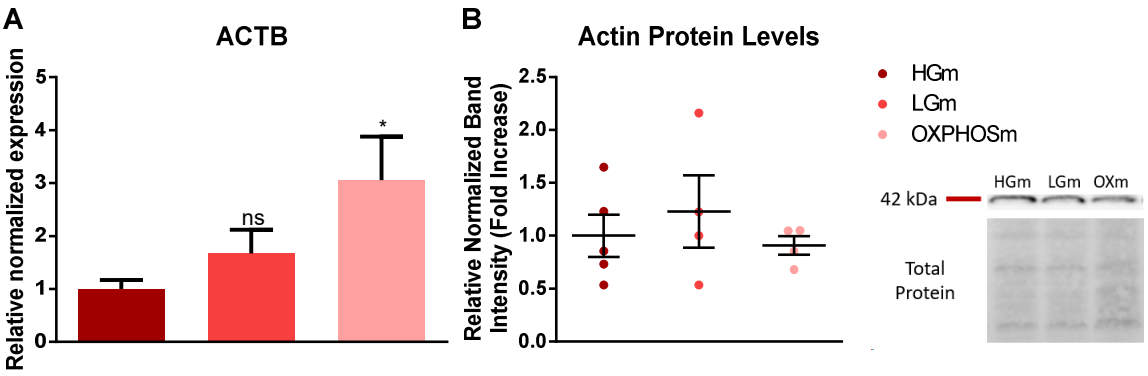

Figure 4.19 A ACTB gene expression in NHDF cells grown in HGm or adapted to LGm or OXPHOSm. Total RNA was extracted, purified, converted into cDNA, and amplified by qRT-PCR. Gene expression was measured and normalized to B2M, HPRT1 and RNA18S levels, and divided by the mean of the values obtained for HGm-grown cells. Data are expressed as mean ± SEM of 5 independent experiments. *: $p<0.05$, ns: $p\geq0.05$, with p being calculated using Kruskal-Wallis test with Dunn's multiple comparisons test vs HGm. **B** ACTB Protein Levels in cells grown in HGm or adapted to LGm or OXPHOSm. ACTB protein levels were measured by Western Blot and normalized to total protein levels. Image at right shows the blot represented in the data at the graph. Data are expressed as mean ± SEM of 4-5 independent experiments. Dots represent individual measurements.

4.7.2 Adaptation to OXPHOSm promoted changes in mitochondrial network.

Mitochondrial network formation in cells is associated with several physiological functions, including the increase in the efficiency of ATP production (Hoitzing et al., 2015). Thus, metabolic remodeling associated with adaptation to OXPHOSm might lead to mitochondrial network structural reorganization. In this subchapter, we intended to understand whether the increase in mitochondrial content, reported in the previous subchapters, was translated into an increase in mitochondrial area, and in that case a change in mitochondrial morphology could be a possible cause. Images were obtained by fluorescence microscopy, using TMRM dye for mitochondria labeling and Hoechst dye for nuclei labeling.

Representative images of each condition are shown in Figure 4.20A to C. It is possible to observe a bigger mitochondrial area per cell in cells adapted either to OXPHOSm and to LGm, when compared to cells grown in HGm. These data were quantified in Figure 4.20D. These results were actually the opposite to what was observed by Rossignol *et al.* (2004) in HeLa cells, in which cellular area was higher in cells grown with glucose. However, in the same work, contrarily to what was observed by us in NHDF cells, mitochondrial content was also not increased in OXPHOSm-adapted cells (Rossignol et al., 2004). Rossignol and colleagues also showed that mitochondria in OXPHOSm-adapted cells were more elongated, which was also observed by Pereira *et al.* (2018) (Rossignol et al., 2004, Pereira et al., 2018). However, in our images, it is not possible to visualize this, due to the low amplification used by us.

Using the same images, TMRM intensity was measured, to quantify mitochondrial membrane potential. This is possible because the probe accumulates in mitochondria proportionally to its membrane potential (Scaduto and Grotyohann, 1999). Results are in Figure 4.20E, showing increased membrane potential not only in OXPHOSm-adapted NHDF cells but also in their LGm-adapted counterparts. The results related to OXPHOSm-adapted cells are in accordance to what was previously described, since the metabolism of these cells was found to be more reliant in OXPHOS in the previous subchapters, being that supported by several works found on literature (Sanuki et al., 2017, Pereira et al., 2018).

The same cannot be said about the results obtained for LGm-adapted NHDF cells, since most metabolism-related parameters were more similar to HGm-grown cells than to OXPHOSm-adapted cells, suggesting a more glycolytic phenotype. Confirmation of this result should be a priority, given the apparently contradiction. One way to do that is by evaluating complex V activity, since proton gradient is used to other ends rather than ATP synthesis, for example, heat production through Uncoupling Proteins (UCP) (Krauss et al., 2005). Seahorse results, shown in Subchapters 4.1 and 4.2, seem to suggest that complex V activity is indeed decreased,

given the lower ATP Production-linked respiration in LGm-adapted cells in comparison with OXPHOSm-adapted cells, although no differences in proton leak were found.

In the future, fluorescence microscopy with higher amplifications or other techniques should be performed in cells grown under these conditions, in order to evaluate structural parameters that are difficult to evaluate with this amplification, including not only mitochondria elongation, but also cristae number or intra-cristal area, which were found to be increased in HeLa cells grown without glucose (Rossignol et al., 2004).

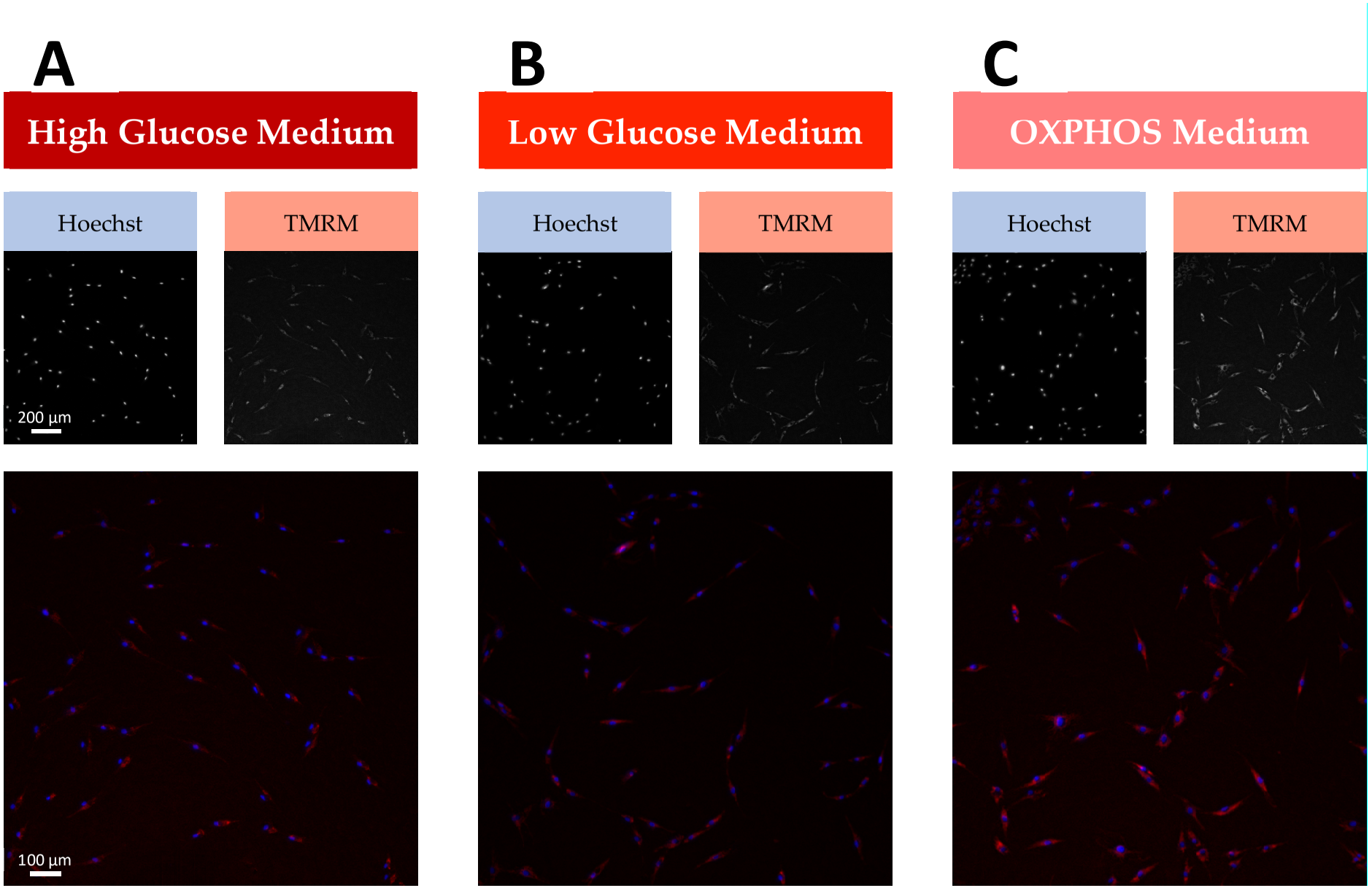
A
High Glucose Medium
Hoechst
TMRM
200 µm
100 µm
B
Low Glucose Medium
Hoechst
TMRM
C
OXPHOS Medium
Hoechst
TMRM

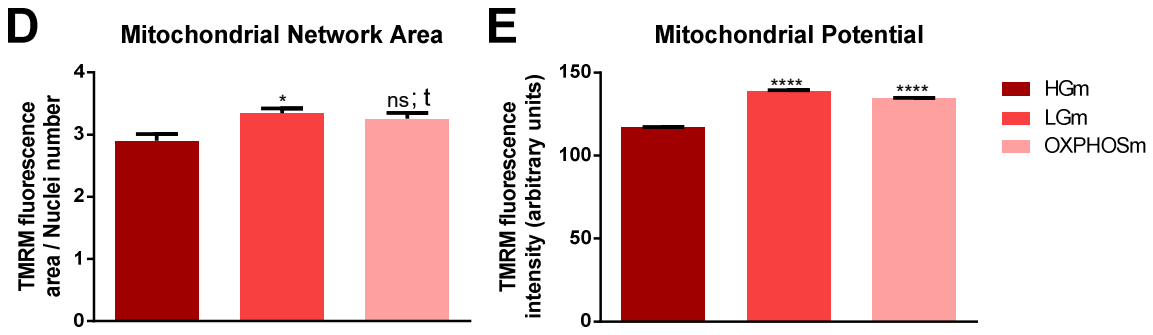

Figure 4.20 Mitochondria in NHDF cells grown in HGm and adapted to OXPHOSm or to LGm. NHDF cells were plated with a density of 2000 cells/well and incubated with 100 nM TMRM and 0.5 µg/ml Hoechst. Imaging was performed by fluorescence microscopy, with 10x ampliation. Representative images of HGm-grown, LGm-adapted or OXPHOSm-adapted cells are in figures **A to C**, respectively. **D** Mitochondrial network area, normalized to nuclei number. **E** Mitochondrial membrane potential, assessed by measuring TMRM fluorescence intensity. Data are expressed as mean ± SEM of 3 independent experiments performed 8-16 times. ****: $p<0.0001$, *: $p<0.05$, ns: $p\geq0.05$, with p being calculated using Kruskal-Wallis test with Dunn's multiple comparisons test; t: $p<0.05$, with p being calculated using two-tailed Mann-Whitney test.

Chapter V
Conclusions

Adaptation of cells to media without glucose gained relevance in the last years, given their effect in sensitizing cells to mitochondrial toxicants. However, this methodology has more applications. A first example is biomedicine, since it may allow to detect if mitochondrial defects are involved in the etiology of diseases, as shown by Ghelli *et al.* for LHON (Ghelli et al., 2003). Another example that is quite unexplored is related with drug development, concretely, mitochondrial protection studies, given that reproducibility of the results for tBHP toxicity was much higher for OXPHOSm-adapted NHDF cells, when compared to cells grown with glucose, and given that were able to observe protection by mitochondria-targeted antioxidants.

As mentioned before, one of the big gaps regarding this methodology is the lack of standardization, which is something that prevents comparisons between the works found in literature. Having this in mind, our work focused on the technique more than in the applications.

Usually, the adaptation period depends on the cell line used (Marroquin et al., 2007, Swiss and Will, 2011). For the NHDF cell line, we found that adaptation in one passage was enough for OXPHOS stimulation. In regard to media composition, our work offers some interesting contributions to what was already known, although we ended up choosing the traditionally used OXPHOSm. The major contribution is the conclusion that pyruvate supplementation is unnecessary in the culture media when sugars are present, since its removal produced a small effect on OCR and in OCR-associated parameters (Figure 4.8). Therefore, although in this work pyruvate was used, for upcoming works its supplementation should be discarded, since we may be introducing a variable that seems to be useless.

Despite all the results shown in this work, there are still some points that can be tested, such as the impact of the substitution of glutamine by glutamate or α-

ketoglutarate, both having the advantage of theoretically decreasing nitrogen levels in cells.

Another important contribution from the present work is the observation that NHDF cells cultured in LGm are more similar to NHDF cells cultured in HGm, than to cells cultured in OXPHOSm. Therefore, for *in vitro* testing, LGm can be a replacer of HGm, and not of OXPHOSm, as we wanted to test. In this work, it was shown that LGm-adapted cells are metabolically much closer to HGm-grown cells than to OXPHOSm-adapted cells, although some important differences were pointed. For many purposes, including the most important applications of this methodology, LGm can be used instead of HGm, with the big advantage of being closer to the physiological conditions that cells experience. The biggest handicap was related with antioxidant defenses, since these cells were much more sensitive to tBHP than HGm-grown cells, and since SOD2 levels also seemed to be decreased. Evaluation of other endogenous antioxidant defenses should be done to confirm this result.

To sum up, our method to stimulate OXPHOS in NHDF cells seemed to increase their OXPHOS-reliance, as desired, which did not occur shortly after exposure to this medium, as was shown for HepG2 cell line (Sanuki et al., 2017). This adaptation sensitized cells for the toxic effects of some mitochondrial drugs, such as antimycin A, rotenone and oligomycin. In addition, our method also seems to have potential for mitochondrial protection studies, as explored in Subchapter 4.5. These effects were accompanied by several molecular changes, such as in gene expression and/or in the protein levels of OXPHOS complexes subunits and other metabolism-related proteins, complex I activity, mitochondrial content and mitochondrial membrane potential. These changes, however, were not translated into changes in cellular energetic state, given that both energy charge and ATP/ADP ratio values were similar in all conditions tested, underlining that whatever are the components available for metabolization, cells adapt and produce what they need with those components.

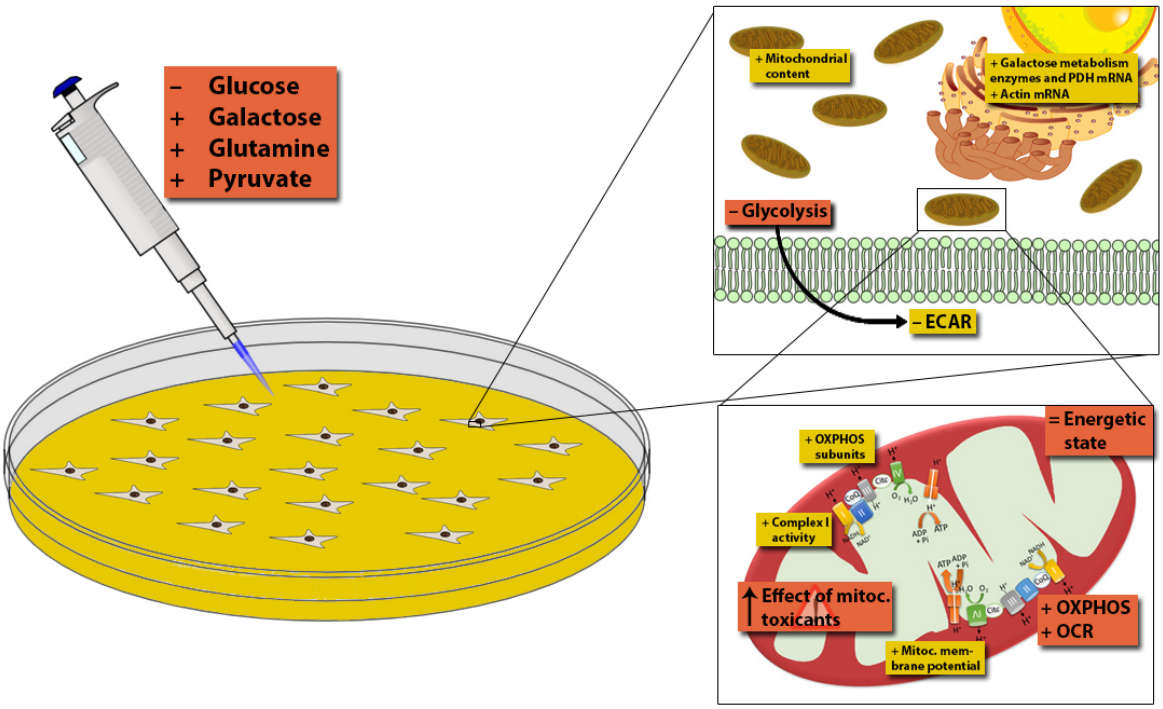

Figure 5.1 Growing cells in media without glucose induces several molecular changes in NHDF cells, such as increases in transcription of galactose metabolism enzymes, PDH and actin, in mitochondrial content, in OXPHOS subunits gene expression and protein levels, in complex I activity and in mitochondrial membrane potential. Associated to these changes, a decrease in glycolysis and an increase in OXPHOS were observed, without changes in energetic state, which sensitized cells to the toxic effect of mitochondrial drugs.

Chapter VI

Image Copyrights

Figures 1.1, 1.2, 1.4, 1.5 and 1.6 were used under a Creative Commons License. Figure 1.3 is available at Agilent® website (http://www.agilent.com/en-us/products/cell-analysis-(seahorse)/mitochondrial-respiration-the-xf-cell-mito-stress-test). Remaining figures are original.

Chapter VII
References

Aguer C, Gambarotta D, Mailloux RJ, Moffat C, Dent R, McPherson R, Harper ME (2011) Galactose enhances oxidative metabolism and reveals mitochondrial dysfunction in human primary muscle cells. PloS one 6:e28536.

Ahn BH, Kim HS, Song S, Lee IH, Liu J, Vassilopoulos A, Deng CX, Finkel T (2008) A role for the mitochondrial deacetylase Sirt3 in regulating energy homeostasis. Proceedings of the National Academy of Sciences of the United States of America 105:14447-14452.

Altamirano C, Illanes A, Becerra S, Cairo JJ, Godia F (2006) Considerations on the lactate consumption by CHO cells in the presence of galactose. Journal of biotechnology 125:547-556.

Ambrosi G, Ghezzi C, Sepe S, Milanese C, Payan-Gomez C, Bombardieri CR, Armentero MT, Zangaglia R, Pacchetti C, Mastroberardino PG, Blandini F (2014) Bioenergetic and proteolytic defects in fibroblasts from patients with sporadic Parkinson's disease. Biochimica et biophysica acta 1842:1385-1394.

Atkinson DE, Walton GM (1967) Adenosine triphosphate conservation in metabolic regulation. Rat liver citrate cleavage enzyme. The Journal of biological chemistry 242:3239-3241.

Auburger G, Klinkenberg M, Drost J, Marcus K, Morales-Gordo B, Kunz WS, Brandt U, Broccoli V, Reichmann H, Gispert S, Jendrach M (2012) Primary skin fibroblasts as a model of Parkinson's disease. Molecular neurobiology 46:20-27.

Aussel C, Coudray-Lucas C, Lasnier E, Cynober L, Ekindjian OG (1996) alpha-Ketoglutarate uptake in human fibroblasts. Cell biology international 20:359-363.

Babich H, Liebling EJ, Burger RF, Zuckerbraun HL, Schuck AG (2009) Choice of DMEM, formulated with or without pyruvate, plays an important role in assessing the in vitro cytotoxicity of oxidants and prooxidant nutraceuticals. In vitro cellular & developmental biology Animal 45:226-233.

Benfeito S, Oliveira C, Soares P, Fernandes C, Silva T, Teixeira J, Borges F (2013) Antioxidant therapy: still in search of the 'magic bullet'. Mitochondrion 13:427-435.

Berg JM, Tymoczko JL, Stryer L (2002) Biochemistry. New York: W.H. Freeman.

Blomme EA, Will Y (2016) Toxicology Strategies for Drug Discovery: Present and Future. Chemical research in toxicology 29:473-504.

Bogdan Allemann I, Baumann L (2008) Antioxidants used in skin care formulations. Skin therapy letter 13:5-9.

Bradford MM (1976) A rapid and sensitive method for the quantitation of microgram quantities of protein utilizing the principle of protein-dye binding. Analytical biochemistry 72:248-254.

Brand MD, Nicholls DG (2011) Assessing mitochondrial dysfunction in cells. The Biochemical journal 435:297-312.

Broer S (2014) The SLC38 family of sodium-amino acid co-transporters. Pflugers Archiv : European journal of physiology 466:155-172.

Brown MD, Voljavec AS, Lott MT, Torroni A, Yang CC, Wallace DC (1992) Mitochondrial DNA complex I and III mutations associated with Leber's hereditary optic neuropathy. Genetics 130:163-173.

Brunmair B, Lest A, Staniek K, Gras F, Scharf N, Roden M, Nohl H, Waldhausl W, Furnsinn C (2004) Fenofibrate impairs rat mitochondrial function by inhibition of respiratory complex I. The Journal of pharmacology and experimental therapeutics 311:109-114.

Byrne AM, Lemasters JJ, Nieminen AL (1999) Contribution of increased mitochondrial free Ca2+ to the mitochondrial permeability transition induced by tert-butylhydroperoxide in rat hepatocytes. Hepatology 29:1523-1531.

Chen Q, Zhang T, Roshetsky JF, Ouyang Z, Essers J, Fan C, Wang Q, Hinek A, Plow EF, Dicorleto PE (2009) Fibulin-4 regulates expression of the tropoelastin gene and consequent elastic-fibre formation by human fibroblasts. The Biochemical journal 423:79-89.

Coelho AI, Rubio-Gozalbo ME, Vicente JB, Rivera I (2017) Sweet and sour: an update on classic galactosemia. Journal of inherited metabolic disease 40:325-342.

Cura AJ, Carruthers A (2012) Role of monosaccharide transport proteins in carbohydrate assimilation, distribution, metabolism, and homeostasis. Comprehensive Physiology 2:863-914.

Daenzer JM, Sanders RD, Hang D, Fridovich-Keil JL (2012) UDP-galactose 4'-epimerase activities toward UDP-Gal and UDP-GalNAc play different roles in the development of Drosophila melanogaster. PLoS genetics 8:e1002721.

Dall'Asta V, Gazzola GC, Franchi-Gazzola R, Bussolati O, Longo N, Guidotti GG (1983) Pathways of L-glutamic acid transport in cultured human fibroblasts. The Journal of biological chemistry 258:6371-6379.
Dall'Asta V, Rossi PA, Bussolati O, Guidotti GG, Gazzola GC (1990) The transport of L-glutamine into cultured human fibroblasts. Biochimica et biophysica acta 1052:106-112.
Davit-Spraul A, Pourci ML, Soni T, Lemonnier A (1994) Metabolic effects of galactose on human HepG2 hepatoblastoma cells. Metabolism: clinical and experimental 43:945-952.
De Rasmo D, Signorile A, Santeramo A, Larizza M, Lattanzio P, Capitanio G, Papa S (2015) Intramitochondrial adenylyl cyclase controls the turnover of nuclear-encoded subunits and activity of mammalian complex I of the respiratory chain. Biochimica et biophysica acta 1853:183-191.
DeFronzo RA (2004) Pathogenesis of type 2 diabetes mellitus. The Medical clinics of North America 88:787-835, ix.
Dervartanian DV, Veeger C (1964) Studies on Succinate Dehydrogenase. I. Spectral Properties of the Purified Enzyme and Formation of Enzyme-Competitive Inhibitor Complexes. Biochimica et biophysica acta 92:233-247.
Deus CM, Zehowski C, Nordgren K, Wallace KB, Skildum A, Oliveira PJ (2015) Stimulating basal mitochondrial respiration decreases doxorubicin apoptotic signaling in H9c2 cardiomyoblasts. Toxicology 334:1-11.
Dimmer KS, Friedrich B, Lang F, Deitmer JW, Broer S (2000) The low-affinity monocarboxylate transporter MCT4 is adapted to the export of lactate in highly glycolytic cells. The Biochemical journal 350 Pt 1:219-227.
Dobbing J (1989) Dietary starches and sugars in man : a comparison. London ; New York: Springer-Verlag.
Dominguez R, Holmes KC (2011) Actin structure and function. Annual review of biophysics 40:169-186.
Dott W, Mistry P, Wright J, Cain K, Herbert KE (2014) Modulation of mitochondrial bioenergetics in a skeletal muscle cell line model of mitochondrial toxicity. Redox biology 2:224-233.
Drahota Z, Krivakova P, Cervinkova Z, Kmonickova E, Lotkova H, Kucera O, Houstek J (2005) Tert-butyl hydroperoxide selectively inhibits mitochondrial respiratory-chain enzymes in isolated rat hepatocytes. Physiological research 54:67-72.
Driskell RR, Watt FM (2015) Understanding fibroblast heterogeneity in the skin. Trends in cell biology 25:92-99.
Dudzinska W, Lubkowska A, Dolegowska B, Safranow K (2010) Blood uridine concentration may be an indicator of the degradation of pyrimidine nucleotides during physical exercise with increasing intensity. Journal of physiology and biochemistry 66:189-196.
Duong A, Che Y, Ceylan D, Pinguelo A, Andreazza AC, Trevor Young L, Berk M (2016) Regulators of mitochondrial complex I activity: A review of literature and evaluation in postmortem prefrontal cortex from patients with bipolar disorder. Psychiatry research 236:148-157.
Dykens JA, Jamieson J, Marroquin L, Nadanaciva S, Billis PA, Will Y (2008a) Biguanide-induced mitochondrial dysfunction yields increased lactate production and cytotoxicity of aerobically-poised HepG2 cells and human hepatocytes in vitro. Toxicology and applied pharmacology 233:203-210.
Dykens JA, Jamieson JD, Marroquin LD, Nadanaciva S, Xu JJ, Dunn MC, Smith AR, Will Y (2008b) In vitro assessment of mitochondrial dysfunction and cytotoxicity of nefazodone, trazodone, and buspirone. Toxicological sciences : an official journal of the Society of Toxicology 103:335-345.
Elkalaf M, Andel M, Trnka J (2013) Low glucose but not galactose enhances oxidative mitochondrial metabolism in C2C12 myoblasts and myotubes. PloS one 8:e70772.
Endlicher R, Krivakova P, Rauchova H, Nuskova H, Cervinkova Z, Drahota Z (2009) Peroxidative damage of mitochondrial respiration is substrate-dependent. Physiological research 58:685-692.
Fagerberg L, Hallstrom BM, Oksvold P, Kampf C, Djureinovic D, Odeberg J, Habuka M, Tahmasebpoor S, Danielsson A, Edlund K, Asplund A, Sjostedt E, Lundberg E, Szigyarto CA, Skogs M, Takanen JO, Berling H, Tegel H, Mulder J, Nilsson P, Schwenk JM, Lindskog C, Danielsson F, Mardinoglu A, Sivertsson A, von Feilitzen K, Forsberg M, Zwahlen M, Olsson I, Navani S, Huss M, Nielsen J, Ponten F, Uhlen M (2014) Analysis of the human tissue-specific expression by genome-wide integration of transcriptomics and antibody-based proteomics. Molecular & cellular proteomics : MCP 13:397-406.
Fedotcheva NI, Mokhova EN (2013) Mechanism of induction of oxidative stress in liver mitochondria by low concentrations of tert-butyl hydroperoxide. Biochemistry Biokhimiia 78:75-79.
Ghelli A, Zanna C, Porcelli AM, Schapira AH, Martinuzzi A, Carelli V, Rugolo M (2003) Leber's hereditary optic neuropathy (LHON) pathogenic mutations induce mitochondrial-dependent apoptotic death in transmitochondrial cells incubated with galactose medium. The Journal of biological chemistry 278:4145-4150.
Gibson JB, Reynolds RA, Palmieri MJ, Berry GT, Elsas LJ, 2nd, Levy HL, Segal S (1995) Comparison of erythrocyte uridine sugar nucleotide levels in normals, classic galactosemics, and patients with other metabolic disorders. Metabolism: clinical and experimental 44:597-604.

Gohil VM, Sheth SA, Nilsson R, Wojtovich AP, Lee JH, Perocchi F, Chen W, Clish CB, Ayata C, Brookes PS, Mootha VK (2010) Nutrient-sensitized screening for drugs that shift energy metabolism from mitochondrial respiration to glycolysis. Nature biotechnology 28:249-255.

Grinnell F (1994) Fibroblasts, myofibroblasts, and wound contraction. The Journal of cell biology 124:401-404.

Grollman EF, Philp NJ, McPhie P, Ward RD, Sauer B (2000) Determination of Transport Kinetics of Chick MCT3 Monocarboxylate Transporter from Retinal Pigment Epithelium by Expression in Genetically Modified Yeast. Biochemistry 39:9351-9357.

Halestrap AP, Meredith D (2004) The SLC16 gene family-from monocarboxylate transporters (MCTs) to aromatic amino acid transporters and beyond. Pflugers Archiv : European journal of physiology 447:619-628.

Hayashi T, Ishimori C, Takahashi-Niki K, Taira T, Kim YC, Maita H, Maita C, Ariga H, Iguchi-Ariga SM (2009) DJ-1 binds to mitochondrial complex I and maintains its activity. Biochemical and biophysical research communications 390:667-672.

Hinkle PC, Kumar MA, Resetar A, Harris DL (1991) Mechanistic stoichiometry of mitochondrial oxidative phosphorylation. Biochemistry 30:3576-3582.

Hoitzing H, Johnston IG, Jones NS (2015) What is the function of mitochondrial networks? A theoretical assessment of hypotheses and proposal for future research. BioEssays : news and reviews in molecular, cellular and developmental biology 37:687-700.

Hu W, Qiu B, Guan W, Wang Q, Wang M, Li W, Gao L, Shen L, Huang Y, Xie G, Zhao H, Jin Y, Tang B, Yu Y, Zhao J, Pei G (2015) Direct Conversion of Normal and Alzheimer's Disease Human Fibroblasts into Neuronal Cells by Small Molecules. Cell stem cell 17:204-212.

Hynes J, Nadanaciva S, Swiss R, Carey C, Kirwan S, Will Y (2013) A high-throughput dual parameter assay for assessing drug-induced mitochondrial dysfunction provides additional predictivity over two established mitochondrial toxicity assays. Toxicology in vitro : an international journal published in association with BIBRA 27:560-569.

Johnson RJ, Rivard C, Lanaspa MA, Otabachian-Smith S, Ishimoto T, Cicerchi C, Cheeke PR, Macintosh B, Hess T (2013) Fructokinase, Fructans, Intestinal Permeability, and Metabolic Syndrome: An Equine Connection? Journal of equine veterinary science 33:120-126.

Kamalian L, Chadwick AE, Bayliss M, French NS, Monshouwer M, Snoeys J, Park BK (2015) The utility of HepG2 cells to identify direct mitochondrial dysfunction in the absence of cell death. Toxicology in vitro : an international journal published in association with BIBRA 29:732-740.

Kase ET, Nikolic N, Bakke SS, Bogen KK, Aas V, Thoresen GH, Rustan AC (2013) Remodeling of oxidative energy metabolism by galactose improves glucose handling and metabolic switching in human skeletal muscle cells. PloS one 8:e59972.

Kennedy CH, Church DF, Winston GW, Pryor WA (1992) tert-Butyl hydroperoxide-induced radical production in rat liver mitochondria. Free radical biology & medicine 12:381-387.

Khlyntseva SV, Bazel' YR, Vishnikin AB, Andruch V (2009) Methods for the determination of adenosine triphosphate and other adenine nucleotides. Journal of Analytical Chemistry 64:657-673.

Kim H, Esser L, Bilayet Hossain M, Xia D, Yu CA, Rizo J, van der Helm D, Deisenhofer J (1999) Structure of Antimycin A1, a Specific Electron Transfer Inhibitor of Ubiquinol-Cytochrome c Oxidoreductase. J Am Chem Soc 121:4902-4903.

Krauss S, Zhang C-Y, Lowell BB (2005) The mitochondrial uncoupling-protein homologues. Nature Reviews Molecular Cell Biology 6:248-261.

Kucera O, Endlicher R, Rousar T, Lotkova H, Garnol T, Drahota Z, Cervinkova Z (2014) The effect of tert-butyl hydroperoxide-induced oxidative stress on lean and steatotic rat hepatocytes in vitro. Oxidative medicine and cellular longevity 2014:752506.

Lapointe J, Hekimi S (2010) When a theory of aging ages badly. Cellular and molecular life sciences : CMLS 67:1-8.

Larsen S, Nielsen J, Hansen CN, Nielsen LB, Wibrand F, Stride N, Schroder HD, Boushel R, Helge JW, Dela F, Hey-Mogensen M (2012) Biomarkers of mitochondrial content in skeletal muscle of healthy young human subjects. The Journal of physiology 590:3349-3360.

Latt SA, Stetten G (1976) Spectral studies on 33258 Hoechst and related bisbenzimidazole dyes useful for fluorescent detection of deoxyribonucleic acid synthesis. The journal of histochemistry and cytochemistry : official journal of the Histochemistry Society 24:24-33.

Latt SA, Stetten G, Juergens LA, Willard HF, Scher CD (1975) Recent developments in the detection of deoxyribonucleic acid synthesis by 33258 Hoechst fluorescence. The journal of histochemistry and cytochemistry : official journal of the Histochemistry Society 23:493-505.

Lee Y, Zacharias NM, Piwnica-Worms D, Bhattacharya PK (2014) Chemical reaction-induced multi-molecular polarization (CRIMP). Chemical communications 50:13030-13033.

Leese HJ, Bronk JR (1975) Lactate formation by rat small intestine in vitro. Biochimica et biophysica acta 404:40-48.
Lin J, Redies C (2012) Histological evidence: housekeeping genes beta-actin and GAPDH are of limited value for normalization of gene expression. Development genes and evolution 222:369-376.
Lin MT, Beal MF (2006) Mitochondrial dysfunction and oxidative stress in neurodegenerative diseases. Nature 443:787-795.
Lin RY, Vera JC, Chaganti RS, Golde DW (1998) Human monocarboxylate transporter 2 (MCT2) is a high affinity pyruvate transporter. The Journal of biological chemistry 273:28959-28965.
Lin ZX, Hoult JR, Raman A (1999) Sulphorhodamine B assay for measuring proliferation of a pigmented melanocyte cell line and its application to the evaluation of crude drugs used in the treatment of vitiligo. Journal of ethnopharmacology 66:141-150.
Lodish HF (2000) Molecular cell biology. New York: W.H. Freeman.
Luo Y, Rana P, Will Y (2012) Palmitate increases the susceptibility of cells to drug-induced toxicity: an in vitro method to identify drugs with potential contraindications in patients with metabolic disease. Toxicological sciences : an official journal of the Society of Toxicology 129:346-362.
Mackenzie B, Erickson JD (2004) Sodium-coupled neutral amino acid (System N/A) transporters of the SLC38 gene family. Pflugers Archiv : European journal of physiology 447:784-795.
Maldonado EN, Lemasters JJ (2014) ATP/ADP ratio, the missed connection between mitochondria and the Warburg effect. Mitochondrion 19 Pt A:78-84.
Malik AN, Czajka A (2013) Is mitochondrial DNA content a potential biomarker of mitochondrial dysfunction? Mitochondrion 13:481-492.
Malik AN, Shahni R, Rodriguez-de-Ledesma A, Laftah A, Cunningham P (2011) Mitochondrial DNA as a non-invasive biomarker: accurate quantification using real time quantitative PCR without co-amplification of pseudogenes and dilution bias. Biochemical and biophysical research communications 412:1-7.
Marie SK, Shinjo SM (2011) Metabolism and brain cancer. Clinics 66 Suppl 1:33-43.
Marroquin LD, Hynes J, Dykens JA, Jamieson JD, Will Y (2007) Circumventing the Crabtree effect: replacing media glucose with galactose increases susceptibility of HepG2 cells to mitochondrial toxicants. Toxicological sciences : an official journal of the Society of Toxicology 97:539-547.
Masubuchi Y, Kano S, Horie T (2006) Mitochondrial permeability transition as a potential determinant of hepatotoxicity of antidiabetic thiazolidinediones. Toxicology 222:233-239.
McKeehan WL (1982) Glycolysis, glutaminolysis and cell proliferation. Cell biology international reports 6:635-650.
Mills EL, Kelly B, Logan A, Costa ASH, Varma M, Bryant CE, Tourlomousis P, Dabritz JHM, Gottlieb E, Latorre I, Corr SC, McManus G, Ryan D, Jacobs HT, Szibor M, Xavier RJ, Braun T, Frezza C, Murphy MP, O'Neill LA (2016) Succinate Dehydrogenase Supports Metabolic Repurposing of Mitochondria to Drive Inflammatory Macrophages. Cell 167:457-470 e413.
Mitchell P (1961) Coupling of phosphorylation to electron and hydrogen transfer by a chemi-osmotic type of mechanism. Nature 191:144-148.
Mookerjee SA, Brand MD (2015) Measurement and Analysis of Extracellular Acid Production to Determine Glycolytic Rate. Journal of visualized experiments : JoVE e53464.
Morais VA, Haddad D, Craessaerts K, De Bock PJ, Swerts J, Vilain S, Aerts L, Overbergh L, Grunewald A, Seibler P, Klein C, Gevaert K, Verstreken P, De Strooper B (2014) PINK1 loss-of-function mutations affect mitochondrial complex I activity via NdufA10 ubiquinone uncoupling. Science 344:203-207.
Moreadith RW, Lehninger AL (1984) The pathways of glutamate and glutamine oxidation by tumor cell mitochondria. Role of mitochondrial NAD(P)+-dependent malic enzyme. The Journal of biological chemistry 259:6215-6221.
Nakamoto RK, Baylis Scanlon JA, Al-Shawi MK (2008) The rotary mechanism of the ATP synthase. Archives of biochemistry and biophysics 476:43-50.
Nelson DL, Cox MM (2013) Lehninger principles of biochemistry. New York: W.H. Freeman.
Nieminen AL, Saylor AK, Tesfai SA, Herman B, Lemasters JJ (1995) Contribution of the mitochondrial permeability transition to lethal injury after exposure of hepatocytes to t-butylhydroperoxide. The Biochemical journal 307 (Pt 1):99-106.
Nirwane A, Majumdar A (2018) Understanding mitochondrial biogenesis through energy sensing pathways and its translation in cardio-metabolic health. Archives of physiology and biochemistry 124:194-206.
Nolan JJ, Ludvik B, Beerdsen P, Joyce M, Olefsky J (1994) Improvement in glucose tolerance and insulin resistance in obese subjects treated with troglitazone. The New England journal of medicine 331:1188-1193.
O'Brien J, Wilson I, Orton T, Pognan F (2000) Investigation of the Alamar Blue (resazurin) fluorescent dye for the assessment of mammalian cell cytotoxicity. European journal of biochemistry 267:5421-5426.

Oh JY, In YS, Kim MK, Ko JH, Lee HJ, Shin KC, Lee SM, Wee WR, Lee JH, Park M (2007) Protective effect of uridine on cornea in a rabbit dry eye model. Investigative ophthalmology & visual science 48:1102-1109.

Oliveira C, Cagide F, Teixeira J, Amorim R, Sequeira L, Mesiti F, Silva T, Garrido J, Remiao F, Vilar S, Uriarte E, Oliveira PJ, Borges F (2018) Hydroxybenzoic Acid Derivatives as Dual-Target Ligands: Mitochondriotropic Antioxidants and Cholinesterase Inhibitors. Frontiers in chemistry 6:126.

Palmfeldt J, Vang S, Stenbroen V, Pedersen CB, Christensen JH, Bross P, Gregersen N (2009) Mitochondrial proteomics on human fibroblasts for identification of metabolic imbalance and cellular stress. Proteome science 7:20.

Papa S, Rasmo DD, Technikova-Dobrova Z, Panelli D, Signorile A, Scacco S, Petruzzella V, Papa F, Palmisano G, Gnoni A, Micelli L, Sardanelli AM (2012) Respiratory chain complex I, a main regulatory target of the cAMP/PKA pathway is defective in different human diseases. FEBS letters 586:568-577.

Papa S, Scacco S, Sardanelli AM, Vergari R, Papa F, Budde S, van den Heuvel L, Smeitink J (2001) Mutation in the NDUFS4 gene of complex I abolishes cAMP-dependent activation of the complex in a child with fatal neurological syndrome. FEBS letters 489:259-262.

Patra KC, Hay N (2014) The pentose phosphate pathway and cancer. Trends in biochemical sciences 39:347-354.

Pereira CV, Oliveira PJ, Will Y, Nadanaciva S (2012) Mitochondrial bioenergetics and drug-induced toxicity in a panel of mouse embryonic fibroblasts with mitochondrial DNA single nucleotide polymorphisms. Toxicology and applied pharmacology 264:167-181.

Pereira SP, Deus CM, Serafim TL, Cunha-Oliveira T, Oliveira PJ (2018) Metabolic and Phenotypic Characterization of Human Skin Fibroblasts After Forcing Oxidative Capacity. Toxicological sciences : an official journal of the Society of Toxicology 164:191-204.

Petry KG, Reichardt JK (1998) The fundamental importance of human galactose metabolism: lessons from genetics and biochemistry. Trends in genetics : TIG 14:98-102.

Picca A, Mankowski RT, Burman JL, Donisi L, Kim JS, Marzetti E, Leeuwenburgh C (2018) Mitochondrial quality control mechanisms as molecular targets in cardiac ageing. Nature reviews Cardiology.

Pogson JH, Ivatt RM, Sanchez-Martinez A, Tufi R, Wilson E, Mortiboys H, Whitworth AJ (2014) The complex I subunit NDUFA10 selectively rescues Drosophila pink1 mutants through a mechanism independent of mitophagy. PLoS genetics 10:e1004815.

Prieur I, Lunardi J, Dupuis A (2001) Evidence for a quinone binding site close to the interface between NUOD and NUOB subunits of Complex I. Biochimica et biophysica acta 1504:173-178.

Rana P, Nadanaciva S, Will Y (2011) Mitochondrial membrane potential measurement of H9c2 cells grown in high-glucose and galactose-containing media does not provide additional predictivity towards mitochondrial assessment. Toxicology in vitro : an international journal published in association with BIBRA 25:580-587.

Reitzer LJ, Wice BM, Kennell D (1979) Evidence that glutamine, not sugar, is the major energy source for cultured HeLa cells. The Journal of biological chemistry 254:2669-2676.

Rijken F, Bruijnzeel PL, van Weelden H, Kiekens RC (2004) Responses of black and white skin to solar-simulating radiation: differences in DNA photodamage, infiltrating neutrophils, proteolytic enzymes induced, keratinocyte activation, and IL-10 expression. The Journal of investigative dermatology 122:1448-1455.

Rittie L, Fisher GJ (2002) UV-light-induced signal cascades and skin aging. Ageing research reviews 1:705-720.

Robinson BH, Petrova-Benedict R, Buncic JR, Wallace DC (1992) Nonviability of cells with oxidative defects in galactose medium: a screening test for affected patient fibroblasts. Biochemical medicine and metabolic biology 48:122-126.

Rodriguez-Enriquez S, Juarez O, Rodriguez-Zavala JS, Moreno-Sanchez R (2001) Multisite control of the Crabtree effect in ascites hepatoma cells. European journal of biochemistry 268:2512-2519.

Rossignol R, Gilkerson R, Aggeler R, Yamagata K, Remington SJ, Capaldi RA (2004) Energy substrate modulates mitochondrial structure and oxidative capacity in cancer cells. Cancer research 64:985-993.

Saada A (2014) Mitochondria: mitochondrial OXPHOS (dys) function ex vivo--the use of primary fibroblasts. The international journal of biochemistry & cell biology 48:60-65.

Sadoul K, Boyault C, Pabion M, Khochbin S (2008) Regulation of protein turnover by acetyltransferases and deacetylases. Biochimie 90:306-312.

Sanuki Y, Araki T, Nakazono O, Tsurui K (2017) A rapid mitochondrial toxicity assay utilizing rapidly changing cell energy metabolism. The Journal of toxicological sciences 42:349-358.

Sanz A, Stefanatos RK (2008) The mitochondrial free radical theory of aging: a critical view. Current aging science 1:10-21.

Scaduto RC, Jr., Grotyohann LW (1999) Measurement of mitochondrial membrane potential using fluorescent rhodamine derivatives. Biophysical journal 76:469-477.

Schmidt JA, Rinaldi S, Scalbert A, Ferrari P, Achaintre D, Gunter MJ, Appleby PN, Key TJ, Travis RC (2016) Plasma concentrations and intakes of amino acids in male meat-eaters, fish-eaters, vegetarians and vegans: a cross-sectional analysis in the EPIC-Oxford cohort. European journal of clinical nutrition 70:306-312.

Shchepina LA, Pletjushkina OY, Avetisyan AV, Bakeeva LE, Fetisova EK, Izyumov DS, Saprunova VB, Vyssokikh MY, Chernyak BV, Skulachev VP (2002) Oligomycin, inhibitor of the F0 part of H+-ATP-synthase, suppresses the TNF-induced apoptosis. Oncogene 21:8149-8157.

Silva AM, Barbosa IA, Seabra C, Beltrao N, Santos R, Vega-Naredo I, Oliveira PJ, Cunha-Oliveira T (2016a) Involvement of mitochondrial dysfunction in nefazodone-induced hepatotoxicity. Food and chemical toxicology : an international journal published for the British Industrial Biological Research Association 94:148-158.

Silva FS, Starostina IG, Ivanova VV, Rizvanov AA, Oliveira PJ, Pereira SP (2016b) Determination of Metabolic Viability and Cell Mass Using a Tandem Resazurin/Sulforhodamine B Assay. Current protocols in toxicology 68:2 24 21-22 24 15.

Smith PK, Krohn RI, Hermanson GT, Mallia AK, Gartner FH, Provenzano MD, Fujimoto EK, Goeke NM, Olson BJ, Klenk DC (1985) Measurement of protein using bicinchoninic acid. Analytical biochemistry 150:76-85.

Stein WH, Moore S (1954) The free amino acids of human blood plasma. The Journal of biological chemistry 211:915-926.

Sullivan SG, Stern A (1983) Effects of physiologic concentrations of lactate, pyruvate and ascorbate on glucose metabolism in unstressed and oxidatively stressed human red blood cells. Biochemical pharmacology 32:2891-2902.

Sun F, Huo X, Zhai Y, Wang A, Xu J, Su D, Bartlam M, Rao Z (2005) Crystal structure of mitochondrial respiratory membrane protein complex II. Cell 121:1043-1057.

Swiss R, Niles A, Cali JJ, Nadanaciva S, Will Y (2013) Validation of a HTS-amenable assay to detect drug-induced mitochondrial toxicity in the absence and presence of cell death. Toxicology in vitro : an international journal published in association with BIBRA 27:1789-1797.

Swiss R, Will Y (2011) Assessment of mitochondrial toxicity in HepG2 cells cultured in high-glucose- or galactose-containing media. Current protocols in toxicology Chapter 2:Unit2 20.

Teixeira J, Cagide F, Benfeito S, Soares P, Garrido J, Baldeiras I, Ribeiro JA, Pereira CM, Silva AF, Andrade PB, Oliveira PJ, Borges F (2017a) Development of a Mitochondriotropic Antioxidant Based on Caffeic Acid: Proof of Concept on Cellular and Mitochondrial Oxidative Stress Models. Journal of medicinal chemistry 60:7084-7098.

Teixeira J, Deus CM, Borges F, Oliveira PJ (2018a) Mitochondria: Targeting mitochondrial reactive oxygen species with mitochondriotropic polyphenolic-based antioxidants. The international journal of biochemistry & cell biology 97:98-103.

Teixeira J, Oliveira C, Amorim R, Cagide F, Garrido J, Ribeiro JA, Pereira CM, Silva AF, Andrade PB, Oliveira PJ, Borges F (2017b) Development of hydroxybenzoic-based platforms as a solution to deliver dietary antioxidants to mitochondria. Scientific reports 7:6842.

Teixeira J, Oliveira C, Cagide F, Amorim R, Garrido J, Borges F, Oliveira PJ (2018b) Discovery of a new mitochondria permeability transition pore (mPTP) inhibitor based on gallic acid. Journal of enzyme inhibition and medicinal chemistry 33:567-576.

Teixeira J, Silva T, Andrade PB, Borges F (2013) Alzheimer's disease and antioxidant therapy: how long how far? Current medicinal chemistry 20:2939-2952.

Teixeira J, Soares P, Benfeito S, Gaspar A, Garrido J, Murphy MP, Borges F (2012) Rational discovery and development of a mitochondria-targeted antioxidant based on cinnamic acid scaffold. Free radical research 46:600-611.

Thompson RA, Isin EM, Li Y, Weidolf L, Page K, Wilson I, Swallow S, Middleton B, Stahl S, Foster AJ, Dolgos H, Weaver R, Kenna JG (2012) In vitro approach to assess the potential for risk of idiosyncratic adverse reactions caused by candidate drugs. Chemical research in toxicology 25:1616-1632.

Traut TW (1994) Physiological concentrations of purines and pyrimidines. Molecular and cellular biochemistry 140:1-22.

Uhlen M, Fagerberg L, Hallstrom BM, Lindskog C, Oksvold P, Mardinoglu A, Sivertsson A, Kampf C, Sjostedt E, Asplund A, Olsson I, Edlund K, Lundberg E, Navani S, Szigyarto CA, Odeberg J, Djureinovic D, Takanen JO, Hober S, Alm T, Edqvist PH, Berling H, Tegel H, Mulder J, Rockberg J, Nilsson P, Schwenk JM, Hamsten M, von Feilitzen K, Forsberg M, Persson L, Johansson F, Zwahlen M, von Heijne G, Nielsen J, Ponten F (2015) Proteomics. Tissue-based map of the human proteome. Science 347:1260419.

Vichai V, Kirtikara K (2006) Sulforhodamine B colorimetric assay for cytotoxicity screening. Nature protocols 1:1112-1116.

Villegas J, McPhaul M (2005) Establishment and culture of human skin fibroblasts. Current protocols in molecular biology Chapter 28:Unit 28 23.
Voet D, Voet JG (2011) Biochemistry. Hoboken, NJ: John Wiley & Sons.
Wagner A, Marc A, Engasser JM, Einsele A (1991) Growth and metabolism of human tumor kidney cells on galactose and glucose. Cytotechnology 7:7-13.
Wang X, Perez E, Liu R, Yan LJ, Mallet RT, Yang SH (2007) Pyruvate protects mitochondria from oxidative stress in human neuroblastoma SK-N-SH cells. Brain research 1132:1-9.
Wang YA, Kammenga JE, Harvey SC (2017) Genetic variation in neurodegenerative diseases and its accessibility in the model organism Caenorhabditis elegans. Human genomics 11:12.
Wilkins HM, Carl SM, Swerdlow RH (2014) Cytoplasmic hybrid (cybrid) cell lines as a practical model for mitochondriopathies. Redox biology 2:619-631.
Will Y, Dykens JA (2018) Mitochondrial dysfunction caused by drug and environmental toxicants. Hoboken, NJ: John Wiley & Sons.
Will Y, Dykens JA, Nadanaciva S, Hirakawa B, Jamieson J, Marroquin LD, Hynes J, Patyna S, Jessen BA (2008) Effect of the multitargeted tyrosine kinase inhibitors imatinib, dasatinib, sunitinib, and sorafenib on mitochondrial function in isolated rat heart mitochondria and H9c2 cells. Toxicological sciences : an official journal of the Society of Toxicology 106:153-161.
Wilson K, Walker JM (2009) Principles and techniques of biochemistry and molecular biology. Cambridge, UK New York: Cambridge University Press.
Yang C, Ko B, Hensley CT, Jiang L, Wasti AT, Kim J, Sudderth J, Calvaruso MA, Lumata L, Mitsche M, Rutter J, Merritt ME, DeBerardinis RJ (2014) Glutamine oxidation maintains the TCA cycle and cell survival during impaired mitochondrial pyruvate transport. Molecular cell 56:414-424.
Yu L, Lu M, Jia D, Ma J, Ben-Jacob E, Levine H, Kaipparettu BA, Onuchic JN (2017) Modeling the Genetic Regulation of Cancer Metabolism: Interplay between Glycolysis and Oxidative Phosphorylation. Cancer research 77:1564-1574.
Yu X, Hiromasa Y, Tsen H, Stoops JK, Roche TE, Zhou ZH (2008) Structures of the human pyruvate dehydrogenase complex cores: a highly conserved catalytic center with flexible N-terminal domains. Structure 16:104-114.
Zhao FQ, Keating AF (2007) Functional properties and genomics of glucose transporters. Current genomics 8:113-128.
Zhou W, Zhu M, Wilson MA, Petsko GA, Fink AL (2006) The oxidation state of DJ-1 regulates its chaperone activity toward alpha-synuclein. Journal of molecular biology 356:1036-1048.

Chapter VIII
Supplementary Data

8.1 Supplementary Data #1

Supplementary Data present in this subchapter was obtained from a XF Cell MitoStress Seahorse™ assay in which we do not have complete confidence. Cells were grown in LGm and adapted to OXPHOSm or to HGm as schematized in Figure 2.1. Cellular oxygen consumption and extracellular acidification measurements were performed as described in Subchapter 2.2.1.3. Figure 8.1 represents the initial respiration (defined as the sum of basal respiration and non-mitochondrial respiration), basal ECAR, and the Energy Map obtained from analyzing OCR and ECAR at the third OCR measurement in this assay. The results were interesting, although OCR values were higher than normal and NHDF cells did not respond to the mitochondrial-modulator drugs in the following measurements.

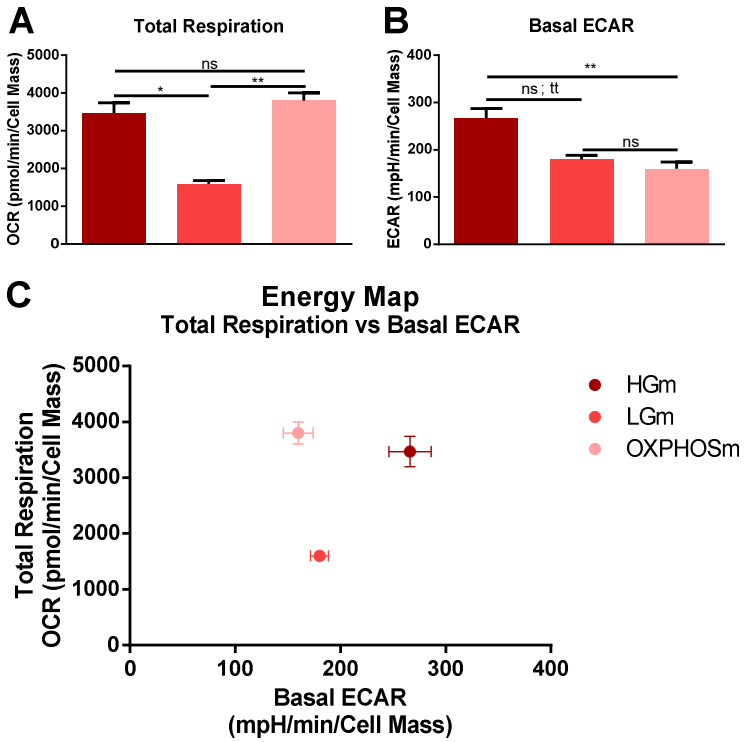

Figure 8.1 A Total Respiration, **B** Basal ECAR and **C** Energy Map of NHDF cells grown in LGm and adapted to OXPHOSm or HGm. NHDF cells were plated with a density of 7500 cells/well and OCR and ECAR were read. Data

are expressed as mean ± SEM of 3 independent experiments performed 2-3 times. **: p<0.01, *: p<0.05, ns: p≥0.05, with p being calculated using Kruskal-Wallis test with Dunn's multiple comparisons test; tt: p<0.01, with p being calculated using two-tailed Mann-Whitney test.

8.2 Supplementary Data #2

Supplementary Data present in this subchapter corresponds to complex IV in-gel activity measurements, performed as described in the Methods section. Although no changes are found in this complex activity, the method was not fully optimized, meaning that the confidence level of these measurements is low.

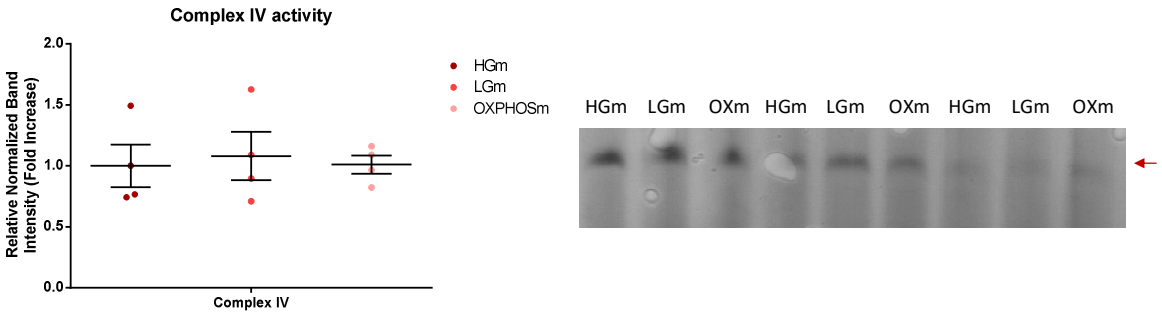

Figure 8.2 Complex IV activity in cells grown in HGm or adapted to LGm or OXPHOSm. Activity was measured in-gel, through the appearance of brown bands, correspondent to the oxidation of cytochrome c by DAB. Image at right shows representative gel. Arrow indicate the location of the band. Data are expressed as mean ± SEM of 4 independent experiments. Dots represent individual measurements.

8.3 Supplementary Data #3

Supplementary Data present in this subchapter is correspondent to gene expression measurements of some genes relevant for mitochondria biogenesis, including Cardiolipin Synthase 1 (CRLS1), GA binding protein transcription factor, alpha and beta 1 subunits (GABPA and GABPB1, which are components of the Nuclear Respiratory Factor 2), NRF1, PGC1α, TFAM. These measurements were performed in cells already adapted, in which the process of biogenesis has already occurred, giving little information about the process.

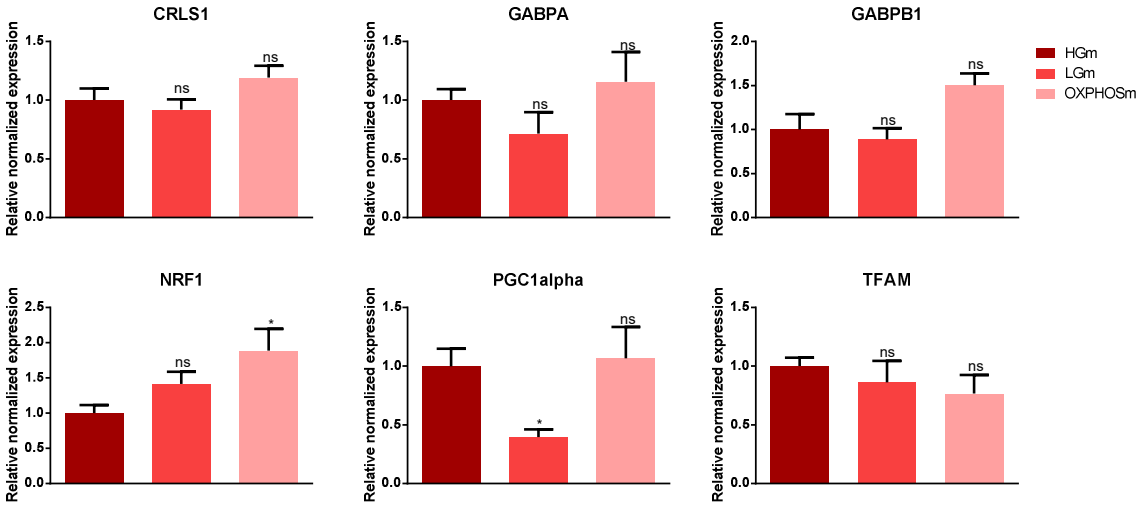

Figure 8.3 CRLS1, GABPA, GABPB1, NRF1, PGC1α and TFAM gene expression in cells grown in HGm or adapted to LGm or OXPHOSm. Total RNA was extracted, purified, converted into cDNA, and amplified by qRT-PCR. Gene expression was measured and normalized to B2M, HPRT1 and RNA18S levels, and divided by the mean of the values obtained for HGm-grown cells. Data are expressed as mean ± SEM of 5 independent experiments. *: $p<0.05$, ns: $p\geq0.05$, with p being calculated using Kruskal-Wallis test with Dunn's multiple comparisons test vs HGm